National Technical University of Athens
School of Civil Engineering
Geotechnical Division

Εθνικό Μετσόβιο Πολυτεχνείο
Σχολή Πολιτικών Μηχανικών
Τομέας Γεωτεχνικής

Diploma Thesis by

Papakyriakopoulos Orestis

Supervised by

Assistant Professor N. Gerolymos

MACROELEMENT MODELING OF THE NON-LINEAR RESPONSE OF PILES AND PILE-GROUPS SUBJECTED TO COMBINED LATERAL AND AXIAL LOADING

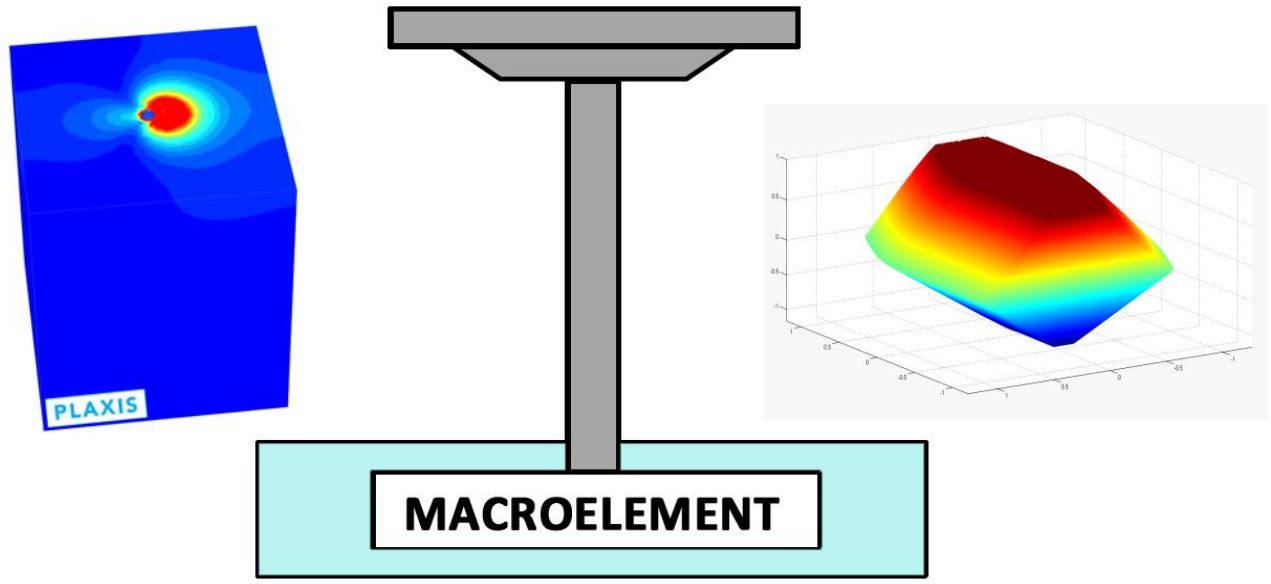

ΜΑΚΡΟΣΤΟΙΧΕΙΟ ΓΙΑ ΤΗ ΜΗ ΓΡΑΜΜΙΚΗ ΑΠΟΚΡΙΣΗ ΠΑΣΣΑΛΟΥ ΚΑΙ ΟΜΑΔΑΣ ΠΑΣΣΑΛΩΝ ΣΕ ΣΥΝΔΥΑΣΜΕΝΗ ΕΓΚΑΡΣΙΑ ΚΑΙ ΑΞΟΝΙΚΗ ΦΟΡΤΙΣΗ

Διπλωματική Εργασία

Παπακυριακόπουλου Ορέστη

Επιβλέπων

Επίκουρος Καθηγητής Ν. Γερόλυμος

July 2013

Acknowledgements

Upon completing my diploma thesis, I feel the need to thank the people that supported and encouraged me throughout my work.

This thesis would not have been possible without my supervisor, assistant Professor N. Gerolymos, to whom I owe my respectful gratitude not only for the inspiration provided, but also for his guidance, help and patience. His contribution to solving the challenging obstacles that arised throughout this thesis was really considerable.

I would also like to express my deepest appreciation and gratitude to Professor G. Gazetas, for his valuable guidance throughout my studies. He has been an endless source of inspiration and has greatly contributed to the love that I have developed towards Engineering in general and Geotechnical Engineering in particular.

I would like to thank assistant Professor I. Anastasopoulos for the interest shown and all the people of the Geotechnical Department and Soil Mechanics laboratory for their kind embrace as well as my fellow students and friends for the experiences we shared.

Finally, above all, I feel the need to thank my family for their consistent support and encouragement.

Table of Contents

Chapter 1

Introduction

1 Introduction

1.1 Scope

In this thesis, the response of pile foundations under combined axial, horizontal and moment loading is investigated. Assuming undrained soil conditions, primary goal is the extraction of the total 3D (in M-Q-N space) failure Envelope or ‘’Interaction Diagram’’ of the foundation system. Moreover the comprehension and the description of all physical attributes that rule the specific cases is targeted, explaining the physical meaning that governs the failure envelopes. To achieve this, a new macroscopic approach is developed to capture the accurate pile behavior. In addition, analytical expressions able to describe the capacity of each foundation type and their yield surface are proposed, utilizing the results of the Finite Element Analysis. Final aim of this thesis is the connection of all the above mentioned objectives and their integration in the theoretical framework of the development of an innovative mathematical tool known as ‘’macro-element’’ -similar to those already developed by researchers in the case of shallow foundations, which ‘’obeys’’ the plasticity theory laws that correlates the hardening of the system with the anticipated work (work–hardening plasticity theory). This approach is driven by the lack of complete tools that can effectively capture the behavior of pile foundations under combined loading and that would enhance the cooperation of structural and geotechnical engineers. In the following sections we provide a layout of the thesis as well as a short review of the literature regarding the analysis of deeply embedded foundations.

1.2 Layout

The second chapter deals with the development of a macroscopic (in M-Q-N space) Mohr-Coulomb based approach of the behavior of circular piles. The analytical extraction of the method is outlined, its calibration method through an optimization procedure is described while it is verified through an engineering calculation method and finite element modeling.

In the third chapter, a single pile and two pile-groups in cohesive soil in undrained conditions are studied, while sliding and gapping is allowed at the soil-pile interface. Through the limit equilibrium approach analytical expressions for the complete representation of the ultimate capacities of the foundations are derived and assess their ability to effectively capture all major trends. Their calibration and validation is performed through numerous finite element analyses. The methods for the conduction of the numerical analyses and present the results in terms of ultimate capacities and failure envelopes, Furthermore the total 3-D failure envelope in M-Q-N space of foundations is derived. Finally, insight is provided to the different types of failure mechanisms and to the shape of the interaction diagrams.

In the fourth chapter a macro-element model for pile foundations is developed. The extraction and incorporation of all necessary tools is described for the appropriate capture of the foundation behavior in elasticity and plasticity. Furthermore the results are compared with the data from the numerical experiments, while swipe tests are performed to validate the approach.

In the last chapter, the basic conclusions derived from this thesis are summed up and further research recommendations are given.

1.3 Use of Pile Foundations

Fig 1.1 presents a rough categorization of the types of foundations that are generally used in order to support structural systems. Surface or shallow embedded foundations are distinguished by small slenderness ratios, while pile foundations are generally more slender elements. Caisson foundations lie somewhere in between in terms of slenderness or embedment; yet their limits are vague. The compressibility of the soil and the structural element should also be taken into consideration for a more realistic distinction of different foundation types.

Pile foundations are typically made from steel or reinforced concrete and possibly timber. They are principally used to transfer the loads from a superstructure, through weak, compressible strata or water onto stronger, more compact, less compressible and stiffer soil or rock at depth, increasing the effective size of a foundation and resisting horizontal loads (Tomlinson & Woodward, 2007). They are used in very large buildings, off-shore structures, bridge piers and in situations where the soil under the superstructure is not suitable to prevent excessive settlement.

Piles can be classified by their function:

- End bearing piles are those where most of the friction is developed at the toe.
- Friction piles are those where most of the pile bearing capacity is developed by shear stresses along the sides of the pile (Atkinson, 2007).

There are two types of pile foundation installations: driven piles and bored piles:

- Driven piles are normally made from pre-cast concrete which is then hammered into the ground once on site.
- Bored piles are cast *in situ*; the soil is bored out of the ground, underreaming is performed and then the concrete is poured into the hole. Alternatively, boring of the soil and pouring of the concrete can take place simultaneously, in which case the piles are called continuous fight augured (CFA) piles.

The choice of pile used depends on the location and type of structure, the ground conditions, durability of the materials in the environment and cost. Most piles use some end bearing and some friction, in order to resist the action of loads. Driven piles are useful in offshore applications, are stable in soft squeezing soils and can densify loose soil. However, bored piles are more popular in urban areas as there is minimal vibration, they can be used where headroom is limited, there is no risk of heave and it is easy to vary their length.

Deeply embedded foundations have been consistently used in major offshore structures, where the study of their response under combined vertical, shear and moment loading is of great importance.

1.4 Piles under lateral loading

In Pile foundations the lateral loads are applied principally in two ways:

- Horizontal static and dynamic loads in the head of the piles, e.g. due to wind, earthquake, forces from the superstructure, sea waves etc.
- Horizontal loads along the length of the pile-side, e.g. in piled walls, bridge pier foundations, piles for soil improvement. These piles are usually vertical and in special circumstances inclined.

The vertical piles undertake horizontal loads with simultaneous bending and lateral displacement, activating in this way not only their resistance but that of the surrounding soil too.

The control of the ultimate capacity in horizontal loading must contain:

- The ultimate capacity of the surrounding soil
- The pile resistance as carrying member in bending due to lateral stresses
- The maximum displacement of the pile head, i.e. acceptable from the superstructure.

The behavior of the piles in horizontal loads depends on many factors as the relative stiffness of the pile soil system, the stress-strain relation (pile and soil), the soil resistance and the fixity conditions of the pile head.

The head of the pile, depending on whether the pile is single, belongs to a pile group, or in other special fixity conditions, might be considered free, pined, or fully fixed. With respect to the forms of the horizontal loads- displacement diagrams of the total pile, the piles might be considered as

- Rigid in the case that they rotate around a specific pivot point, without their significant deformation.
- Flexible in case that their response can be simulated by an elastic beam in elastic soil.

The piles can be categorized also in respect to the ratio L/D (L=length, D=diameter). A short pile behaves and rotates as a rigid body under lateral loads and has a ratio L/D<10. When vertical loads are applied, the loads transferred to the tip of the pile are a percentage of the total. In the case of the long pile (L/D>10), after a certain length (active length l_c) the rest of the pile remains inactive under lateral loading. Under vertical loading the forces are received by the friction of the pile walls at full length.

The active Length l_c is the minimum length after which the displacement at the pile head under a certain lateral load remains unaffected.

- $L \geq l_c$: flexible
- $l_c/2 \prec L \prec l_c$: stiff
- $L \leq l_c/2$: rigid

According to Gazetas (1991) the equations that determine the active length in an elastic half-space, are dependent of the soil elastic modulus distribution.

$l_c \approx 1.5 \cdot d \cdot \left(E_p / E_s \right)^{0.25}$ for uniform distribution (***Fig***.1.2.a)

$l_c \approx 1.5 \cdot d \cdot \left(E_p / \tilde{E}_s \right)^{0.22}$ for linear increase of E_s with depth (***Fig***.1.2.b)

$l_c \approx 1.5 \cdot d \cdot \left(E_p / \tilde{E}_s \right)^{0.20}$ for parabolic increase of E_s with depth (***Fig***.1.2.c)

1.5 Macroelement Modeling

Macroelement modeling provides an efficient alternative for the aforementioned difficulties; it simplifies drastically the consideration of soil-structure interaction effects in structural analyses by dispensing from the need to model explicitly the soil domain. It generally exhibits a straightforward and quick calibration procedure, an excellent degree of qualitative insight on foundation dynamic behavior and sufficiently accurate quantitative performance. Moreover, it minimizes the modeling uncertainty and guarantees repeatability since the entire soil domain is shrunk to a single finite element, characterized by a well-documented constitutive law and a relatively straightforward algorithmic implementation.

As it can be understood, macroelement modeling is related to the process of capturing, from the global response of a complex system that is the soil and the foundation substructure, only those elements that contribute to the interaction with the superstructure. In order to do so, it is important to investigate and understand in depth the characteristics of soil-foundation response. In reference to the examined problem of deep foundations under seismic loading, the prerequisites for macroelement modeling are the following:

• Definition of type of foundations to which the model will be applicable

• Knowledge of the bearing capacity of the foundation

• Knowledge of the lateral response of the foundation from small levels of loading up to failure.

Up to date, macroelement models have been developed only for the case of shallow foundations, where the effect of lateral soil pressures on the foundation can be neglected. Of noteworthy exception, Muir Wood and Kalasin (2004) have formulated a macroelement for the dynamic response of gravity retaining walls in which, issues

such as active and passive lateral earth pressure and bearing failure with significant overburden are successfully confronted.

A second option that has received more and more attention in the recent years is the nonlinear macro-element (NLME) approach, where the entire soil-foundation system is replaced by a single element located at the base of the super-structure, described with a suitable yield surface and plastic potential function. Thus, the footing and the soil are considered as a single 'macro-element', and a 6 DOF in the 3D case or a 3 DOF (2D case) model is formulated, describing the resultant force displacement behavior of a point of the footing (e.g. the center of a surface foundation or the center of head in the case of a pile foundation) in the vertical, horizontal, and rotational directions. The basic assumption beneath this formulation is that the footing is considered as a rigid body. The main advantage with respect to the BNWF approach is that all DOF of the macroelement are coupled.

The first non-linear macro-element (NLME) was proposed by Nova and Montrasio (1991) for strip footings on sand under monotonic loading with an isotropic-hardening elasto-plastic law. The basic idea of this model is first to represent the bearing capacity of the foundation under combined loading as a surface in the space of the resultant vertical and horizontal force and moment acting on the foundation following the reasoning initiated by Butterfield (1980). Then this ultimate surface is identified as the yield surface in the plasticity model regardless the mechanisms governing its origin and is allowed to evolve according to a suitably chosen hardening law. The displacements of the footing are predicted by introducing an experimentally calibrated flow rule, which turns out to be non-associated. This modelling procedure has been followed by subsequent works for different soil conditions (clay, loose or dense sand) and different foundation geometries (strip, rectangular, circular shallow foundations) leading to accurate formulations of the ultimate surface, the hardening rule and the flow rule (e.g. Gottardi et al., 1999; Houlsby and Cassidy, 2002; Cassidy et al., 2005). Di Prisco et al. (2003) extended this model to cyclic loading, introducing a bounding surface plasticity formulation, which allows one to obtain a continuous plastic response for the footing throughout the loading history. Paolucci (1997) initiated the use of macro-element models to study

non-linear dynamic soil-structure interaction problems under seismic loading, considering an elastic-perfectly plastic formulation of the Nova and Montrasio (1991) model. Le Pape and Sieffert (2001) derived a macro-element model to the Nova and Montrasio (1991) model within a thermodynamically coherent framework.

Cremer et al. (2002) introduced footing uplift in the macro-element formulation, which was modeled as a distinct non-linear mechanism with respect to soil plasticity, so that the global footing response was obtained through coupling between two distinct non-linear mechanisms (soil plastification and footing uplift). Uplift was described by a geometric model and soil plastification by a kinematic and isotropic hardening plasticity model. This macro-element model was developed for strip footings on cohesive soils under seismic loading.

Grange et al. (2008) extended Cremer et al (2002) macro-element model to 3D circular footings under monotonic static and cyclic loading and the uplift of the footing was treated into the plasticity model framework. Shirato et al. (2008) introduced the uplift of the footing in the Nova and Motrasio (1991) macro-element model by adding a coupling term in the soil-foundation stiffness matrix. Gajan and Kutter (2009) introduced a contact interface model which tracks the evolution of the soil-footing contact area.

Chatzigogos et al (2011) extended Cremer et al (2002) macro-element model by introducing a third non-linear mechanism, sliding between the soil and the footing, to the ultimate (failure) surface. Finally, Figini et al. (2012) modified the Chatzigogos et al. (2011) macroelement by introducing two main improvements: (i) a new mapping rule that better fits the loading path under seismic loading; and (ii) an uplift-plasticity coupling, described through the concept of footing effective width, with distinction between transient and permanent reduction of the soil-foundation contact area. An asset of the proposed model is that a unique set of parameters for dense sand conditions is introduced that fits reasonably well the results from independent large scale laboratory tests, both cyclic and dynamic, supporting its use for predictive analyses and applications.

Correia et al (2012) proposed a pile-head macro-element as an extension of the macro-element concept previously developed for structures on shallow foundations (Figini et al, 2012), to the case of deep foundations.

Figures

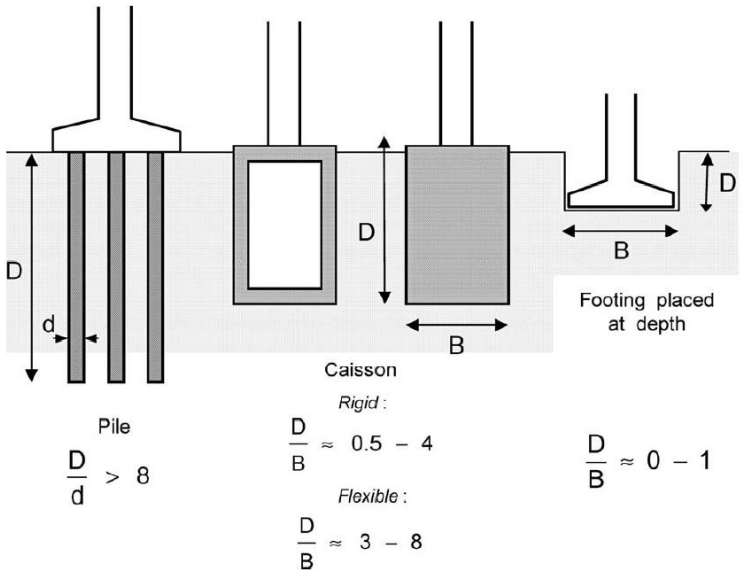

Figure 1.1 *A rough categorization of different foundation types based on their slenderness or embedment ratio D/B. From the left to the right we can distinguish (a) piles, (b) deeply embedded foundations and (c) shallow foundations.* (after Gerolymos & Gazetas, 2006)

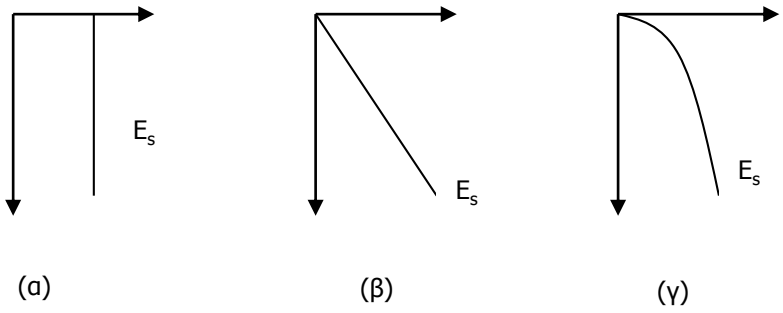

Figure 1.2 *Different distributions of the Elastic Modulus with the depth.*

Chapter 2

Macroscopic Mohr-Coulomb based approach of the behavior of circular piles

2 Macroscopic (in M-N space) Mohr-Coulomb based approach of the behavior of circular piles

The need for a realistic pile behavior and the absence of an accurate pile model aroused the interest in developing a new approach that would be able to overcome the lack in the existing bibliography and Finite Element Modeling.

Until now the pile simulation in FEM was succeeded in two ways:

- The representation of the pile as a soil volume, whose response is governed by a fully elastic model.
- The composure of the pile as a combination of one dimensional elastic or inelastic beam elements and elastic elements that provide the geometrical volume.

The drawback of the first model is the total ignorance of the pile failure, while in the second no installation effects can be taken into account and the pile-soil interaction is modelled at the center rather than the circumference. Moreover, in both cases the satisfying simulation of the properties and the behavior of the pile material is not succeeded.

The aim of the new approach is to:

- include the pile material behavior into the soil-foundation system
- incorporate the effect of the external load combination to the alteration of the pile material properties
- simulate in a uniform approach the elastoplastic pile response
- the realistic representation of the pile-soil interaction

2.1 Soil Constitutive Models

2.1.1 Tresca Failure Criterion

In general, the yield function f depends on various parameters such as stresses, strains and history of loading. The strains from the parameters in the yield function may be excluded since, for the classical perfectly plastic models, they are uniquely related to the stress level. Therefore, the general form may be given by the equation:

$$f(\sigma_{ij}) = f_c \qquad \textbf{(2.1)}$$

Furthermore, in isotropic materials the function f must be unchanged with respect to any transformation of coordinates. This isotropic condition calls for the use of invariants of stresses. Thus the form of f can be represented by:

$$f(\text{invariants of } \sigma_j) = f_c \qquad \textbf{(2.2)}$$

Since the hydrostatic pressure has little or no effect on the plastic deformation and yielding of a material in undrained conditions the equation takes the form:

$$f(\text{invariants of } S_{ij}) = f_c \qquad \textbf{(2.3)}$$

Among various invariants of deviatoric stress tensor S_{ij} only two are independent and other invariants can be expressed in terms of these two. The invariants J_2 and J_3 are independent and express the yield criterion in the form:

$$f(J_2, J_3) = f_c \qquad \textbf{(2.4)}$$

The Tresca criterion (or the maximum shear stress criterion) implies that yielding occurs when the maximum shear stress reaches a critical level. For the special case $\sigma_1 \geq \sigma_2 \geq \sigma_3$, the Tresca yield condition can be written as:

$$\frac{1}{2}(\sigma_1 - \sigma_3) = k \qquad \textbf{(2.5)}$$

Where σ_1, σ_3 are maximum and minimum principal stresses respectively and k is the yield stress of the material determined from pure shear test. More generally the previous equation can be written as:

$$\left[(\sigma_1 - \sigma_3)^2 - 4k^2\right]\left[(\sigma_2 - \sigma_3)^2 - 4k^2\right]\left[(\sigma_3 - \sigma_1) - 4k^2\right] = 0 \qquad \textbf{(2.6)}$$

Or in terms of stress invariants J_2 and J_3:

$$f - f_c = 4J_2^3 - 27J_3^2 - 36k^2J_2^2 + 96k^4J_2 - 64k^6 = 0 \qquad \textbf{(2.7)}$$

The three-dimensional view of the Tresca yield criterion in principal stress is shown in ***Fig 2.1*** where ***Eq. 2.6*** represents a cylindrical surface whose generator is parallel to the hydrostatic $\sigma_1 = \sigma_2 = \sigma_3$ and whose cross sectional shape on the π-plane is a regular hexagon.

In simple tension test with $\sigma_1 = \sigma_2 = \sigma_3$ the yield stress is equal to:

$$\sigma_y = 2k \qquad \textbf{(2.8)}$$

2.1.2 Mohr-Coulomb Model

Realizing that soil strength depends on the hydrostatic pressure, a general yield function of ***Eq. 2.1*** may be written as:

$$f(I_1, J_2, J_3) = f_c \qquad \textbf{(2.9)}$$

The Coulomb criterion is the first criterion that take into consideration the hydrostatic pressure:

$$|\tau| + \sigma \tan\varphi - c = 0 \qquad \textbf{(2.10)}$$

Where C and φ denote the cohesion and the angle of internal friction respectively.

For the special case of frictionless materials for which φ =0, ***Eq. 2.10*** reduces to the maximum shear stress criterion of Tresca $\tau = C$.We consider a state of principal stress (σ_1, σ_2, σ_3) which satisfies the Coulomb criterion of ***Eq.2.10.*** If the condition of stress state is $\sigma_1 > \sigma_2 > \sigma_3$, the Coulomb criterion can be written as:

$$\frac{1}{2}(\sigma_1 - \sigma_3) = -\frac{1}{2}(\sigma_1 - \sigma_3)\sin\varphi + c\cos\varphi \qquad \textbf{(2.11)}$$

Each principal stress can be represented in terms of I_1, J_2, θ(lode angle);

$$\sigma_1 = \frac{2}{\sqrt{3}}\sqrt{J_2}\cos\theta + \frac{1}{3}I_1 \qquad \textbf{(2.12a)}$$

$$\sigma_2 = \frac{2}{\sqrt{3}}\sqrt{J_2}\cos(\theta - \frac{2}{3}\pi) + \frac{1}{3}I_1 \qquad \textbf{(2.12b)}$$

$$\sigma 3 = \frac{2}{\sqrt{3}}\sqrt{J_2}\cos(\theta + \frac{2}{3}\pi) + \frac{1}{3}I_1 \qquad \textbf{(2.12c)}$$

Therefore substitution of ***Eq. 2.12a*** and ***Eq. 2.12c*** and into ***Eq. 2.11*** leads to the stress invariant form of the Coulomb criterion that is

$$\frac{1}{3}I_1\sin\varphi + \sqrt{\frac{J_2}{3}}[(1+\sin\varphi)\cos\theta - (1-\sin\varphi)\cos(\theta + \frac{2}{3}\pi)] - c\cos\varphi = 0 \qquad \textbf{(2.13)}$$

Or

$$I_1\sin\varphi + \frac{1}{2}[3(1-\sin\varphi)\sin\theta + \sqrt{3}(3+\sin\varphi)\cos\theta]\sqrt{J_2} - 3c\cos\varphi = 0 \qquad \textbf{(2.14)}$$

As shown by Shield (1995), the Coulomb's criterion is a hexagonal pyramid in the principal stress space (***Fig 2.2)***. To obtain a better approximation when tensile stress occurs, it is sometimes necessary to combine the Coulomb criterion with a maximum tensile strength cut-off

$$\sigma = f_1 > 0 \qquad \textbf{(2.15)}$$

where f_1 is a tensile strength obtained from an experiment. This modified Coulomb Criterion with a tension cut-off is defined by three material constants such as c , φ and f_1. Note that the uniaxial tensile strength as predicted by the Coulomb criterion should be thought of as a fictitious tensile strength which is not the same as the true uniaxial tensile strength of a material from experiment. The main advantages and limitations of the Coulomb criterion with a tension cut-off are summarized in detail in the book by Chen (1982).

Even though the Coulomb criterion, as mentioned above, is generally simple in graphical form, the Coulomb surface exhibits corners or singularities in a three-dimensional generalization. The resulting general yield or failure function with singularities gives rise to some difficulties in numerical analysis. In addition to these

limitations, the Coulomb criterion neglects the influence of intermediate principal shear stress on shear strength. Nevertheless, for the most part, this criterion has in the past been used for necessity and simplicity to obtain reasonable solutions to important and practical problems in geotechnical engineering.

2.2 Analytical Solution

When the pile is subjected to moment and axial load in full plasticity, on a random section there is the stress distribution of ***Fig. 2.3***

According to the Tresca failure theory in this case, the maximum stress capacity is equal with:

$$\sigma_y = 2c = \sigma_c \,, \qquad \textbf{(2.16)}$$

while the tensile stress of the section cannot exceed the tensile capacity σt.

Applying for the bending stresses the Newton's law Equilibrium $\Sigma\vec{F} = 0$,

$$\sigma_{MC} A_C = \sigma_{Mt} A_t \,, \qquad \textbf{(2.17)}$$

where

$$\sigma_{MC} = 2c - \frac{4N}{\pi D^2} \qquad \textbf{(2.18a)}$$

The maximum compressive stress that can be expended by the bending stress

$$\sigma_{Mt} = \sigma t + \frac{4N}{\pi D^2} \qquad \textbf{(2.18b)}$$

The maximum tensile stress that can be expended by the bending stress

$$A_C = 2\int_0^{\frac{\pi}{2}} \int_0^{\frac{2x\cos^2\theta - D\cos^2\theta + \frac{\sqrt{2}\cos\theta\sqrt{D^2 - 4x^2 + D^2\cos 2\theta + 4Dx + 4x^2\cos 2\theta - 4Dx\cos 2\theta}}{2}}{2\cos\theta}} r dr d\theta \qquad \textbf{(2.19a)}$$

$$A_C = 2\int_0^{\frac{\pi}{2}} \int_0^{\frac{2x\cos^2\theta - D\cos^2\theta + \frac{\sqrt{2}\cos\theta\sqrt{D^2-4x^2+D^2\cos 2\theta+4Dx+4x^2\cos 2\theta-4Dx\cos 2\theta}}{2}}{2\cos\theta}} rdrd\theta \quad \textbf{(2.19a)}$$

$$A_t = 2\int_0^{\frac{\pi}{2}} \int_0^{\frac{2(D-x)\cos^2\theta - D\cos^2\theta + \frac{\sqrt{2}\cos\theta\sqrt{D^2-4(D-x)^2+D^2\cos 2\theta+4D(D-x)+4(D-x)^2\cos 2\theta-4D(D-x)\cos 2\theta}}{2}}{2\cos\theta}} rdrd\theta \quad \textbf{(2.19b)}$$

where x is the compression zone, D the pile diameter, A_C and A_t the area of the section that it is under compression and tension respectively.

Finally the ultimate bending imposing moment is given by the following equation:

$$M = \sigma_{MC}\iint dA_c dy + 2\sigma_{Mt}\iint dA_t dy + (\frac{D}{2} - x)\,\mathrm{N} \quad \textbf{(2.20)}$$

,with:

$$\iint dA_c dy = \quad \textbf{(2.21a)}$$

$$= 2\int_0^{\frac{\pi}{2}} \int_0^{\frac{2x\cos^2\theta - D\cos^2\theta + \frac{\sqrt{2}\cos\theta\sqrt{D^2-4x^2+D^2\cos 2\theta+4Dx+4x^2\cos 2\theta-4Dx\cos 2\theta}}{2}}{2\cos\theta}} r^2\cos\theta drd\theta$$

$$\iint dA_t dy = \quad \textbf{(2.21b)}$$

$$= 2\int_0^{\frac{\pi}{2}} \int_0^{\frac{2(D-x)\cos^2\theta - D\cos^2\theta + \frac{\sqrt{2}\cos\theta\sqrt{D^2-4(D-x)^2+D^2\cos 2\theta+4D(D-x)+4(D-x)^2\cos 2\theta-4D(D-x)\cos 2\theta}}{2}}{2\cos\theta}} r^2\cos\theta d\theta$$

dy the momentarm of the infinitesimal area.

For the variables input in the finite-element platform, due to the fact that the Finite-Element Method forms the stress distribution in a hyperbolic shape (***Fig.2.4***) the following correction factor that represents the difference between the rectangular and the hyperbolic stress distribution is inserted in the ***Eq.2.18a*** and ***2.18.b***:

$$\frac{x_0}{\int_0^{x0}\tanh(3\frac{x}{x_0})} = 1.299, \quad \textbf{(2.22)}$$

where $X0$ the compressive zone length and X the coordinate of the stress distribution.

Changing them to:

$$\sigma_{MC} = 2.598c - \frac{4N}{\pi D^2} \quad \textbf{(2.23a)}$$

$$\sigma_{Mt} = 1.299\sigma_t - \frac{4N}{\pi D^2} \quad \textbf{(2.23b)}$$

2.3 Optimization

Reinforced Concrete Piles of 3 different diameters (0.8m,1m,1.5m) with varying steel bar section Area (1%,1.5%,2%) and a length of 16 m are chosen. Modulus of elasticity is picked $30 \cdot 10^6$ *KN/m*^{2} and the Poisson's ratio v=0.2. Their failure Envelopes in M-N space and their Moment-Curvature diagrams are extracted through USC-RC, a fiber analysis calculation tool for reinforced concrete members.

The data are imported to Matlab and the variables c , σ_t from the previously derived equations are optimized to fit to the failure envelope of the pile. This nonlinear optimization problem is addressed with the use of two different solvers:

The use of a hybrid algorithm, incorporating a genetic algorithm and a constrained minimizing function of Matlab. A genetic algorithm (GA) is a method for solving both constrained and unconstrained optimization problems based on a natural selection process that mimics biological evolution. The algorithm repeatedly modifies a population of individual solutions. At each step, the genetic algorithm randomly selects individuals from the current population and uses them as parents to produce the children for the next generation. Over successive generations, the population "evolves" toward an optimal solution. In fact, the former is utilized in order to locate the global minimum and in a second step, the latter captures the optimum solution,

as visualized in ***Figure 2.5*** for an equivalent 3-dimensional problem. Choosing the most efficient goal function and the right parameters of the genetic algorithm's structure (initial population, generations, mutation, migration and crossover) is of great importance in order to efficiently solve the problem. Various structure characteristics were utilized, before concluding to a 40-individual initial population, 1000-generation-limited, constraint dependent-mutation, forward-migration, scattered-crossover approach that could effectively solve the problem. We ensured the good fit by accepting a solution to the optimization problem that provides a goal function value below an acceptable limit.

The use of Generalized Pattern Search solver, which uses a pattern search method that implements a minimal and maximal positive basis pattern. A similar procedure as above is followed, giving a start point to the solver and adopting a GPS Positive basis 2N method. Good fitting was ensured by accepting a solution below an acceptable limit.

Two different optimization procedures are performed. The first aiming at the calibration of the approach to the total failure Envelope and the latter from full tensile to the half compressive strength of the pile, point where all stiff soils have reached their ultimate capacity.

2.4 Verification

The proposed values for C , σt are inserted in the failure equations of the pile and through the engineering calculation platform Mathcad and Plaxis 3D the approach is verified.

2.4.1 The Finite Element Model

The Finite-Element Platform Plaxis 3D is used. The pile is represented as a soil volume with a Mohr- Coulomb Model ruling its response that has the above mentioned properties and the corresponding failure parameters. The cohesion is set equal with C , the angle of friction is equal with zero and tension cut-off is activated with a strength factor equal with σt . A total displacement fixity is placed at the pile

bottom, while a stress distribution is applied on the pile head simulating the load ***Fig.2.6***. The Moment is derived out of the horizontal load multiplied by the length of the pile. The M-N Failure Envelope of the pile is calculated and through a mesh sensitivity analysis (***Fig.2.7***) the appropriate pile discretization is elected. As expected, the pile failure Envelope for the variable values without the stress shape correction factor cannot represent the pile behavior satisfactorily. Finally a pile consistent of 7659 elements is chosen for the further analysis.

2.4.2 Results

The Failure Envelopes of the piles are compared with the ones extracted through calculations and through FEM. Each time, the appropriate variable values, derived out of an optimization procedure matching the total failure envelope, are inserted into the equations (***Fig 2.8-2.10***)***.*** Moreover the Moment-Curvature Diagram derived from FEM fits satisfactorily with the one extracted from the fiber analysis (***Fig 2.11).***

Taking into consideration the soil capacity, a more focused calibration of the approach is conducted ***(Fig 2.12-2.14)***, as mentioned above***.*** More specifically, assuming that a very stiff clay has an undrained strength Su=200 KPa, its maximum compressive capacity is equal with:

$$Q_u = S_u \pi D l + A S_u \pi \frac{D^2}{4}, \qquad \textbf{(2.24)}$$

where it is assumed that A=10. In addition, according to the American Petroleum Institute (API) the maximum compressive resistance of sand is equal to:

$$Q_u = 114.8 \pi D l + 12000 \pi \frac{D^2}{4} \qquad \textbf{(2.25)}$$

As it is illustrated, the approach reproduces the pile behavior brilliantly. Thus the development of a very useful tool is succeded. The methodology of the calibration of the approach can be summed up in the following steps:

- Extraction of the failure envelope of the circular pile.
- Using the equations ***2.17,2.20*** through an optimization algorithm the appropriate variable values are derived.

- The variable values are inserted in the soil model in the Finite Element model together with the other material properties. (poisson's ratio, modulus of elasticity)
- The verification can be performed in two ways: a) conducting the failure envelopes through Finite Element Modelling b) compering the Moment-Curvature Diagrams.

Figures

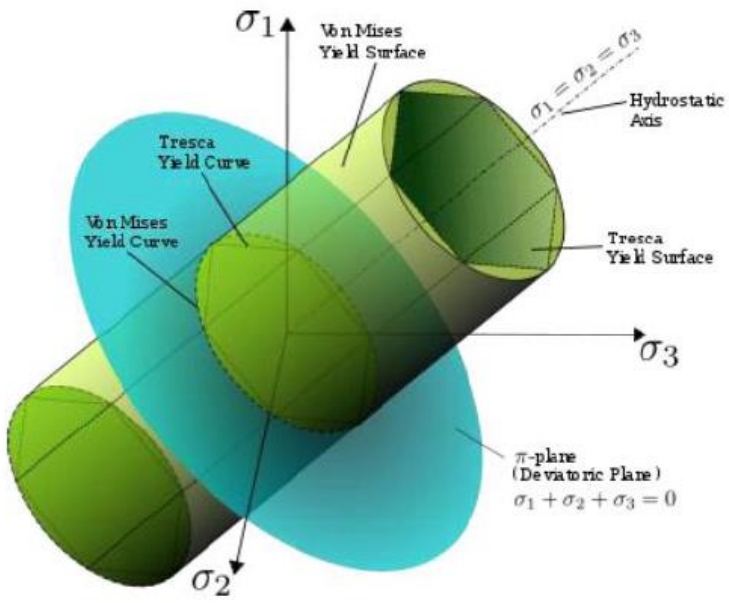

Figure 2.1 *The Tresca criterion is represented by a hexagon that runs along the hydrostatic axis in the σ1-σ2-σ3 space. The yield surface is compared with that proposed by Von Mises.*

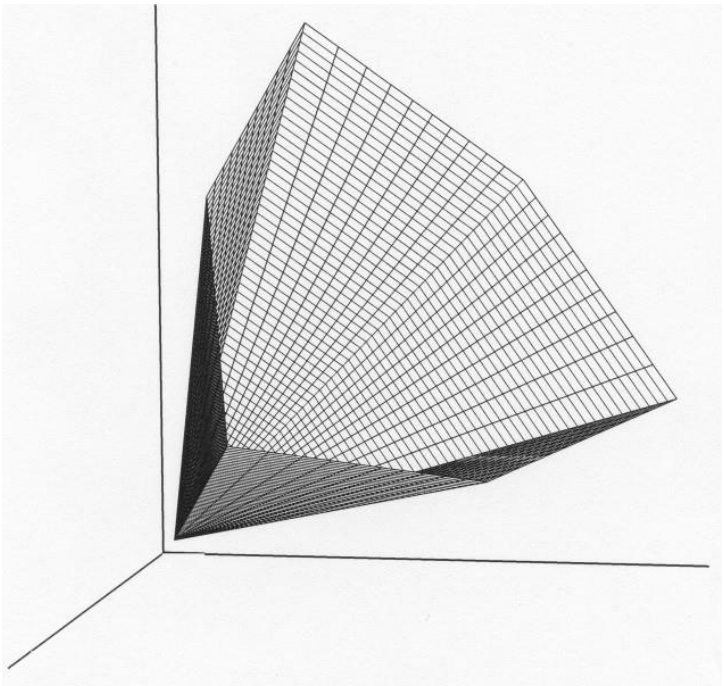

Figure 2.2 *The Coulomb's failure criterion is represented by a irregular hexagon pyramid in the principal stress space.*

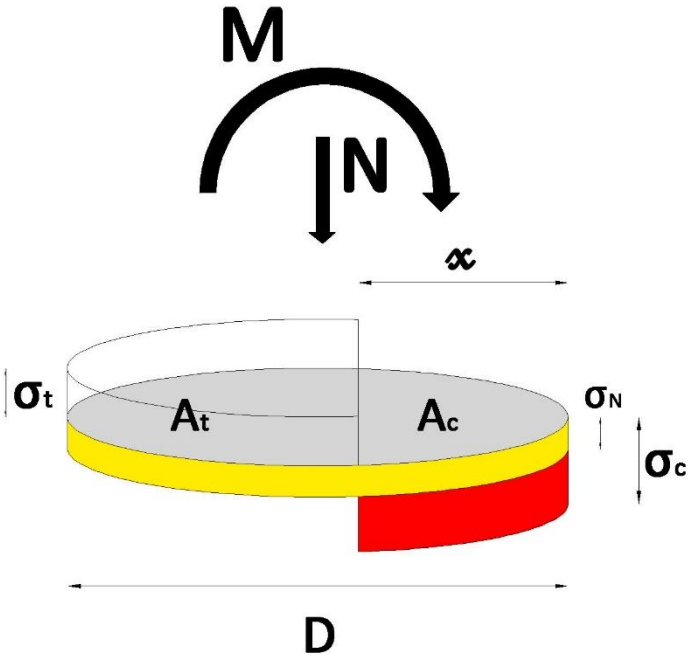

Figure 2.3 *Stress Distribution on a random Pile Section under Moment and Axial Load in full Plasticity*

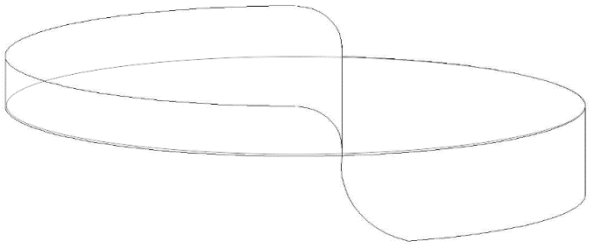

Figure 2.4 *Stress distribution on a random pile section in full plasticity in Finite Element Modelling*

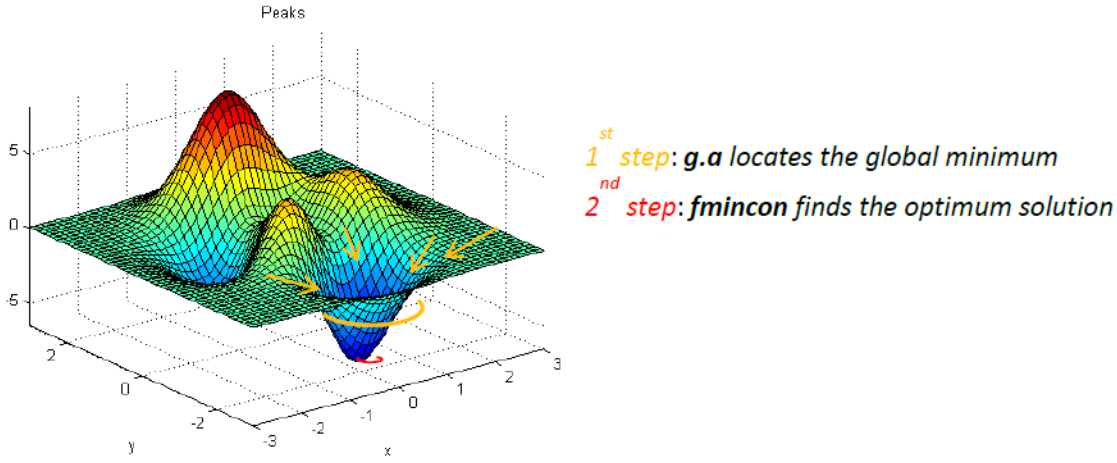

Figure 2.5 *Visualization of the optimization procedure in an equivalent 3-dimensional problem.*

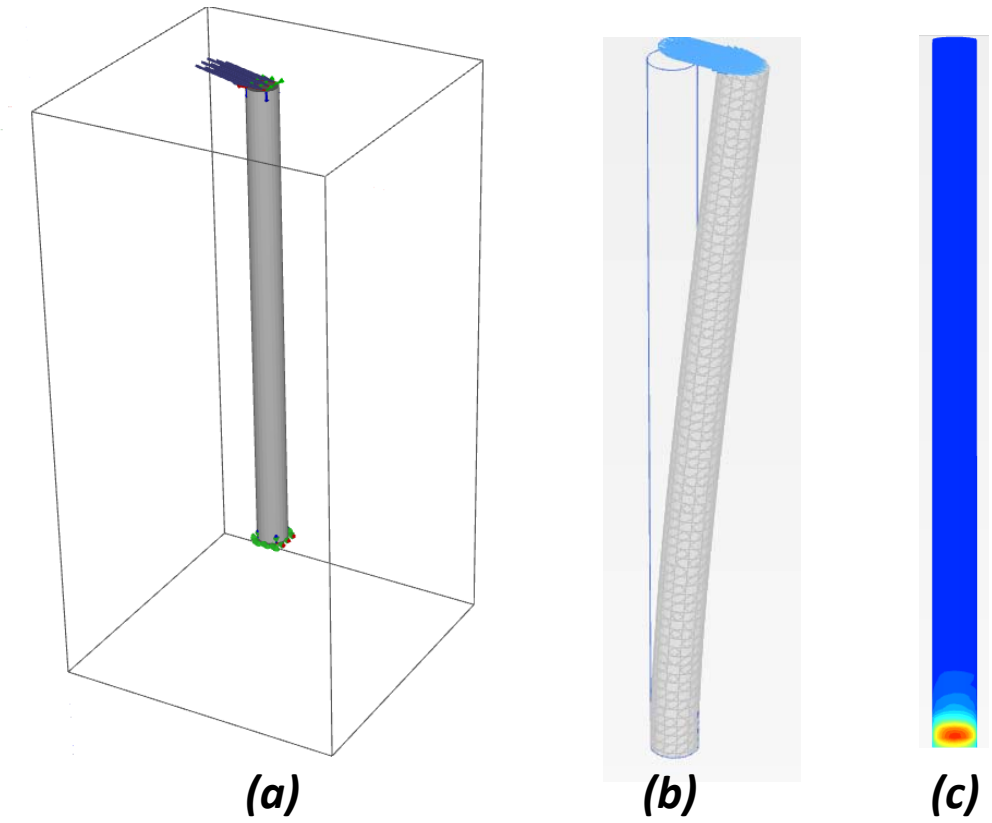

Figure 2.6 *3D Visualizaton of the FE pile model* ***a)*** *showing the bottom fixity and the stress distribution* ***b)*** *under lateral loading* ***c)*** *the plastic hinge developed at the bottom of the pile is visible through the incremental deviatoric strain Δγ.*

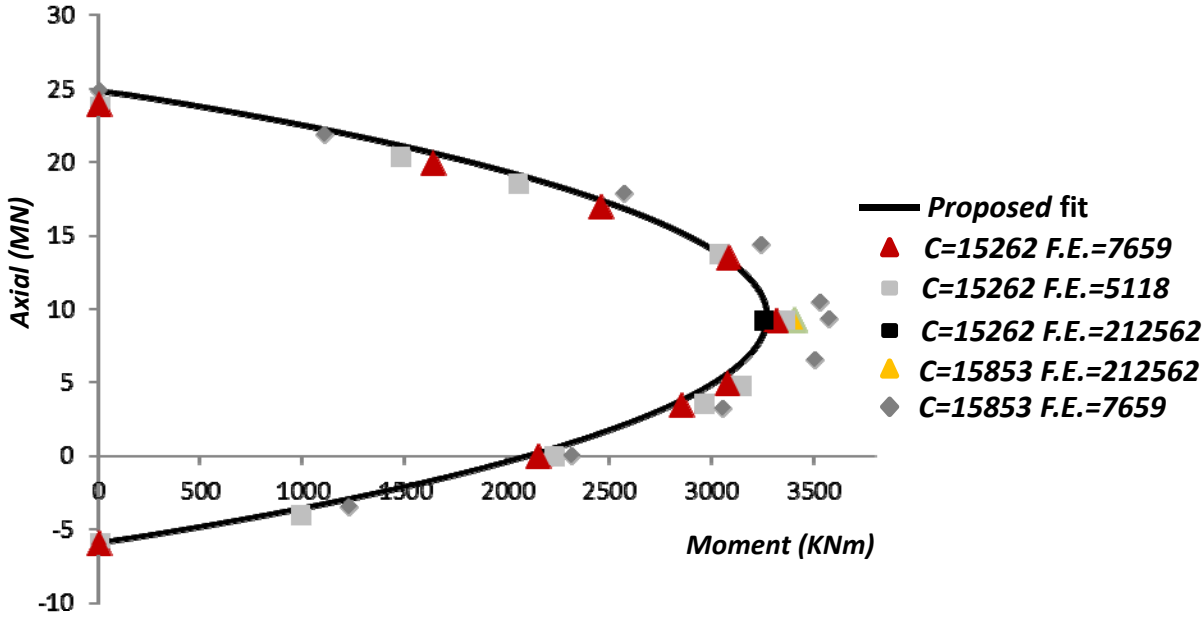

Figure 2.7 *Pile Sensitivity Analysis. As expected the variable values without the stress shape correction factor cannot represent the pile behavior satisfactorily*

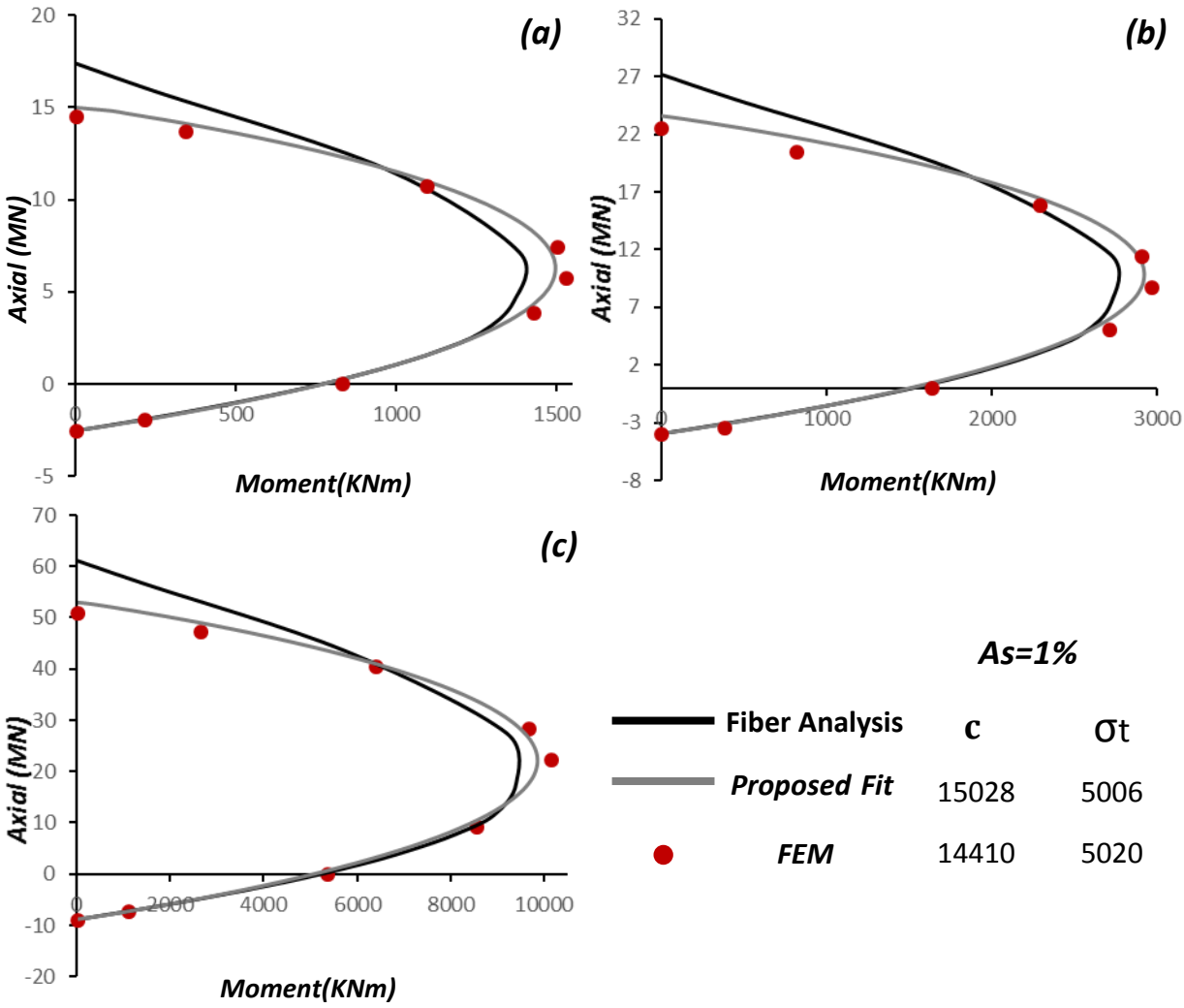

Figure 2.8 *Comparison between the data derived from the numerical experiments (points), the failure Envelope that is extracted from the fiber analysis and the proposed fit from the macroscopic approach for As=1% and a) D= 0.8 m, b) D=1 mc) D=1.5 m.*

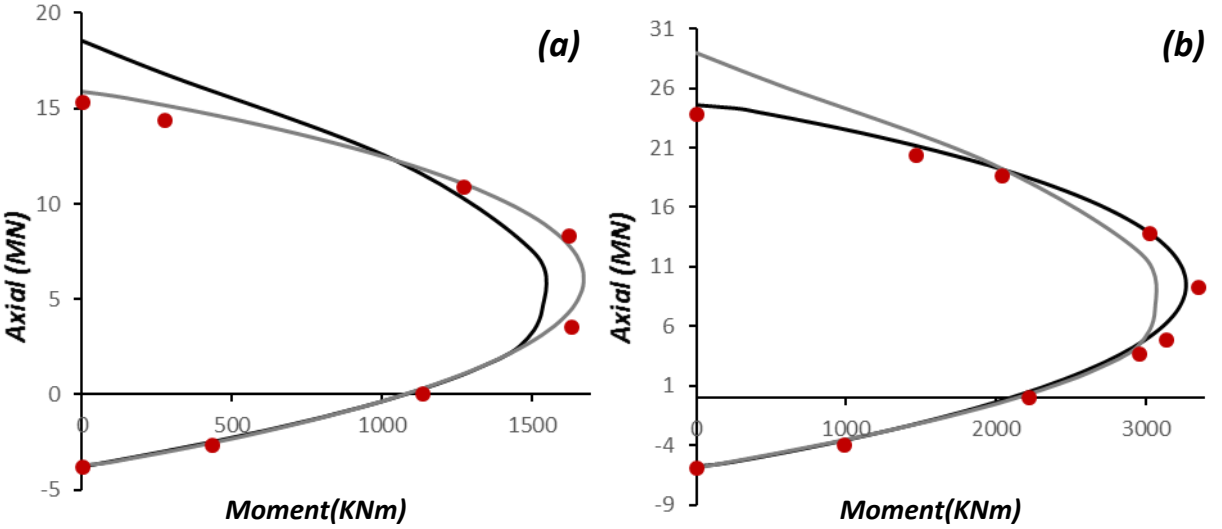

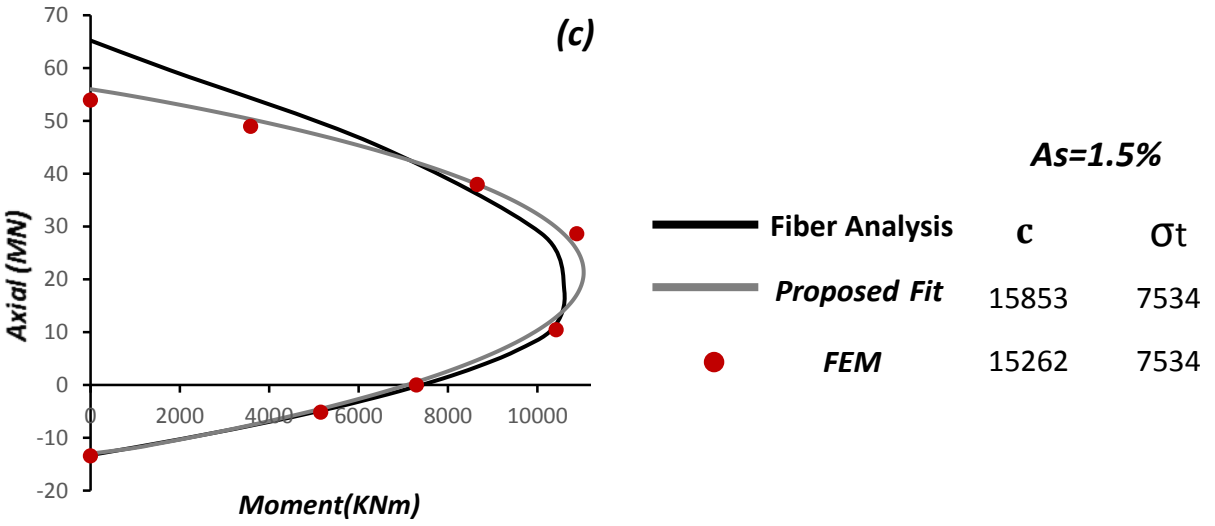

Figure 2.9 *Comparison between the data derived from the numerical experiments (points), the failure Envelope that is extracted from the fiber analysis and the proposed fit from the macroscopic approach for As=1.5% and a) D= 0.8 m, b) D=1 mc) D=1.5 m.*

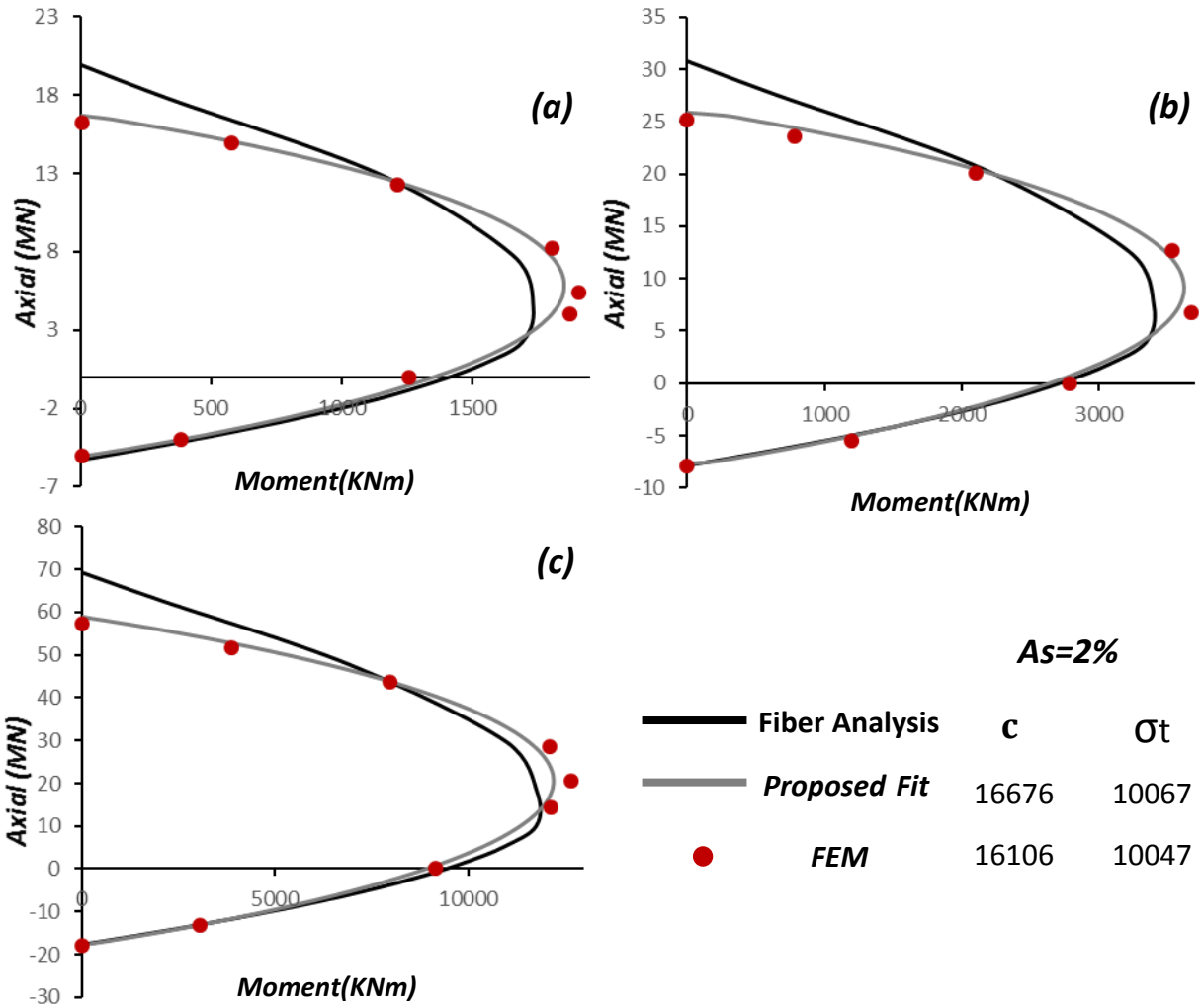

Figure 2.10 *Comparison between the data derived from the numerical experiments (points), the failure Envelope that is extracted from the fiber analysis and the proposed fit from the macroscopic approach for As=2% and a) D= 0.8 m, b) D=1 m c) D=1.5 m.*

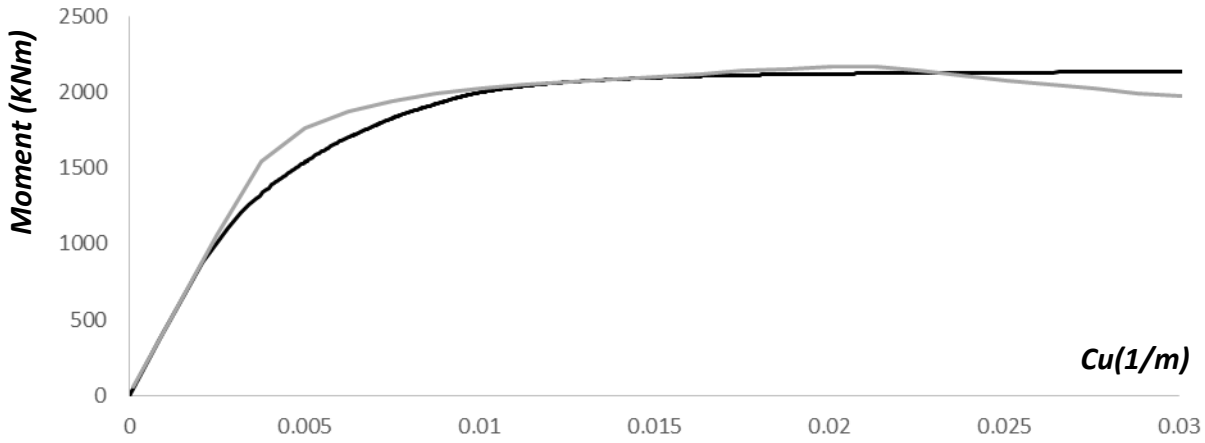

Figure 2.11 *Comparison between the Moment-Curvature Diagram from the numerical experiments and the one derived from the fiber analysis for As=1.5%, D=1 m*

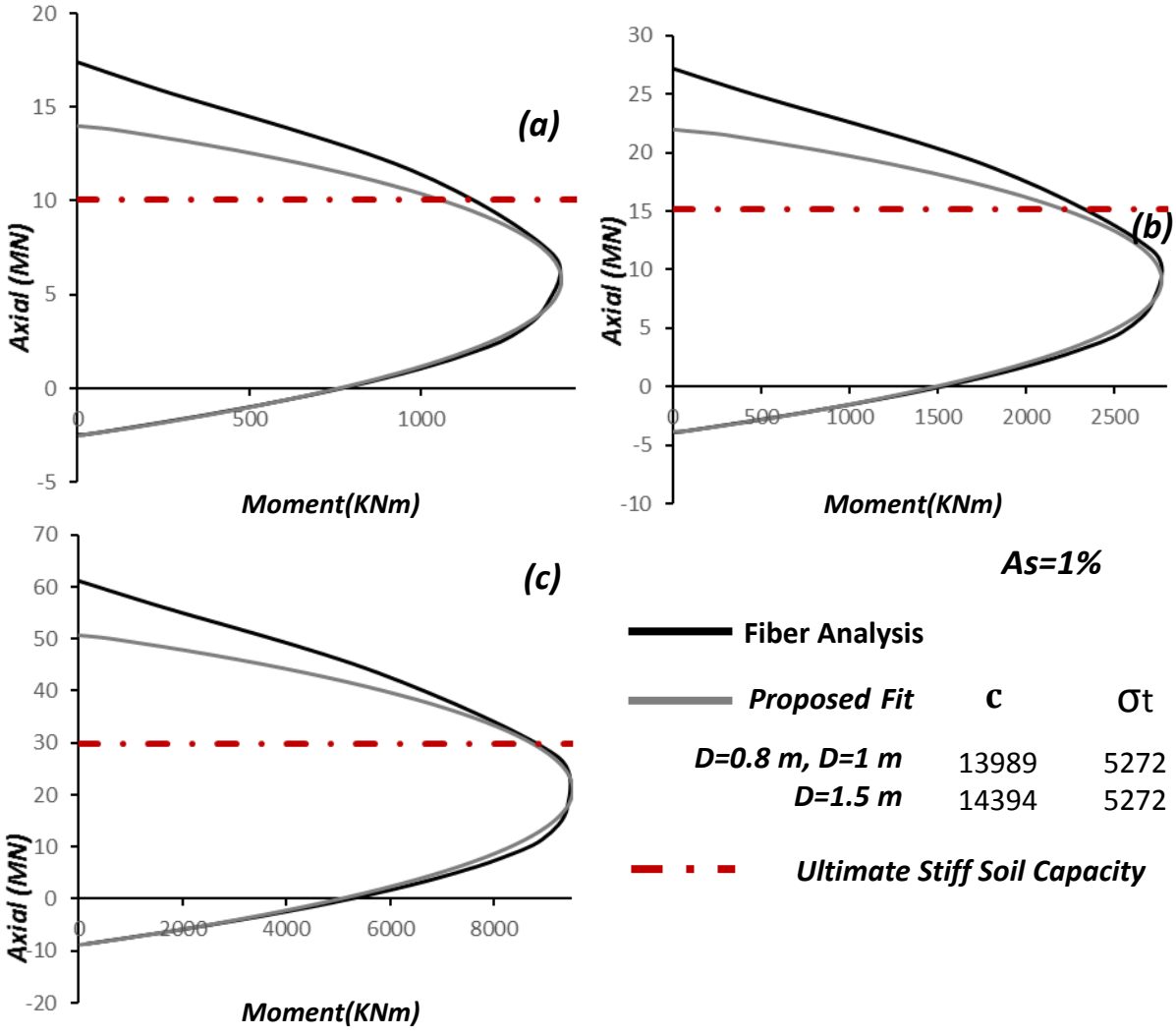

Figure 2.12 *Comparison between the data derived from proposed fit focused* from full tensile to the where all stiff soils have reached their compressive ultimate capacity. *(points), and the failure Envelope that is extracted from the fiber analysis for As=1% and a) D= 0.8 m, b) D=1 m, c) D=1.5 m.*

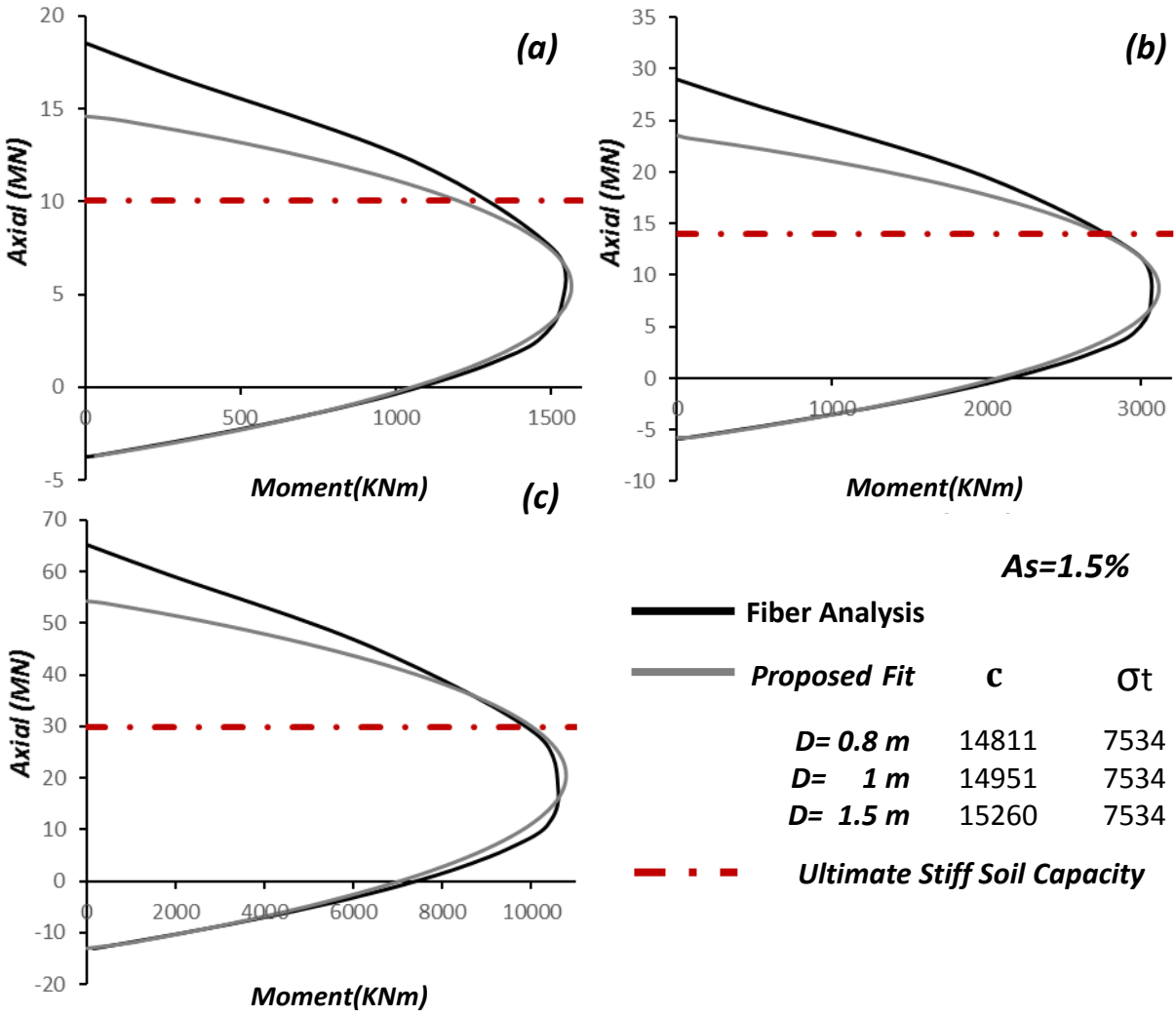

Figure 2.13 *Comparison between the data derived from proposed fit focused* from full tensile to the where all stiff soils have reached their compressive ultimate capacity. *(points), and the failure Envelope that is extracted from the fiber analysis for As=1.5% and a) D= 0.8 m, b) D=1 m, c) D=1.5 m.*

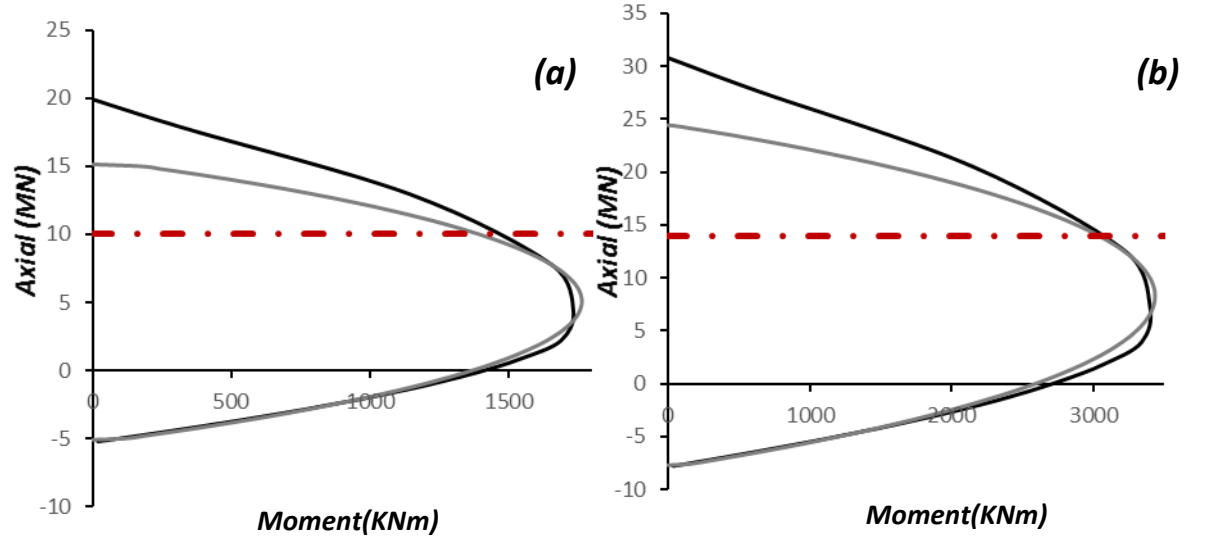

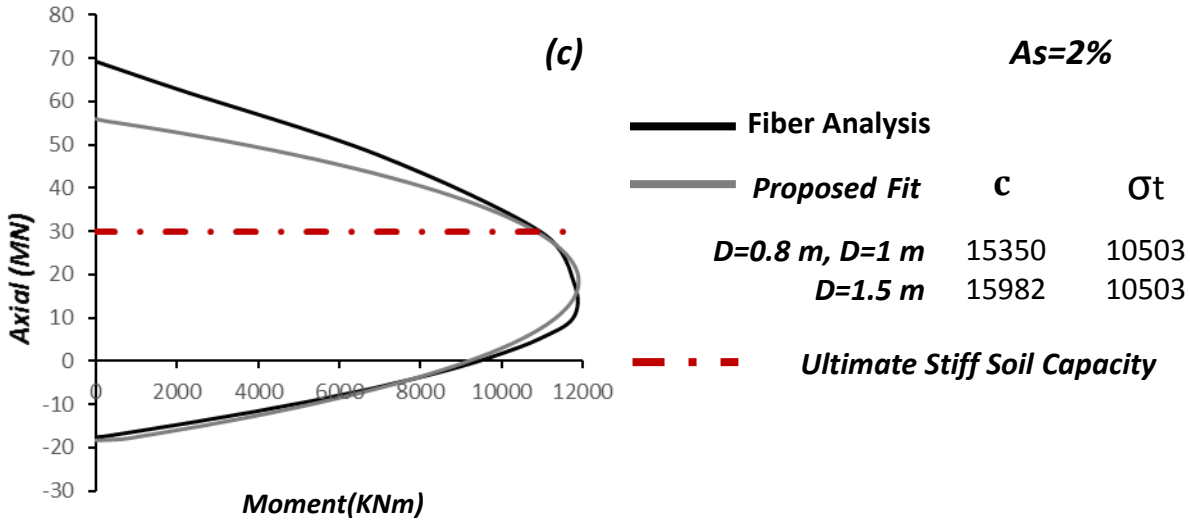

Figure 2.14 *Comparison between the data derived from proposed fit focused* from full tensile to the where all stiff soils have reached their compressive ultimate capacity. *(points), and the failure Envelope that is extracted from the fiber analysis for As=2% and a) D= 0.8 m, b) D=1 m, c) D=1.5 m.*

Chapter 3

Failure Envelopes

3 Failure Envelopes

Introduction

The term “failure envelope” defines the locus of the points that represent failure of the foundation in *M-Q-N* space. The relationship between two of the above – in other words a cross-section of the failure envelope – is conventionally termed an “interaction curve”. ***Figures 3.1 (a)*** and (***b)*** depict typical failure envelopes of surface foundations on sand [*Nova and Montrasio 1991; Gottardi and Butterfield 1995; Chatzigogos, Figini, Pecker, Salençon 2011*] and clay respectively [*Cremer, Pecker, Davenne 2001*]). As part of this thesis, we aim to produce failure envelopes in the case of pile foundations in clay under undrained conditions with constant Su with the depth. The cases of a single pile, a 1x2 and a 2x2 Pile Group are investigated, while gapping and slipping are also taken into consideration.

3.1 Flexibe Pile **in cohesive soil**

3.1.1 Limit Equilibrium Approach

The case of a free-head flexible pile embedded in clay with constant undrained shear strength Su is studied **(*Fig.3.2*).** In this case the soil resistance is

$$P_y = A S_u D\,, \qquad \textbf{(3.1)}$$

where $A = \lambda_2 + \frac{\sigma'_v}{S_u} + J\frac{z}{D}$, (Matlock 1970) **(3.2)**

for $z \le \frac{(\lambda_1 - \lambda_2)}{\frac{\gamma' s D}{Su} + J} D$

And $A = \lambda_2$ otherwise.

From static equilibrium:

$$P_y f = Q \qquad \textbf{(3.3)}$$

$$P_y f \frac{f}{2} = Qf + M - M_{pl} \qquad \textbf{(3.4)}$$

From ***(3.3):***

$$f = \frac{Q}{Py} \qquad \textbf{(3.5)}$$

and by applying ***(3.5)*** in ***(3.4)***

$$M_{pl} + Py(\frac{Q}{P_y})^2 \frac{1}{2} = Q\frac{Q}{P_y} + M \Rightarrow$$

$$\frac{M}{M_{pl}} + (\frac{Q}{\sqrt{2P_y M_{pl}}})^2 = 1 \qquad \textbf{(3.6)}$$

By setting:

$$M_y = M_{pl}$$

$$Q_y = \sqrt{2P_y M_{pl}}$$

equation ***(3.6)*** becomes:

$$\frac{M}{M_y} + (\frac{Q}{Q_y})^2 = 1 \qquad \textbf{(3.7)}$$

By taking into consideration all possible N-Q-M combinations at the pile head the failure envelope for a flexible pile embedded in clay with constant undrained shear strength:

$$f = \left|\mathrm{sgn}(Q)(\frac{Q}{Q_y})^2 + \mathrm{sgn}(M)\left|\frac{M}{M_y}\right|\right| - 1 = 0 \quad \text{for} \quad \left|\frac{M}{M_y}\right| < 1 \qquad \textbf{(3.8)}$$

$$f = \left|\frac{M}{M_y}\right| - 1 = 0 \quad \text{for} \quad \left|\frac{M}{M_y}\right| = 1 \qquad \textbf{(3.9)}$$

$$f = \left|\frac{N}{N_y}\right| - 1 = 0 \qquad \textbf{(3.10)}$$

where:

$$N_y = N_t + (\frac{N_c}{2} - \frac{N_t}{2})(sign(N) + 1) \qquad \textbf{(3.11)}$$

N_c , N_t the ultimate compressive and tensile capacity respectively.

Assuming an associated flow rule (in which the plastic potential function g coincides with the yield function f) the plastic displacement u^{pl} and the plastic rotation ϕ^{pl} give:

$$\frac{u^{pl}}{\varphi^{pl}} = \frac{2QM_y}{Q_y{}^2} = f \qquad \textbf{(3.12)}$$

confirming that the incremental plastic displacement vectors at the point of failure are normal to the yield locus.

3.1.2 Finite Element Verification

The proposed failure envelopes are checked against three-dimensional numerical analysis for flexible pile and pile-groups embedded by using the finite element code Plaxis 3D.

3.1.2.1 Static pushover tests

Considering that the foundation supports a 1-DoF oscillator, one expects that radial loading paths on the *M-Q* plane are applied in the system. Through a series of force-controlled analyses the failure envelope is ultimately determined. Prior to that, the foundation has undergone vertical loading *N* to a fraction $\chi = N/Nu$ of its ultimate capacity. [*Cremer, Pecker, Davenne 2001; Gouvernec 2004; Gajan, Kutter, Phalen, Hutchinson, Martin 2005*].

3.1.2.2 Description of the method

The steps followed in our numerical experiments represent the actual conditions in the field. The soil undergoes geostatic loading and then a part of the soil is replaced

by the foundation, on which a vertical load N is applied increasingly till a specified value of $\chi = N/Nu$ is reached. Afterwards, the vertical load is kept constant and a combination of horizontal force and moment is applied at the head of the pile till the complete failure of the system. Apparently, this implies the state in which no further lateral loading can be undertaken. The above procedure is repeated for various factors of safety against vertical loading and for various radial loading paths. Our aim is to extract the ultimate capacities under pure moment *Mu* and pure horizontal force *Qu*, and then sweep the *M-Q* plane so that a cross-section of the failure envelope is revealed. Repeating this procedure from the Ultimate Axial Compression Capacity to the ultimate Axial Tension Capacity the total 3D Failure Envelope in M-Q-N space is designed.

3.1.3 Finite Element Modelling

A 16 m long pile with 1 m diameter is embedded in the soil. The distance from the pile tip to the bottom of the model is 8 m (1/2 L). ***Figure (3.2)*** depicts the finite element discretization of the problem. Approximately 43000 elements were used for each analysis. The soil is modeled with 10-node tetrahedral elements while the pile is modeled as a soil volume calibrated with the previously macroscopic hardening Soil model approach to simulate the behavior of a circular concrete pile with As=1.5% . A sensitivity analysis for the lateral boundaries is carried out to ensure the accuracy of the model, placing them finally at the distance of 0.6L.

The selected Soil is Clay with constant with the depth Undrained Shear Strength Su=50 KPa, specific weight γ=20 KN/m^3 and Es=25000 KN/m and its behavior is described by the Mohr-Coulomb Model. The poisson's ratio is v=0.45 while the angle of friction is ϕ=0 to simulate undrained water conditions. The pile has an elasticity Modulus of Ec=30*10^6 KN/m, a poisson's ratio v=0.2 and a specific weight practically zero (γ=0.01 KN/m^2) to ensure that the derived ultimate loads are the total ones, while cohesion is chosen to be c=15262 KPa, the angle of friction ϕ=0 and tension cut-off strength equal to 7534 KPa in order to capture the correct pile behavior. An

Interface is used between the pile and the soil enabling gapping and slippage with a friction coefficient R=1.

3.1.4 Results

Figure 3.3 displays the failure envelopes of the foundation for 6 different safety factors **FSv** in respect to the maximum axial compressive (+) and tensile capacity (-). The results from the finite element analysis fit marvelously with those extracted from the finite equilibrium approach, confirming the equations proposed by Gerolimos et al and extending them by taking into consideration the influence of the vertical load. This influence can clearly be captivated in ***Fig 3.4***, where the maximum capacities magnify by the increase of the the axial load. This is rationalized through the alternation of the maximum plastic Moment of the pile, in respect to the axial load, as shown in ***Fig.3.5***. In this specific case the proportional behavior of the ultimate capacities and the vertical load is justified, as the maximum soil resistance is reached before the peak Moment Capacity of the reinforced concrete pile. Thus the ultimate pure horizontal and moment capacities (***Fig.3.6)*** behave in the same way, as it is also explained by the limit equilibrium approach. This variation is even more visible at the 3D Failure Envelope in M-Q-N space. (***Fig.3.7-10).*** In order to calibrate the analytical expressions ***3.8, 3.9*** derived by the limit Equilibrium analysis the following values are set for the ***Eq.3.2***: λ_1=10, λ_2=2, which are dimensionless quantities and the factor for the earth pressure distribution J=1.1, value that is between the ones proposed by Matlock (0.25) and Reese (2.83). The alternation of the plastic Moment is inserted by the Equation:

$$\left|M_{pl}\right| = aN^3 + bN^2 + cN + d \qquad \textbf{(3.13)}$$

a formula derived through the Matlab curve fitting tool, where a, b, c, d dimensionless constants dependent to the failure envelope of the specific circular pile.

It must be noted that the results are normalized either to the "pure" capacities (Qy/My) or to the "pure" capacities (Qy*/My*) of the foundation for safety factor $FS_v=\infty$. As shown in ***Fig.3.11*** the interaction diagram follows the same pattern regardless the vertical load, thus the determination and the analytical representation of the pile response is facilitated, especially in the case of captivating the soil-foundation response with the use of a mathematical tool (Macro-Element Modelling), as it will be formulated in the following chapters of this thesis.

Shape of the failure Envelope

As already mentioned the failure envelopes have a constant shape. In the 1st quadrant, the moment-horizontal load relation is almost linear, while in the 4th an overstrength sector is located. The partial presentation of the curves is based on the symmetry that it is displayed. (1st with 3rd, 2nd with 4th quadrant, ***Fig.3.12***)

The shape of the interaction diagram in the 1st quadrant implies that all the external loads contribute in the same way in the failure mechanism, as the effect of the horizontal load and the moment are in the same direction and thus contribute adversely to the soil-foundation system.

In the 4th quadrant the shape differentiates. As the moment is applied in the opposite direction, provides an overstrength sector to the horizontal load capacity ($Q/Qu \geq 1$). In any case the soil-foundation capacity cannot exceed the pile's plastic moment capacity. Thus, when the contribution of the moment to the system is more intense than that of the opposite vertical load, the system reaches its maximum resistance equal with Mu.

Failure Mechanisms

The failure of the pile-soil system is dependent of the influence and the allocation of the external loads, which vary the failure mechanism at each case.

When the pile is under pure Moment a plastic hinge is developed on its top ***(Fig.3.13),*** while the surrounding soil plasticizes, and gapping occurs on the top

section of the pile ***(Fig.3.14)***. The Axial load has no additional major influence rather than the variation of the moment Mpl in the failure, but the plastification of the interface, especially at the tip of the pile is notable in small safety factors.

Under combined moment and vertical load the plastification around the pile is much more significant and the plastic hinge depth increases, especially with the increase of the Horizontal load. As the horizontal displacements are larger, the detached pile area magnifies. The change of direction of the Moment does not vary the ultimate failure state, but provides the system with the previously mentioned overstrength.

Finally, when the moment overcomes the lateral force, the plastic hinge is located on the top of the pile, with almost zero horizontal displacements, a response similar to that of the pile under pure Moment.

The alteration of the plastic hinge depth is illustrated in ***Fig.3.15***. The ratio of the plastic horizontal displacement to the plastic rotation is compared with the depth of the plastic hinge for $F_{sv}=\infty$ and for $F_{sv}=1.25$. As expected there is matching, confirming the normality of the plastic displacements increment, validity of the assumed associated plastic flow rule and that the flow rule is independent from the moment M that acts on the pile and depends only on the lateral force Q.

3.2 1x2 Pile-Group in cohesive soil

3.2.1 Limit Equilibrium Approach

The case of a fixed-head 1x2 Pile-Group embedded in clay with constant undrained shear strength Su is studied.

The Pile Group reaches its ultimate capacity in two possible states: when the moment has a major contribution on the pile-group failure, i.e. when one plastic hinge at each pile is developed in combination with the axial failure of one of the two piles **(*Fig.3.16(a)*)** or when the pile-group resistance is excited by the applied vertical load i.e. two plastic hinges develop at each pile.**(*Fig.3.16(b)*)**

Static Equilibrium for 1x2 pile-group

From static equilibrium:

$$Q = Py1\, f1 + Py2\, f2 \qquad \textbf{(3.14)}$$

$$M = 2M_{pl} - \frac{Q}{2} f1 - \frac{Q}{2} f2 + Py1\, f1 \frac{f1}{2} + Py2\, f2 \frac{f2}{2} - N\frac{l}{2} + \mathrm{N}1l \qquad \textbf{(3.15)}$$

As the vertical load is equally distributed to the piles from ***(3.13):***

$$f1 = \frac{Q}{2Py1}$$
$$f2 = \frac{Q}{2Py2} \qquad \textbf{(3.16)}$$

and by applying ***(3.16)*** in ***(3.15)***

$$M = 2M_{pl} - \frac{Q^2}{8Py1} - \frac{Q^2}{8Py2} + (N_{ys} - \frac{N}{2})l \Rightarrow$$

$$\frac{M}{2M_{pl}} + \frac{Q^2}{M_{pl}}\left(\frac{1}{16P_{y1}} + \frac{1}{16P_{y2}}\right) - \frac{(N_{ys} - \frac{N}{2})l}{2M_{pl}} - 1 = 0 \qquad \textbf{(3.17)}$$

where

$N_{ys} = N_{yt}$ for $N \le 0$

$N_{ys} = N_{yc}$ otherwise

N_{yc} , N_{yt} the ultimate compressive and tensile capacity of the single pile respectively.

By setting:

$$M_y = 2M_{pl}$$
$$Q_y = \sqrt{\frac{M_{pl}}{\left(\frac{1}{16P_{y1}} + \frac{1}{16P_{y2}}\right)}}$$

equation ***(3.17)*** becomes:

$$\frac{M-\left(N_{ys}-\frac{N}{2}\right)l}{My}+\left(\frac{Q}{Q_y}\right)^2=1 \qquad \textbf{(3.18)}$$

Static Equilibrium for pure vertical load

From static equilibrium:

$$Q=Py1\,f1+Py2\,f2 \qquad \textbf{(3.19)}$$

$$N=N1+N2=2N1 \qquad \textbf{(3.20)}$$

From ***(3.16):***

$$f1=\frac{Q}{2Py1}$$
$$f2=\frac{Q}{2Py2} \qquad \textbf{(3.21)}$$

$$4Mpl-\frac{Q}{2}f1--\frac{Q}{2}f2+Py1f1\frac{f1}{2}+Py2\,f2\frac{f2}{2}-N\frac{l}{2}+\mathrm{N}1l=0 \qquad \textbf{(3.22)}$$

and by applying ***(3.20), (3.21)*** in ***(3.22)***

$$Q-\sqrt{\frac{32Mpl}{\left(\frac{1}{Py1}+\frac{1}{Py2}\right)}}=0$$

By setting:

$$Q_y*=\sqrt{\frac{32Mpl}{\left(\frac{1}{Py1}+\frac{1}{Py2}\right)}}$$
$$\frac{Q}{Q_y*}-1=0 \qquad \textbf{(3.23)}$$

By taking into consideration all possible N-Q-M combinations at the pile head the failure envelope for a flexible pile embedded in clay with constant undrained shear strength:

$$f = \left| \operatorname{sgn}(Q)\left(\frac{Q}{Qy}\right)^2 + \operatorname{sgn}(M)\left| \frac{|M| - \left|\left(Nys - \frac{N}{2}\right)\right| l}{My} \right| \right| - 1 = 0 \qquad \textbf{(3.24)}$$

for $\left| \dfrac{|M| - \left|\left(Nys - \dfrac{N}{2}\right)\right| l}{My} \right| < 1$

$$f = \left|\frac{Q}{Qy*}\right| - 1 = 0 \quad \text{for} \quad \left|\frac{Q}{Qy*}\right| = 1 \qquad \textbf{(3.25)}$$

$$f = \left| \frac{|M| - \left|\left(Nys - \frac{N}{2}\right)\right| l}{My} \right| - 1 = 0 \quad \text{for} \quad \left| \frac{|M| - \left|\left(Nys - \frac{N}{2}\right)\right| l}{My} \right| = 1 \qquad \textbf{(3.26)}$$

$$f = \left|\frac{N}{Ny}\right| - 1 = 0 \qquad \textbf{(3.27)}$$

where:

$$Ny = \left| Nt + \left(\frac{Nc}{2} - \frac{Nt}{2}\right)(sign(N) + 1) \right| \qquad \textbf{(3.28)}$$

Nc , Nt the ultimate compressive and tensile capacity of the pile-group respectively.

Static Equilibrium under axial, Horizontal Load and Moment Combination in Vertical Direction

From static equilibrium:

$$Q = 2Pyf \qquad \textbf{(3.28)}$$

$$M = 2Mpl - Qf + 2Pyf\,\frac{f}{2} \qquad \textbf{(3.29)}$$

From ***(3.28):***

$$Q = 2Pyf \qquad \textbf{(3.30)}$$

and by applying ***(3.16),*** in ***(3.15):***

$$M = 2M_{pl} - \frac{Q^2}{4Py} \Rightarrow$$

$$\frac{M}{2Mpl} - \frac{Q^2}{8MplPy} - 1 = 0 \qquad \textbf{(3.31)}$$

By setting:

$$My = 2M_{pl}$$
$$Q_y = \sqrt{8PyM_{pl}}$$

$$\frac{M}{My} - \left(\frac{Q}{Qy}\right)^2 - 1 = 0 \qquad \textbf{(3.32)}$$

By taking into consideration all possible N-Q-M combinations at the pile head the failure envelope for a flexible pile embedded in clay with constant undrained shear strength:

$$f = \left|\text{sgn}(Q)(\frac{Q}{Q_y})^2 + \text{sgn}(M)\left|\frac{M}{M_y}\right|\right| - 1 = 0 \quad \text{for} \quad \left|\frac{M}{M_y}\right| < 1 \qquad \textbf{(3.33)}$$

$$f = \left|\frac{M}{M_y}\right| - 1 = 0 \quad \text{for} \quad \left|\frac{M}{M_y}\right| = 1 \qquad \textbf{(3.34)}$$

$$f = \left|\frac{N}{N_y}\right| - 1 = 0 \qquad \textbf{(3.35)}$$

where:

$$N_y = \left|N_t + (\frac{N_c}{2} - \frac{N_t}{2})(sign(N) + 1)\right| \qquad \textbf{(3.36)}$$

N_c , N_t the ultimate compressive and tensile capacity of the Pile-group respectively.

Assuming an associated flow rule (in which the plastic potential function g coincides with the yield function f) the plastic displacement u^{pl} and the plastic rotation ϕ^{pl} give:

$$\frac{u^{pl}}{\varphi^{pl}} = \frac{4QM_y}{2Q_y^2} = f$$

confirming that the incremental plastic displacement vectors at the point of failure are normal to the yield locus.

3.2.2 Finite Element Verification

The problem studied is a 1x2 Pile-group that is subject to combined vertical load N, horizontal load Q and overturning moment. The problem is analyzed with the use of the advanced Finite Element code Plaxis 3D. ***Figure 3.17*** shows the Finite Element Model. The size of the finite element mesh is LxLx1.5L carefully weighing the effect of boundaries on the pile-group's ultimate response and the computational time. The piles have a diameter D=1 m and the distance between the pile centers is 3 meters. A 4.5x1.5 m plate is used as pile-cap, while a sensitivity analysis is performed to ensure the fixed pile/pile-cap connection, setting its elastic modulus equal to $E=300 \cdot 10^6$ KPa and its thickness of 1 meter. The piles have the aforementioned properties, i.e. an elastic modulus of $E=30 \cdot 10^6$, a specific weight γ=0.1kN/m^3, poisson's ratio v=0.2 and its behavior is governed by the Mohr-Coulomb model with c = 15262 KPa, ϕ=0 and tension cut-off strength equal to 7534 KPa. Interfaces are placed between the piles and the soil enabling gapping and slippage with a friction coefficient R=1. The soil is Clay with γ=20kN/m^3 constant with the depth Su=50 KPa and Es=25000kPa, obeying the Mohr-Coulomb model too and the Possion's ratio is v=0.45 to simulate undrained conditions. The final model consists of 43000 elements with a finer discretization around the pile-group.

The steps followed in the numerical experiments are similar to the single pile investigation. The total failure Envelopes of the soil-foundation system are extracted by applying various horizontal load – moment combinations for seven different safety factors from ultimate axial tensile to ultimate compressive capacity for direction X, where the full pile-group function is activated and Y where the system behaves as a sum of two independent piles. (***Fig.3.18)***

3.2.3 Results

X Direction

As demonstrated in ***Fig.3.19*** the proposed analytical expressions fit satisfactorily the failure envelopes extracted from the finite element modelling. There is a normalized partial presentation of the interaction diagrams, exactly as in the case of the single pile, due to the symmetry that is displayed. For their calibration the following values are set for the ***Eq.3.2***: λ_1=10, λ_2=2, which are dimensionless quantities and the factor for the earth pressure distribution J=1, value that is between the ones proposed by Matlock (0.25) and Reese (2.83). The alternation of the plastic Moment is inserted by the already mentioned Equation ***3.13***, and the interaction between the piles is taken into account by introducing the appropriate Py-Multiplayers proposed by Reese et al that reduce the ultimate soil reaction per unit length Py. In this case f_{m1}=0.93 and f_{m2}=0.73 for the leading and trailing pile respectively.

In contrary to the failure envelopes of the single pile, the ones derived for the pile-group do not have a constant pattern, but it differentiates in respect to the applied axial load.

When the pile-group is under moment and axial loading the system reaches its full resistance when 1 plastic hinge is developed at each pile – pile-cap connection and one pile reaches its ultimate compressive or tensile axial capacity, depending on which will be reached first. Thus when the pile-group is subjected to compressive or tensile axial load, the pile fails in compression or tension respectively, while when no axial load is applied, the pile reaches its tensile capacity.

Under the combined moment, axial and horizontal loading the pile-group has the exact same behavior at the failure state, with the depth of the plastic hinge magnifying with the increase of the lateral load, up to the point that a second plastic hinge is developed at the pile-pile-cap connection ***(Eq.25)*** and the failure mechanism is modified. Until then, either the horizontal load and the moment are in the same direction and thus contribute adversely to the soil-foundation system or as the moment is applied in the opposite direction, provides an overstrength sector to the

horizontal load capacity (Q/Qy ≥ 1). The pivot point is located always at the head of a pile.

At the state that two plastic hinges are developed on each pile the lateral load reaches its ultimate value Qmax while the moment has no contribution in the failure as it is surmounted by the opposite lateral load and the axial soil reaction at the tip of the piles, while the foundation is barely rotated. Thus the lateral capacity remains constant regardless the value of the opposite moment until the moment reaches its maximum value Mu, where it overcomes the converse horizontal load and the ultimate state consists of the occurrence of the axial failure of one pile in combination with a plastic hinge at each pile-pile-cap connection.

Fig.3.20 and **Fig.3.21** present an overview of the different failure mechanisms for different factors of safety, displaying the plastic hinge development and the axial strain of the piles, clarifying that regardless the change of the interaction diagram shape, the behavior of the pile-group remains similar.

Finally, the effect of the axial load to the plastic moment of the piles can clearly be identified in the increase of Qmax with the growth of the vertical force ***(Fig.3.22(a)).*** On the contrary the maximum moment is located for safety factor Fsv=∞, as the influence of the axial load has an adverse impact on it ***(Fig3.22(b)).*** A more comprehensive view can be captured from the 3-D failure surface of the foundation. ***(Fig.3.23-26)***

Y Direction

The Interaction Diagrams for the 1x2 Pile-Group loaded in combined moment, axial and vertical load in Y-Direction are presented in ***Fig 3.23***. The matching between the derived expressions from the finite equilibrium approach and the numerical experiments is satisfactory. For their calibration the following values are set for the ***Eq.3.2***: λ_1=10, λ_2=2, which are dimensionless quantities and the factor for the earth pressure distribution J=1.1, value that is between the ones proposed by Matlock (0.25) and Reese (2.83) and equal to the value for the single pile. The alternation of the plastic Moment is inserted by the Equation ***3.13***, and the interaction between the

piles is taken into account by introducing the appropriate Py-Multiplayers proposed by Reese et al that reduce the ultimate soil reaction per unit length Py. In this case f_{m1}= f_{m2}=0.93, as both piles behave as leading piles.

The shape of failure envelopes is equal with that of the single pile, while the pattern remains constant regardless the axial load ***(Fig.3.24).*** The value Mu is equal with 2 times the ultimate moment capacity of the single pile, while the pure lateral resistance is remotely lower than 2 times due to the interaction between the two piles ***(Fig.3.25).***

The failure mechanisms of the pile-group are similar to those of the single pile. When the pile-group is under pure Moment a plastic hinge is developed on its top ***(Fig.3.26),*** while the surrounding soil plasticizes notably around the foundation, and gapping occurs on the top section of the piles ***(Fig.3.27).*** The Axial load has no additional major influence rather than the variation of the moment Mpl in the failure, but the plastification of the interface, especially at the tip of the pile is notable in small safety factors.

Under combined moment and vertical load the plastification around the pile is much more significant and the plastic hinge depth magnifies, in respect to the increase of the Horizontal load. As the horizontal displacements are larger, the detached pile area magnifies. The change of direction of the Moment does not vary the ultimate failure state, but provides the lateral resistance with overstrength.

Finally, when the moment surmounts the lateral force the plastic hinge is located on the top of the piles, as in the case of the pile-group under pure Moment.

Comparison

The overstrength of the pile-group when its full group function is activated is displayed in ***Fig.3.31.*** The difference in the Moment capacity is based on the ability of the foundation to enhance the moment not only through the plastic resistance of the pile material but also by the absorbance of the load as axial force too. This behavior is independent of the axial load applied. Moreover the maximum lateral

resistance is provided for a wider range of moment-horizontal loads combinations, while the slightly lower maximum value is related to the different failure mechanism of the pile-group under that load combination and the higher interaction level of the piles.

3.3 2x2 Pile-Group in **cohesive soil**

3.3.1 Limit Equilibrium Approach

X Direction

The Pile Group reaches its ultimate capacity in two possible states: when the moment has a major contribution on the pile-group failure, i.e. when one plastic hinge at each pile is developed in combination with the axial failure of two of the four piles **(*Fig.3.32(a)*)** or when the pile-group resistance is excited by the applied vertical load i.e. two plastic hinges develop at each pile.**(*Fig.3.32(b)*)**

Static Equilibrium for 2x2 pile-group

From static equilibrium:

$$Q = P_{y1} f_1 + P_{y2} f_2 + P_{y3} f_3 + P_{y4} f_4 = 2P_{y1} f_1 + 2P_{y3} f_3 \qquad \textit{(3.37)}$$

$$M = 4M_{pl} \frac{Q}{2} f_1 - \frac{Q}{2} f_3 + 2P_{y1} f_1 \frac{f_1}{2} + +2P_{y3} f_3 \frac{f_3}{2} - N\frac{l}{2} + \mathrm{N}_1 l + \mathrm{N}_2 l \qquad \textit{(3.38)}$$

As the vertical load is equally distributed to the piles from ***(3.37):***

$$f_1 = \frac{Q}{4P_{y1}}$$
$$f_3 = \frac{Q}{4P_{y3}} \qquad \textit{(3.39)}$$

and by applying ***(3.39)*** in ***(3.38)***

$$M = 4M_{pl} - \frac{Q^2}{16P_{y1}} - \frac{Q^2}{16P_{y3}} + 2(N_{ys} - \frac{N}{4}))l \Rightarrow$$

$$\frac{M}{4M_{pl}}+\frac{Q^2}{M_{pl}}\left(\frac{1}{64p_{y1}}+\frac{1}{64p_{y2}}\right)-\frac{2(N_{ys}-\frac{N}{4})l}{4M_{pl}}-1=0 \qquad \textbf{(3.40)}$$

$N_{ys}=N_{yt}$ for $N\le 0$

$N_{ys}=N_{yc}$ otherwise

N_{yc} , N_{yt} the ultimate compressive and tensile capacity of the single pile respectively.

By setting:

$$M_y=4M_{pl}$$

$$Q_y=\sqrt{\frac{M_{pl}}{\left(\frac{1}{64p_{y1}}+\frac{1}{64p_{y2}}\right)}}$$

equation ***(3.17)*** becomes:

$$\frac{M-2\left(N_{ys}-\frac{N}{4}\right)l}{M_y}+\left(\frac{Q}{Q_y}\right)^2=1 \qquad \textbf{(3.41)}$$

Static Equilibrium for 2x2 pile-group under pure vertical load

From static equilibrium:

$$Q=P_{y1}f_1+P_{y2}f_2+P_{y3}f_3+P_{y4}f_4=2P_{y1}f_1+2P_{y3}f_3 \qquad \textbf{(3.42)}$$

$$N=N_1+N_2+N_3+N_4=4N_1 \qquad \textbf{(3.43)}$$

From ***(3.42):***

$$f_1=\frac{Q}{4P_{y1}}$$
$$f_3=\frac{Q}{4P_{y3}} \qquad \textbf{(3.44)}$$

$$8M_{pl}-\frac{Q}{2}f_1-\frac{Q}{2}f_3+2P_{y1}f_1\frac{f_1}{2}++2P_{y3}f_3\frac{f_3}{2}+N\frac{l}{2}-2N_1l=0 \qquad \textbf{(3.45)}$$

and by applying ***(3.44), (3.43)*** in ***(3.45):***

$$Q-\sqrt{\frac{128Mpl}{\left(\frac{1}{py1}+\frac{1}{py2}\right)}}=0$$

By setting:

$$Qy^{*}=\sqrt{\frac{128Mpl}{\left(\frac{1}{py1}+\frac{1}{py2}\right)}}$$

$$\frac{Q}{Qy^{*}}-1=0 \qquad \textbf{(3.46)}$$

By taking into consideration all possible N-Q-M combinations at the pile head the failure envelope for a flexible pile embedded in clay with constant undrained shear strength:

$$f=\left|\operatorname{sgn}(Q)\left(\frac{Q}{Qy}\right)^{2}+\operatorname{sgn}(M)\left\|\frac{|M|-2\left|\left(Nys-\frac{N}{4}\right)\right|l}{My}\right\|-1=0\right.$$

$$\text{for}\quad \left|\frac{|M|-2\left|\left(Nys-\frac{N}{4}\right)\right|l}{My}\right|<1 \qquad \textbf{(3.47)}$$

$$f=\left|\frac{Q}{Qy^{*}}\right|-1=0 \qquad \text{for}\quad \left|\frac{Q}{Qy^{*}}\right|=1 \qquad \textbf{(3.48)}$$

$$f=\left|\frac{|M|-2\left|\left(Nys-\frac{N}{4}\right)\right|l}{My}\right|-1=0 \qquad \text{for}\quad \left|\frac{|M|-2\left|\left(Nys-\frac{N}{4}\right)\right|l}{My}\right|=1 \qquad \textbf{(3.49)}$$

$$f = \left|\frac{N}{N_y}\right| - 1 = 0 \qquad \textbf{(3.50)}$$

where:

$$N_y = \left| N_t + (\frac{N_c}{2} - \frac{N_t}{2})(sign(N) + 1) \right| \qquad \textbf{(3.51)}$$

N_c , N_t the ultimate compressive and tensile capacity of the Pile-group respectively.

Static Equilibrium for 2x2 pile-group under combined load in diagonal direction

The Pile Group reaches its ultimate capacity in three possible states: when the pivot point is in the center of the pile-cap and the moment has a major contribution on the pile-group failure, i.e. when one plastic hinge at each pile is developed in combination with the axial failure of the outer piles **(*Fig.3.32(a)*)**, when the pivot point is at the head of an outer pile and the moment has a major contribution on the pile-group failure, i.e. when one plastic hinge at each pile is developed in combination with the axial failure of the other three piles or when**(*Fig.3.32(b)*)** the pile-group resistance is excited by the applied vertical load i.e. two plastic hinges develop at each pile**(*Fig.3.32(c)*) .**

Failure type *(a)*

From static equilibrium:

$$Q = P_{y1} f_1 + P_{y2} f_2 + P_{y3} f_3 + P_{y4} f_4 = P_{y1} f_1 + 2P_{y2} f_2 + P_{y4} f_4 \qquad \textbf{(3.52)}$$

$$M = 4M_{pl} - \frac{Q}{4} f_1 - \frac{Q}{2} f_2 - - \frac{Q}{4} f_4 + P_{y1} f_1 \frac{f_1}{2} + 2P_{y2} f_2 \frac{f_2}{2} + P_{y4} f_4 \frac{f_4}{2} - \frac{N}{2}\frac{S}{2} + \frac{N}{2}\frac{S}{2} + N_1 S + N_4 S \qquad \textbf{(3.53)}$$

From ***(3.52):***

$$f1=\frac{Q}{4Py1}$$
$$f2=\frac{Q}{4Py2} \qquad \textbf{(3.54)}$$
$$f4=\frac{Q}{4Py4}$$

and by applying ***(3.54)*** in ***(3.53):***

$$M=4M_{pl}-\frac{Q^2}{32Py1}-\frac{Q^2}{16Py2}-\frac{Q^2}{32Py4}+N_{ys1}\frac{S}{2}+N_{ys4}\frac{S}{2}\Rightarrow$$
$$\frac{M-(Nys1+Nys4)\frac{S}{2}}{4M_{pl}}+\frac{Q^2}{Mpl\left(\frac{1}{128p_{y1}}+\frac{1}{64p_{y2}}+\frac{1}{128p_{y4}}\right)}-1=0 \qquad \textbf{(3.55)}$$

$$N_{ys}=N_{yt} \qquad \text{for } N\le 0$$

$$N_{ys}=N_{yc} \qquad \text{otherwise}$$

N_{yc} , N_{yt} the ultimate compressive and tensile capacity of the single pile respectively.

By setting:

$$M_y=4M_{pl}$$
$$Q_y=\sqrt{\frac{M_{pl}}{\left(\frac{1}{128p_{y1}}+\frac{1}{64p_{y2}}+\frac{1}{128p_{y4}}\right)}}$$

equation ***(3.55)*** becomes:

$$\frac{M-(Nys1+Nys4)\frac{S}{2}}{M_y}+\left(\frac{Q}{Q_y}\right)^2=1 \qquad \textbf{(3.56)}$$

Failure type *(b)*

From static equilibrium:

$$Q = P_{y1} f_1 + P_{y2} f_2 + P_{y3} f_3 + P_{y4} f_4 = P_{y1} f_1 + 2P_{y2} f_2 + P_{y4} f_4 \quad \textbf{(3.57)}$$

$$M = 4M_{pl} - \frac{Q}{4} f_1 - \frac{Q}{2} f_2 - - \frac{Q}{4} f_4 + P_{y1} f_1 \frac{f_1}{2} + 2P_{y2} f_2 \frac{f_2}{2} + P_{y4} f_4 \frac{f_4}{2} - N\frac{S}{2} + N_1 S + N_2 \frac{S}{2} + N_3 \frac{S}{2} \quad \textbf{(3.58)}$$

From ***(3.57):***

$$f_1 = \frac{Q}{4P_{y1}}$$

$$f_2 = \frac{Q}{4P_{y2}} \quad \textbf{(3.59)}$$

$$f_4 = \frac{Q}{4P_{y4}}$$

and by applying ***(3.59)*** in ***(3.58):***

$$M = 4M_{pl} - \frac{Q^2}{32P_{y1}} - \frac{Q^2}{16P_{y2}} - \frac{Q^2}{32P_{y4}} + N_{ys1} S + N_{ys2} \frac{S}{2} + N_{ys3} \frac{S}{2} - N\frac{S}{2} \Rightarrow$$

$$\frac{M - (\frac{N}{2} - N_{ys1} - N_{ys2})S}{4M_{pl}} + \frac{Q^2}{M_{pl}\left(\frac{1}{128 p_{y1}} + \frac{1}{64 p_{y2}} + \frac{1}{128 p_{y4}}\right)} - 1 = 0 \quad \textbf{(3.60)}$$

$N_{ys} = N_{yt}$ for $N \le 0$

$N_{ys} = N_{yc}$ otherwise

N_{yc} , N_{yt} the ultimate compressive and tensile capacity of the single pile respectively.

By setting:

$$M_y = 4M_{pl}$$

$$Q_y = \sqrt{\frac{M_{pl}}{\left(\frac{1}{128 p_{y1}} + \frac{1}{64 p_{y2}} + \frac{1}{128 p_{y4}}\right)}}$$

equation ***(3.60)*** becomes:

$$\frac{M-(\frac{N}{2}-\mathrm{Nys1}-Nys2)S}{My}+\left(\frac{Q}{Qy}\right)^2=1 \qquad \textbf{(3.61)}$$

Failure type *(c)*

From static equilibrium:

$$Q=Py1\,f1+Py2\,f2+Py3\,f3+Py4\,f4=Py1\,f1+2Py2\,f2+Py4\,f4 \qquad \textbf{(3.62)}$$

$$N=N1+N2+N3+N4=4N1 \qquad \textbf{(3.63)}$$

From ***(3.62):***

$$f1=\frac{Q}{4Py1}$$
$$f2=\frac{Q}{4Py2} \qquad \textbf{(3.64)}$$
$$f4=\frac{Q}{4Py4}$$

$$8Mpl-\frac{Q}{4}f1-\frac{Q}{2}f2--\frac{Q}{4}f4+Py1f1\frac{f1}{2}+2Py2f2\frac{f2}{2}+Py4f4\frac{f4}{2}+N\frac{l}{2}-2\mathrm{N1}l=0 \qquad \textbf{(3.65)}$$

and by applying ***(3.63), (3.64)*** in ***(3.65)***

$$Q-\sqrt{\frac{2Mpl}{\left(\frac{1}{128py1}+\frac{1}{64py2}+\frac{1}{128py4}\right)}}=0$$

By setting:

$$Qy^*=\sqrt{\frac{2Mpl}{\left(\frac{1}{128py1}+\frac{1}{64py2}+\frac{1}{128py4}\right)}}$$
$$\frac{Q}{Qy^*}-1=0 \qquad \textbf{(3.66)}$$

By taking into consideration all possible N-Q-M combinations at the pile head the failure envelope for a flexible pile embedded in clay with constant undrained shear strength:

When the pivot point is at the center:

$$f = \left| \operatorname{sgn}(Q)\left(\frac{Q}{Q_y}\right)^2 + \operatorname{sgn}(M)\left\| \frac{|M| - (|Nys1| + |Nys4|)\frac{S}{2}}{M_y} \right\| - 1 = 0 \right. \qquad \textbf{(3.67)}$$

for $\left| \frac{|M| - (|Nys1| + |Nys4|)\frac{S}{2}}{M_y} \right| < 1$

$$f = \left| \frac{|M| - (|Nys1| + |Nys4|)\frac{S}{2}}{M_y} \right| - 1 = 0 \qquad \text{for} \qquad \left| \frac{|M| - (|Nys1| + |Nys4|)\frac{S}{2}}{M_y} \right| = 1$$

(3.68)

When the pivot point is at the outer pile:

$$f = \left| \operatorname{sgn}(Q)\left(\frac{Q}{Q_y}\right)^2 + \operatorname{sgn}(M)\left\| \frac{\left(\left|\frac{N}{2}\right| - |\mathrm{Nys1}| - |Nys2|\right)S}{M_y} \right\| - 1 = 0 \right. \qquad \textbf{(3.69)}$$

for $\left| \frac{\left(\left|\frac{N}{2}\right| - |\mathrm{Nys1}| - |Nys2|\right)S}{M_y} \right| < 1$

$$f = \left| \frac{(\left|\frac{N}{2}\right| - |\mathrm{Nys1}| - |Nys2|)S}{My} \right| - 1 = 0 \quad \text{for} \quad \left| \frac{(\left|\frac{N}{2}\right| - |\mathrm{Nys1}| - |Nys2|)S}{My} \right| = 1$$

(3.70)

$$f = \left| \frac{Q}{Qy*} \right| - 1 = 0 \qquad \textbf{(3.71)}$$

$$f = \left| \frac{N}{Ny} \right| - 1 = 0 \qquad \textbf{(3.72)}$$

where:

$$Ny = \left| Nt + (\frac{Nc}{2} - \frac{Nt}{2})(sign(N) + 1) \right| \qquad \textbf{(3.73)}$$

Nc , Nt the ultimate compressive and tensile capacity of the pile-group respectively.

3.3.2 Finite Element Verification

The problem studied is a 2x2 Pile-group subjected to combined vertical load N, horizontal load Q and overturning moment. The problem is analyzed as previously with the use of the advanced Finite Element code Plaxis 3D. ***Figure 3.33*** shows the Finite Element Model. The size of the finite element mesh is LxLx1.5L taking into consideration the effect of boundaries on the pile-group's ultimate response and the computational time. The piles have a diameter D=1 m and the distance between all the pile centers is 3 meters. A 5x5 m plate is chosen as pile-cap, while a sensitivity analysis is performed to ensure the fixed pile/pile-cap connection, setting its elastic modulus equal to $E=300 \cdot 10^6$ KPa and its thickness of 1 meter. The piles have the aforementioned properties, i.e. an elastic modulus of $E=30 \cdot 10^6$, a specific weight $\gamma=0.1 kN/m^3$, poisson's ratio v=0.2 and its behavior is governed by the Mohr-Coulomb model with c = 15262 KPa, ϕ=0 and tension cut-off strength equal with 7534 KPa. Interfaces are placed between the piles and the soil enabling gapping and slippage with a friction coefficient R=1. The soil is Clay with $\gamma=20 kN/m^3$ constant with the depth Su=50 KPa and Es=25000 KPa, obeying the Mohr-Coulomb model too and the

Possion's ratio is v=0.45 to simulate undrained conditions. The final model consists of 63000 elements with a finer discretization around the pile-group.

The steps followed in the numerical experiments are similar to the previous investigation. The total failure Envelopes of the soil-foundation system are extracted by applying various horizontal load – moment combinations in the normal ($\theta=0^o$) and diagonal direction ($\theta=45^o$) for seven different safety factors from ultimate axial tensile to ultimate compressive capacity. (***Fig.3.34)***

3.3.3 Results

X Direction

As displayed in ***Fig.3.35*** the proposed fit and the results from the numerical experiments match excellently. . For the calibration of the analytical expressions the following values are set for the ***Eq.3.2***: $\lambda_1=10$, $\lambda_2=2$, which are dimensionless quantities and the factor for the earth pressure distribution J=1.1, value that is between the ones proposed by Matlock (0.25) and Reese (2.83). The alternation of the plastic Moment is inserted by the already mentioned Equation ***3.13***, and the interaction between the piles is taken into account by introducing the appropriate Py-Multiplayers proposed by Reese et al that reduce the ultimate soil reaction per unit length Py. In this case $f_{m1}=0.866$ and $f_{m2}=0.62$ for the two leading piles and the two trailing piles respectively.

As the 2x2 pile-group is practically composed by two 1x2 pile-groups and its behavior is similar to the 1x2 pile-group in the x direction the shape of the failure envelopes is the same. This can clearly be depicted in the 3-dimensional failure surface of the 2x2 pile-group ***(Fig.3.36-39)***, which is identical in terms of normalized values. Thus there is no constant shape of the interaction diagram, but it changes in respect to the axial load. Moreover in terms of pure capacities, the lateral resistance magnifies by the increase of the axial load, due to the increase of the plastic moment resistance, while the axial load has a negative effect in the moment capacity ***(Fig.40)***.

The failure mechanisms have the same resemblance and are divided in three parts ***(Fig.3.41-42).*** One part where one plastic hinge is developed at each pile and either the leading or the trailing piles reach their ultimate capacities ***(a)***. The place of the plastic hinge from the top of the piles for pure moment load is shifted deeper under the increase of the horizontal load. In this case the pivot point is always located at the head of a pile. The other part is when the lateral load overcomes the contribution of the moment at the system and two plastic hinges are developed at each pile, while the foundation's rotation is practically zero ***(b)***. Finally, when the moment surmounts the opposite vertical load, the system reaches the failure state under the same mechanism of the first part, with the plastic hinge being located at the pile-pile-cap connection ***(c)***.

Diagonal direction

The results from the finite element model and the proposed analytical fit are presented in ***Fig.3.43***. For the soil reaction the following values are inserted in the analytical equations: λ_1=10, λ_2=2, which are dimensionless quantities and the factor for the earth pressure distribution J=1.1. In addition, in order to include the interaction between the piles in the system behavior the Py-Multiplayers proposed by Reese are: f_{m1}=0.866 for the trailing pile, f_{m2}=0.77 for the two middle piles and f_{m3}=0.57 for the trailing pile.

As it is displayed, the shape of the failure envelopes are similar with those of the 1x2 and the 2x2 pile-group although the failure mechanism is differs. That is a very interesting conclusion in the research of the generalized pile-group failure expressions. For big safety factors, i.e. for small axial loads, under combined moment and lateral load, the pivot point is located in the center of the pile-group ***(Fig .3.44(a))***. Thus the system reaches its ultimate capacity when one plastic hinge is developed at each pile and one of the outer piles reaches its ultimate compressive or tensile axial capacity, depending on which will be reached first. Thus when the pile-group is subjected to compressive or tensile axial load, the pile fails in compression or tension respectively, while when no axial load is applied, the pile reaches its

tensile capacity. When the axial load has a major contribution in the system's behavior the pivot point is relocated at one of the outer piles ***(Fig .3.44(b))***. The system reaches its ultimate capacity, when one plastic hinge is developed at each pile and the two central piles and the one outer pile fail axially. In both cases when the lateral load increases and the moment nullifies or is applied in the opposite direction the system reaches its maximum horizontal capacity by developing 2 plastic hinges at each pile. Finally the system cannot exceed its maximum moment capacity Mu, even when the horizontal load is applied in the opposite direction.

Comparison

In ***Fig.3.48*** the maximum capacities of the pile-group under loads in X- and diagonal direction are compared. In every case the ultimate lateral reaction is practically the same. The difference in the response under the different loads is visible through the moment capacities. For big safety factors the pile-group loaded in x direction has greater resistance, but as the axial failure is closer the pile-group under diagonal loading has greater capacity loading. This is also explained and from the analytical expressions, as in x-direction the pile-group displays its maximum moment resistance when no axial load is applied, while in the diagonal direction the longer distance of the piles from the pivot point leads to longer moment arm i.e. increased moment resistance.

Figures

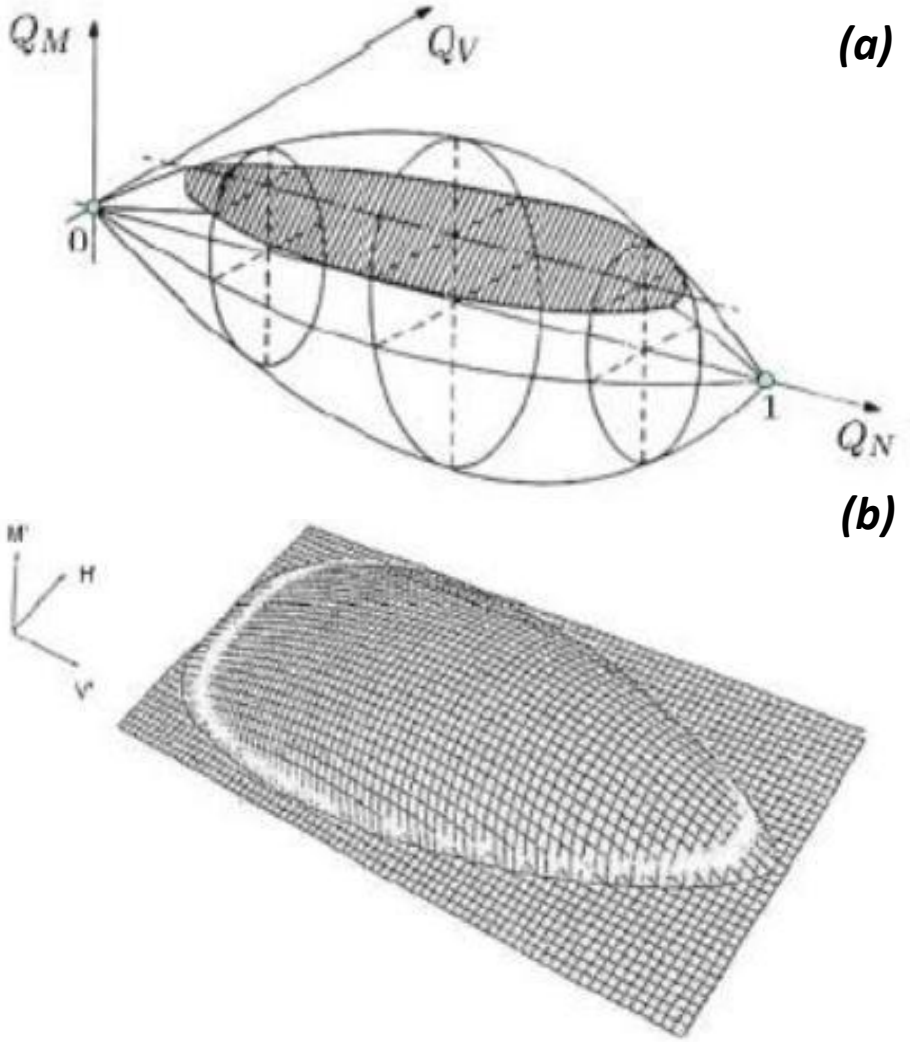

Figure 3.1 *a) Rugby-balls shaped yield surface for surface foundations in cohesionless soil and b) yield surface for surface foundations on cohesive soil.*

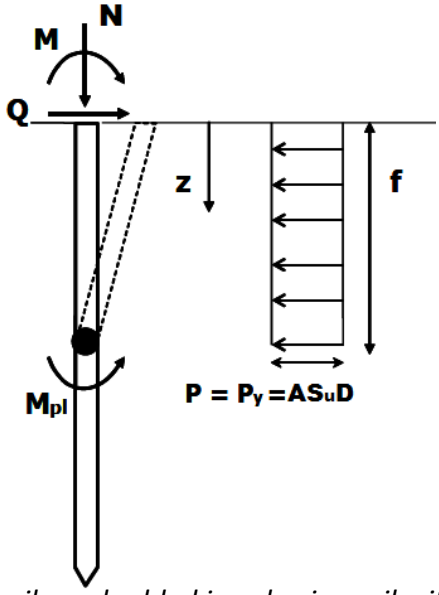

Figure 3.2 *flexible pile embedded in cohesive soil with constant Su distribution with depth*

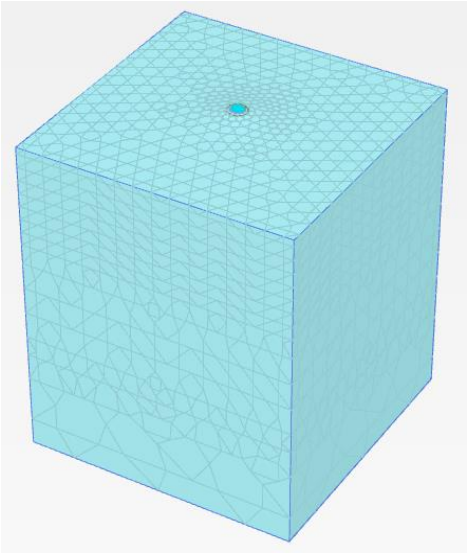

Figure 3.2 *Finite Element Model for flexible pile in clay*

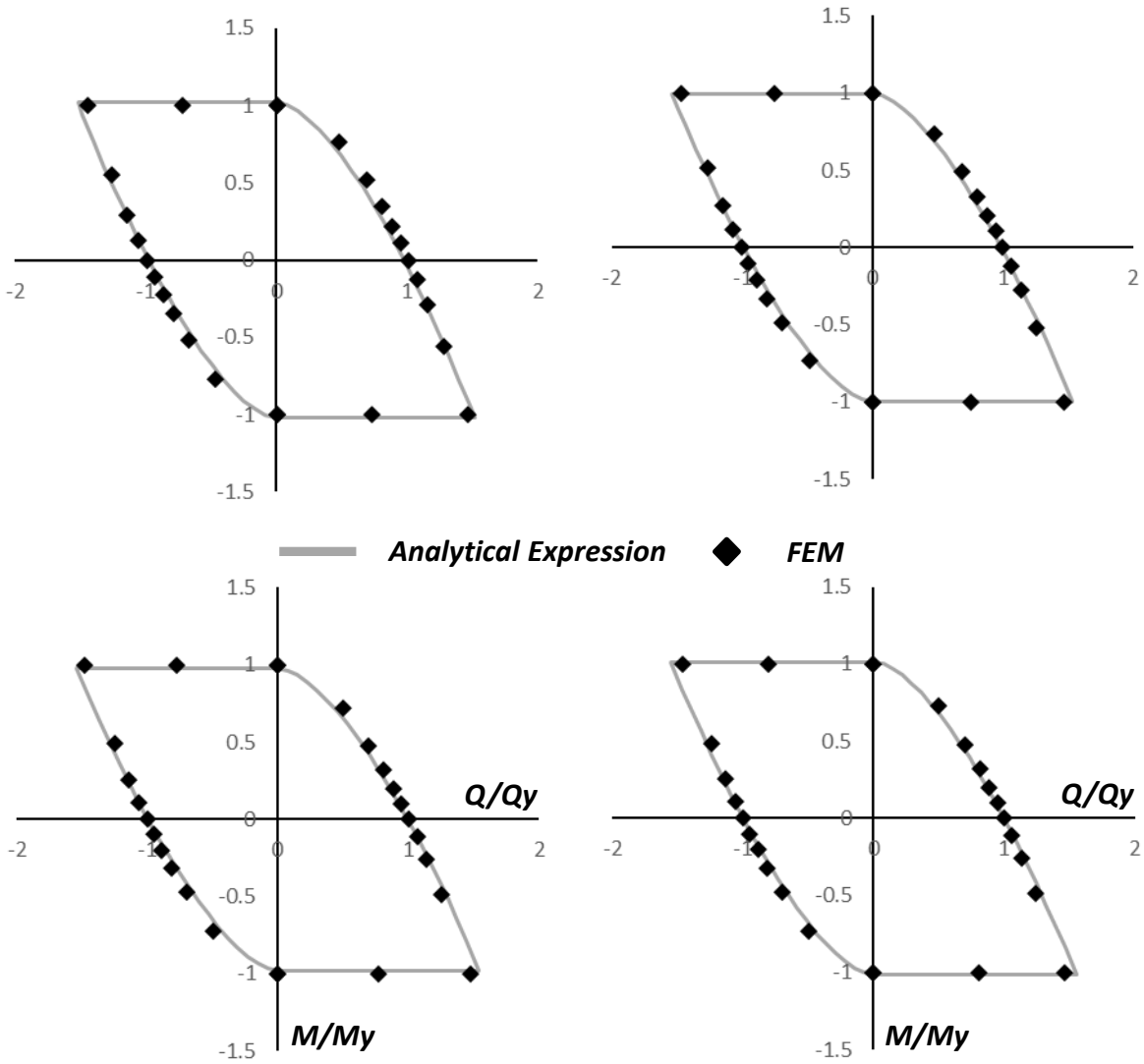

Figure 3.3(a) *Comparison between the data derived from the numerical experiments (points) and the analytical expression proposed for the yield surfaces of flexible piles for 6 different factors, given in normalized values.*

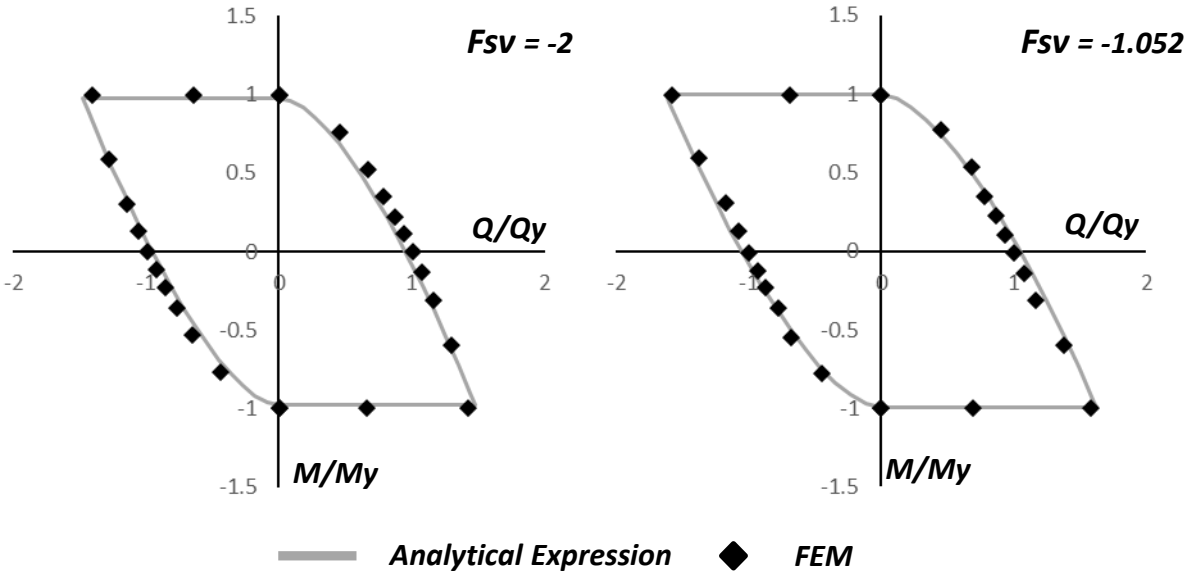

Figure 3.3(b) *Comparison between the data derived from the numerical experiments (points) and the analytical expression proposed for the yield surfaces of flexible piles for 6 different factors, given in normalized values. The foundation may experience gapping and slippage according to a Coulomb friction law with a coefficient of R = 1.*

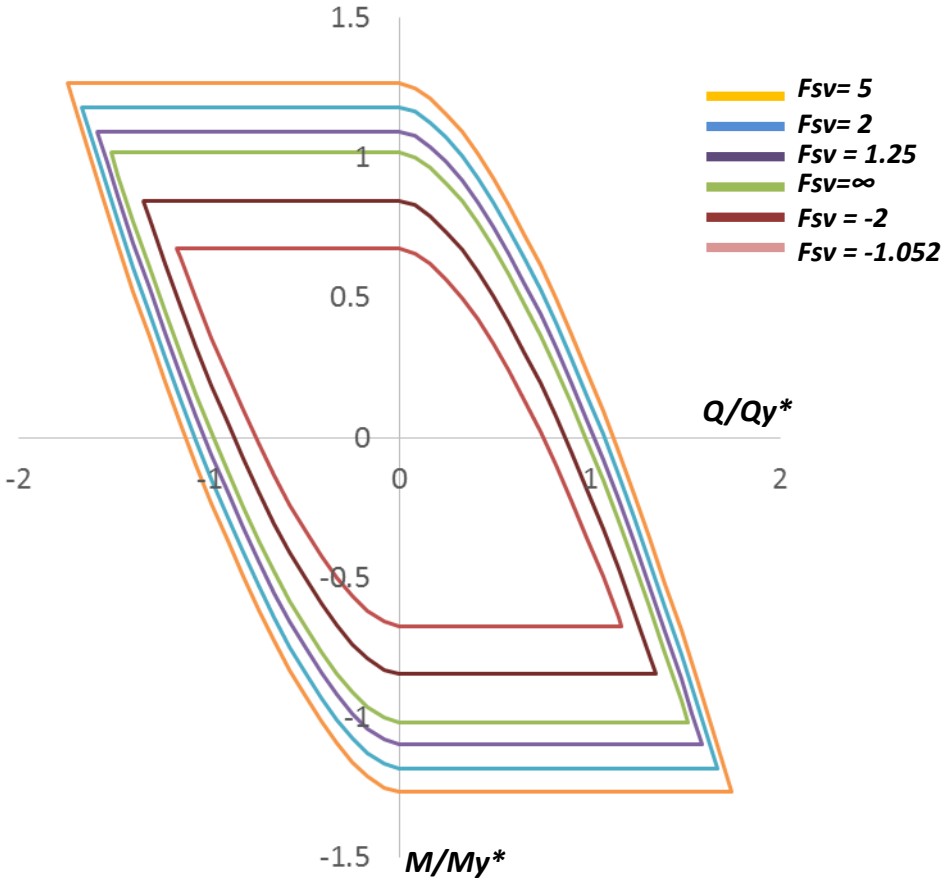

Figure 3.4 *Illustration of the effect of the factor of safety against vertical bearing capacity failure to the magnitude of the normalized interaction curves*

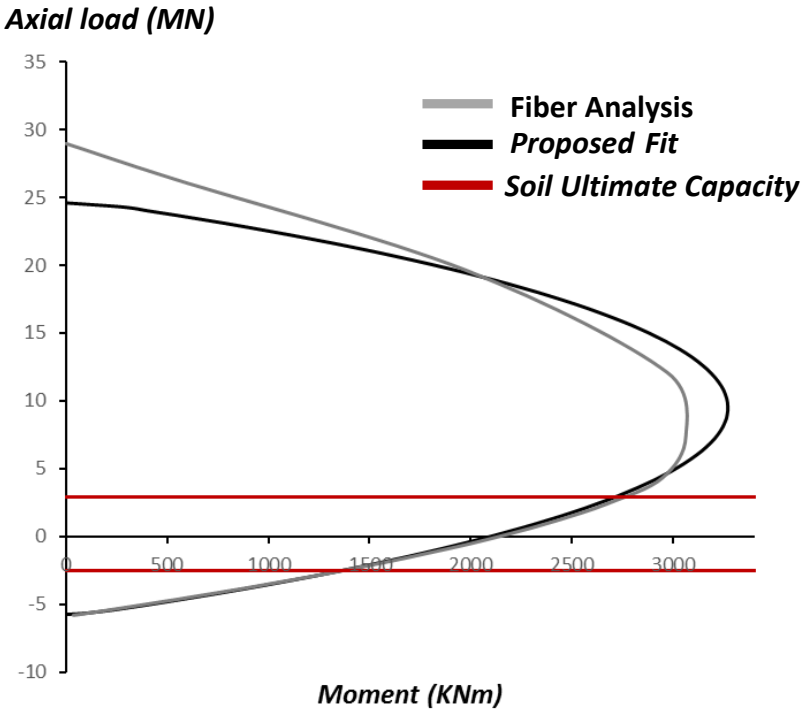

Figure 3.5 *Illustration of the alteration of the pile's plastic moment in respect to the axial load*

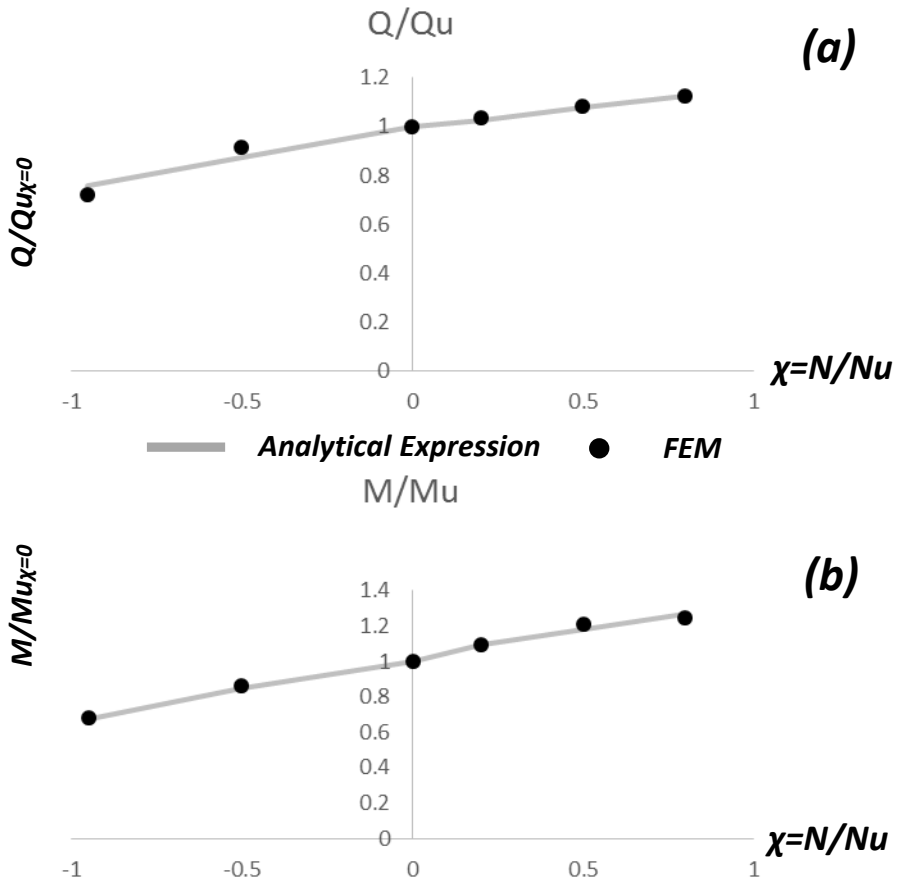

Figure 3.6 *The dimensionless* ***(α)*** *pure horizontal capacities* ***(b)*** *moment capacities derived from the FE analyses (data points) are compared to the proposed analytical expression (lines).*

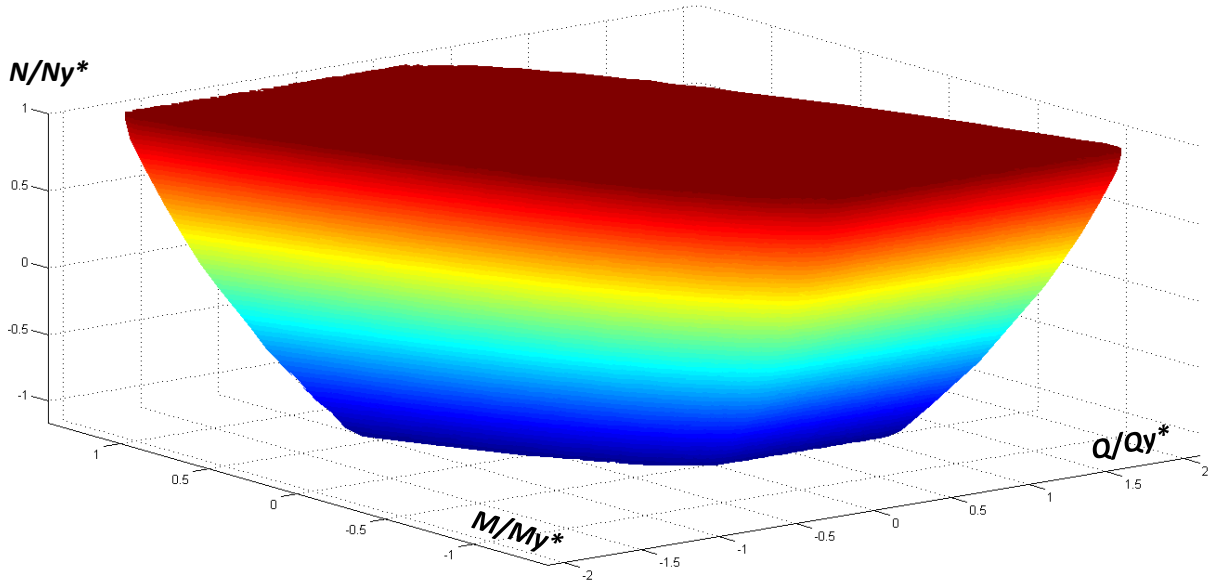

Figure 3.7 *Failure Surface (in 3-Dimensional M-Q-N space) of flexible Pile in cohesive soil*

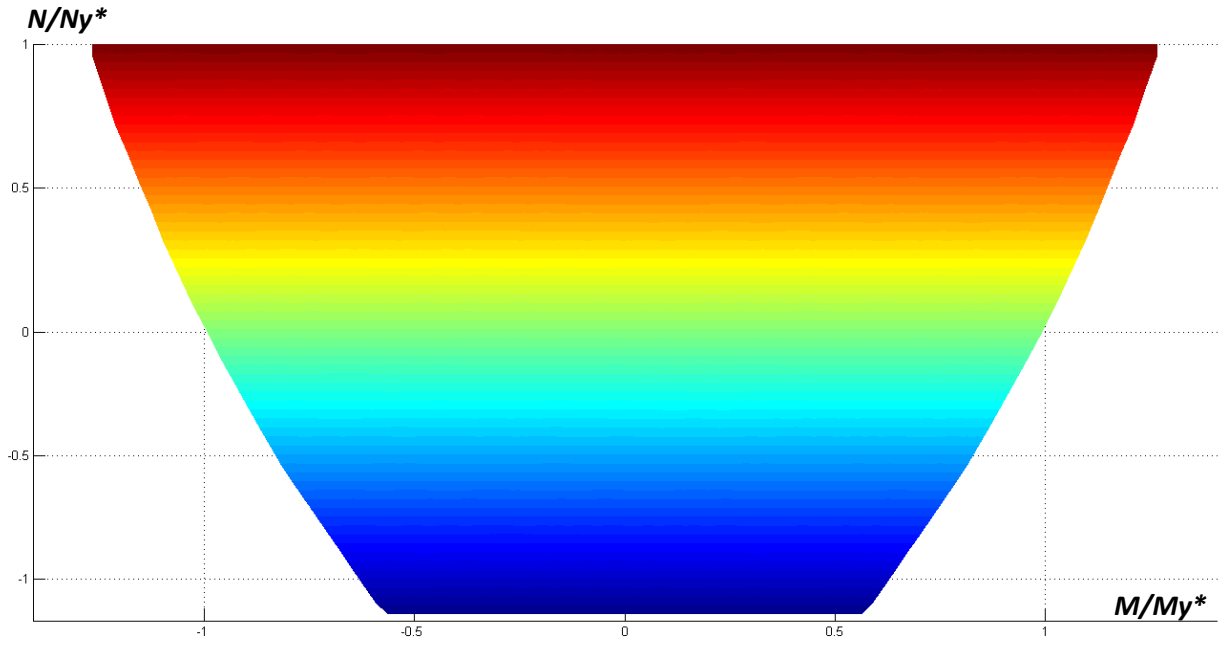

Figure 3.8 *Perspective of M-N Failure Surface (in 3-Dimensional M-Q-N space) of flexible Pile in cohesive soil*

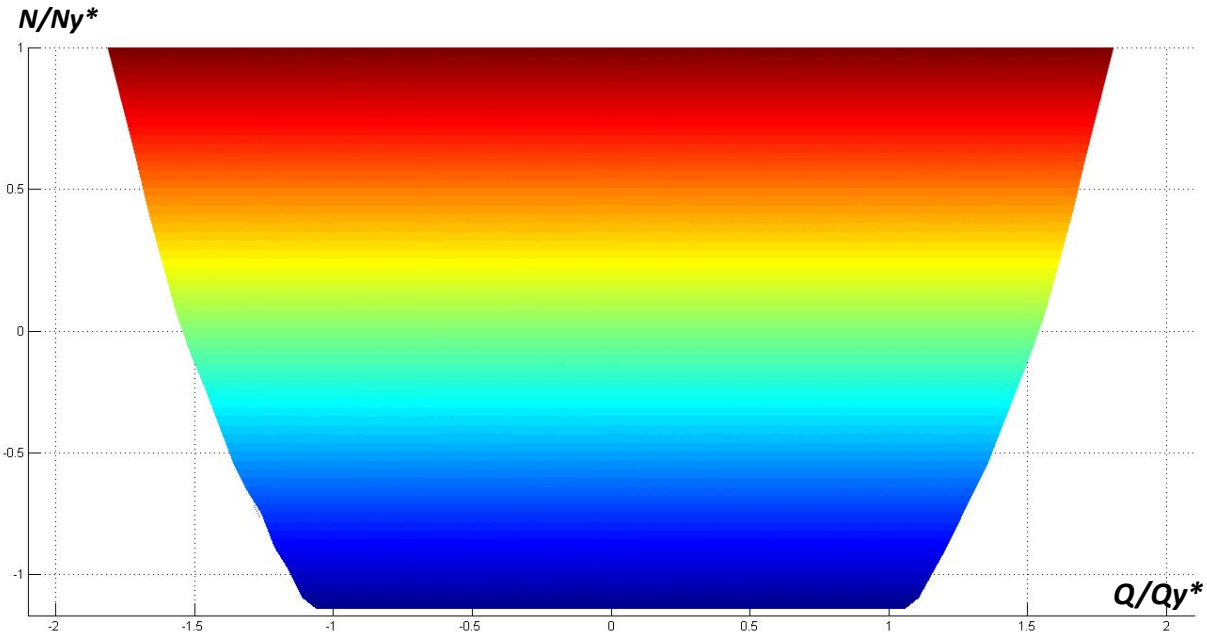

Figure 3.9 *Perspective of Q-N Failure Surface (in 3-Dimensional M-Q-N space) of flexible Pile in cohesive soil*

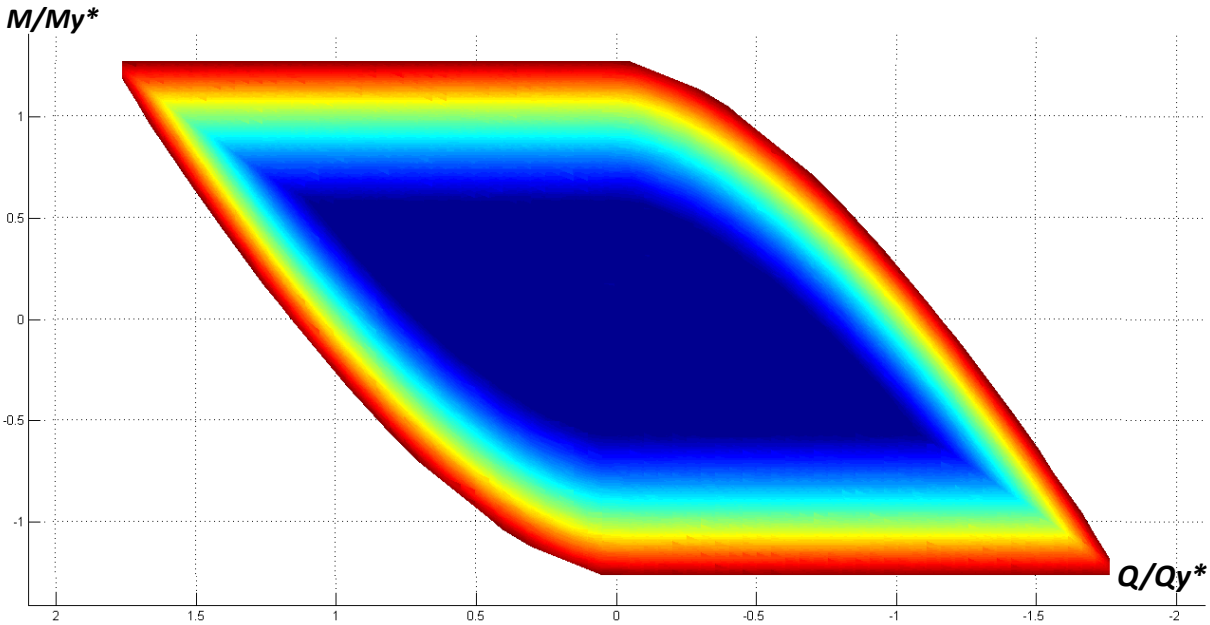

Figure 3.10 *Perspective of Q-M Failure Surface (in 3-Dimensional M-Q-N space) of flexible Pile in cohesive soil*

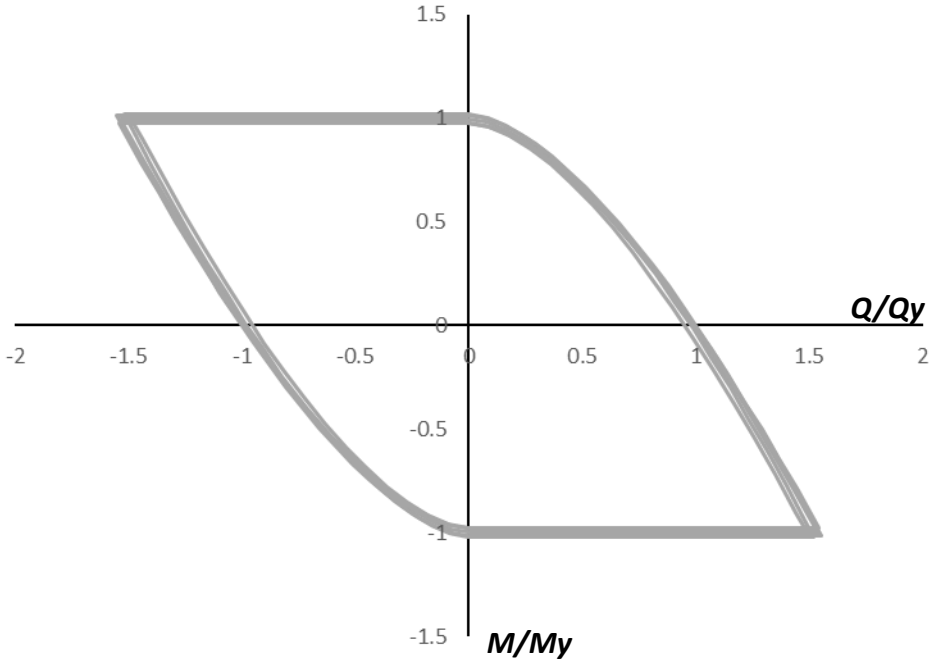

Figure 3.11 *Illustration of the effect of the factor of safety against vertical bearing capacity failure to the shape of the normalized interaction curves*

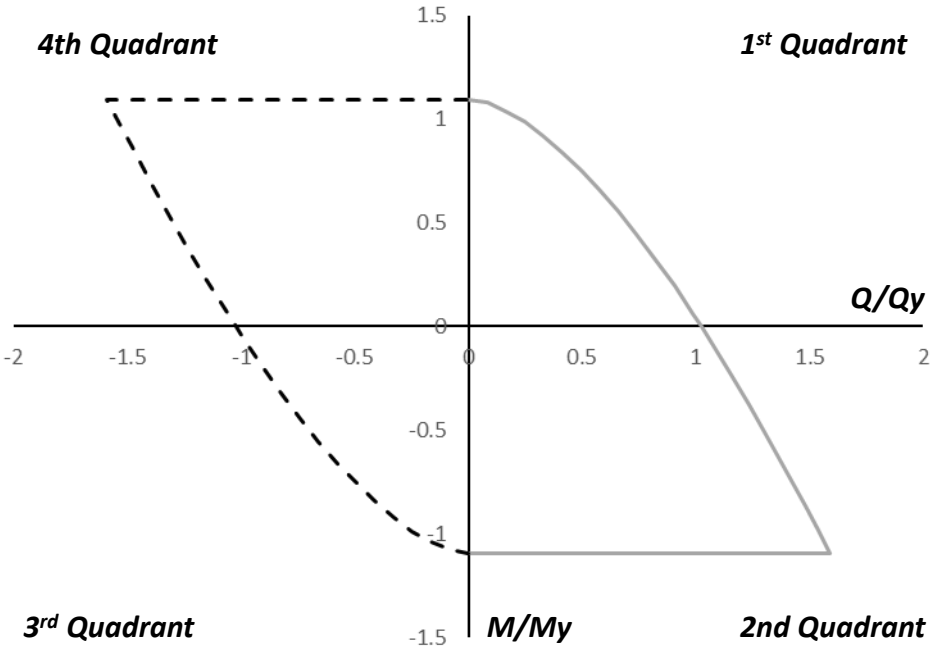

Figure 3.12 *Representation of the symmetry displayed in the interaction diagram. (1st with 3rd, 2nd with 4th quadrant)*

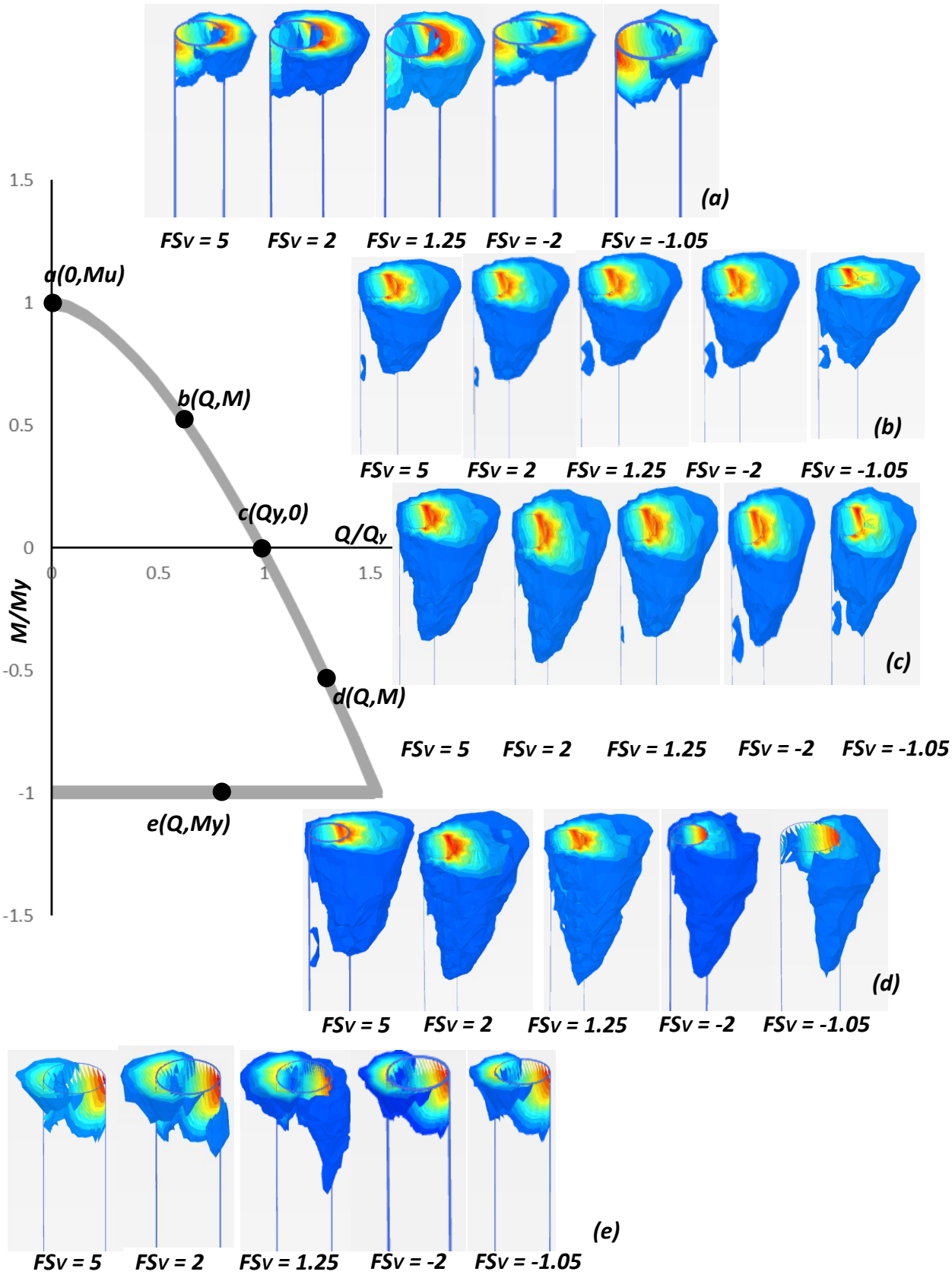

Figure 3.13 *Illustration of the plastic strain magnitude contours developed at characteristic points along the yield surface for 5 distinct factors of safety against vertical loading*

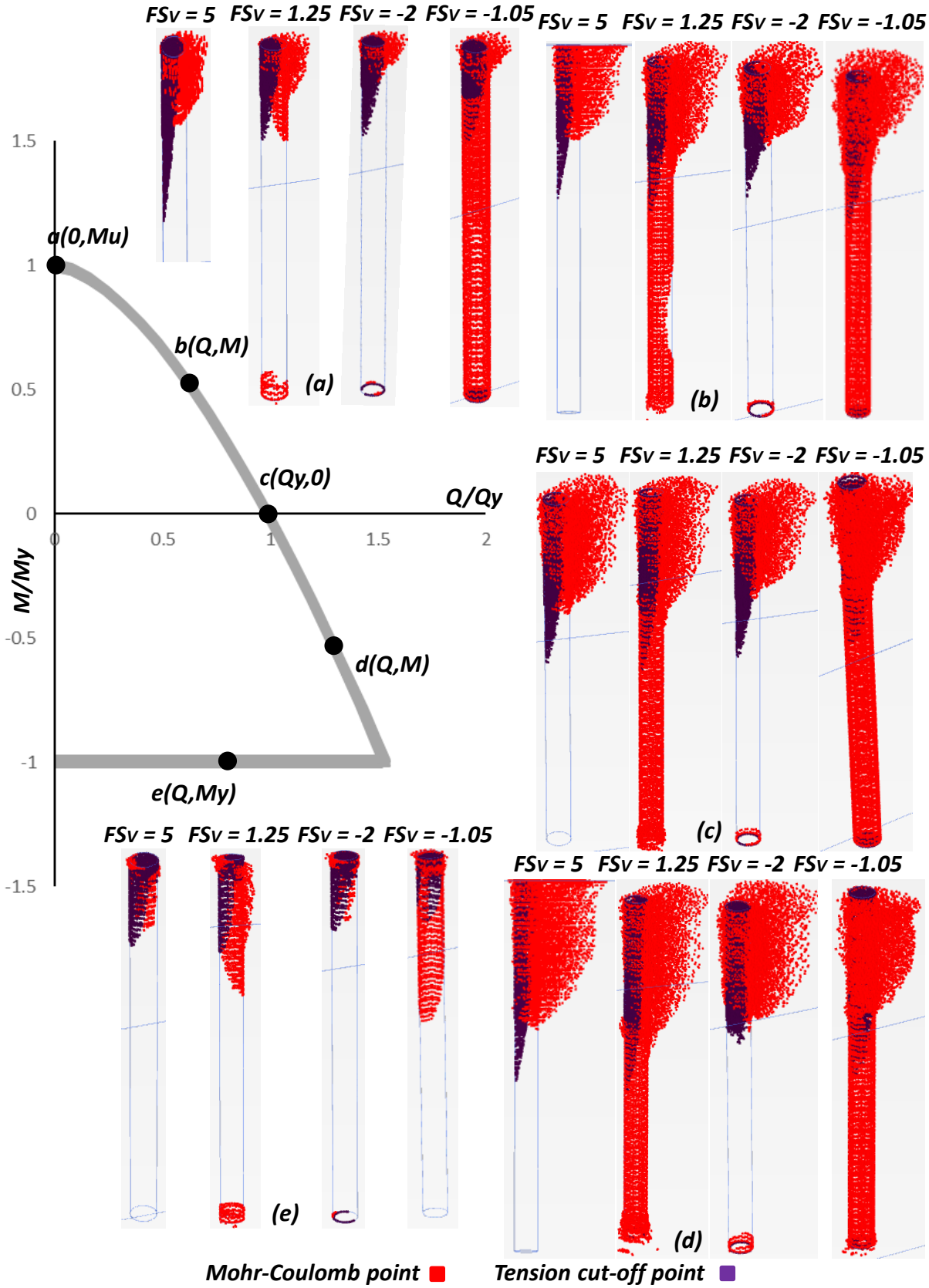

Figure 3.14 *Illustration of the Mohr-Coulomb and Tension cut-off points developed at characteristic points along the yield surface for 5 distinct factors of safety against vertical loading*

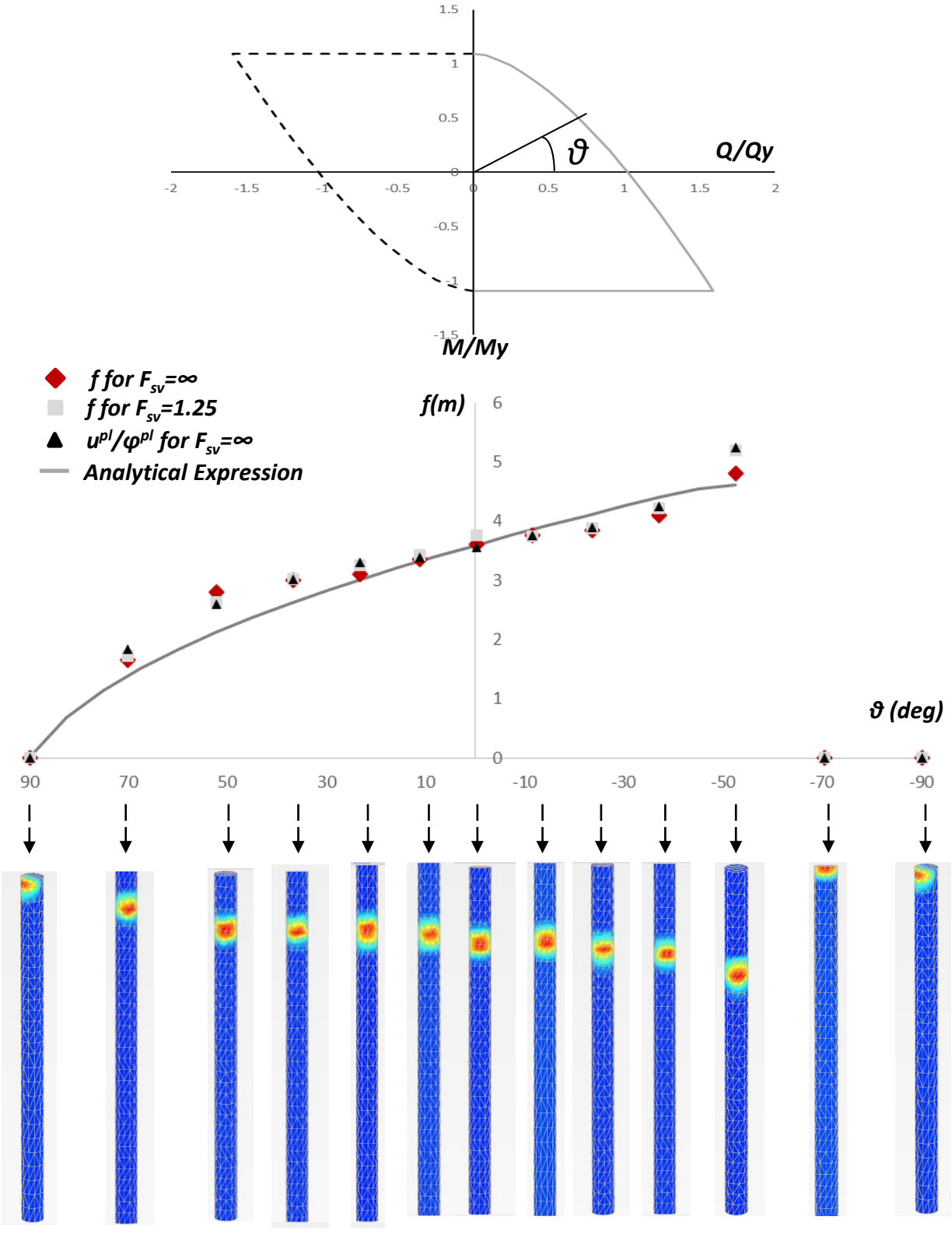

Figure 3.15 Illustration of the plastic hinge depth ***f*** in respect to the load combination angle ***ϑ*** Comparison of the ratio of the plastic horizontal displacements to the plastic rotation with the depth of the plastic hinge for $F_{sv}=\infty$,$F_{sv}=1.25$ and the analytical expression.

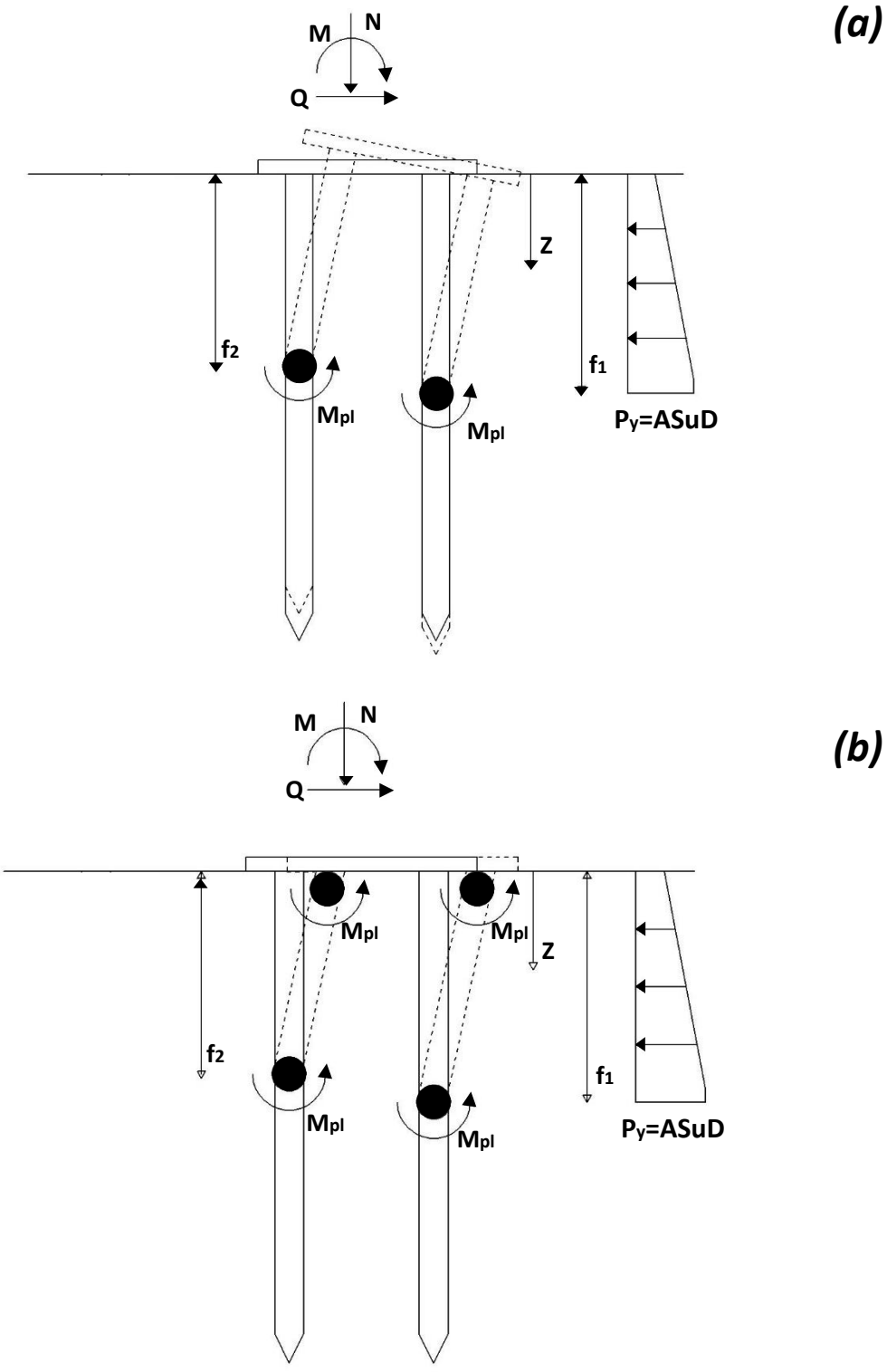

Figure 3.16(a) *Pile-group embedded in cohesive soil with constant Su distribution with depth, where one plastic hinge at each pile is developed* ***(b)*** *Pile-group embedded in cohesive soil with constant Su distribution with depth, where two plastic hinges at each pile are developed*

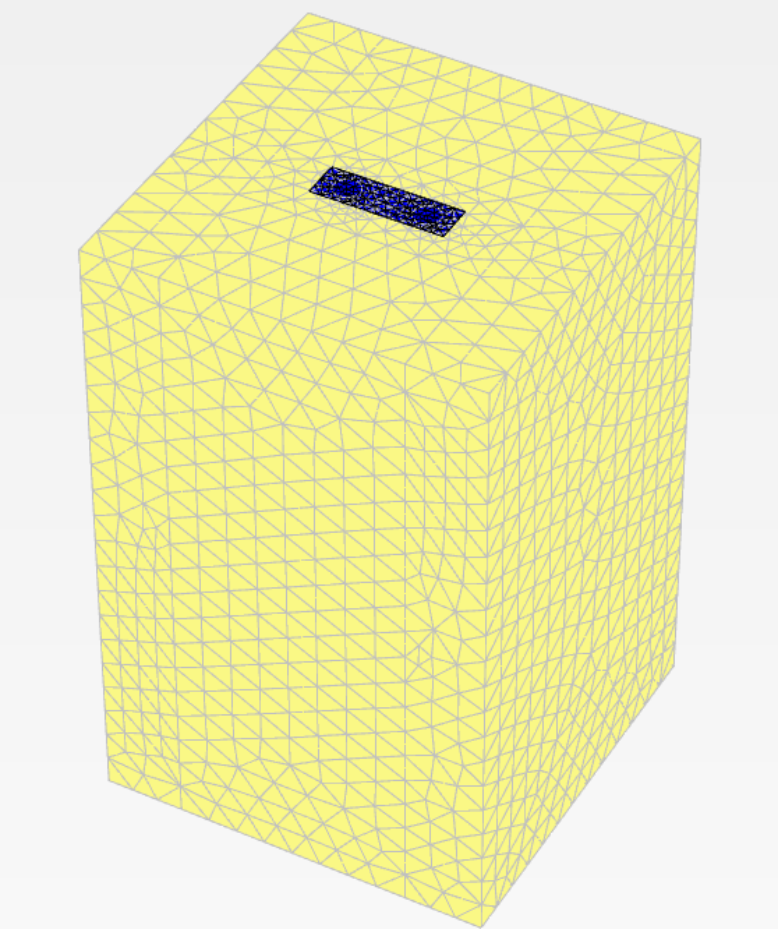

Figure 3.17 *Finite Element Model for 1x2 Pile-group in clay*

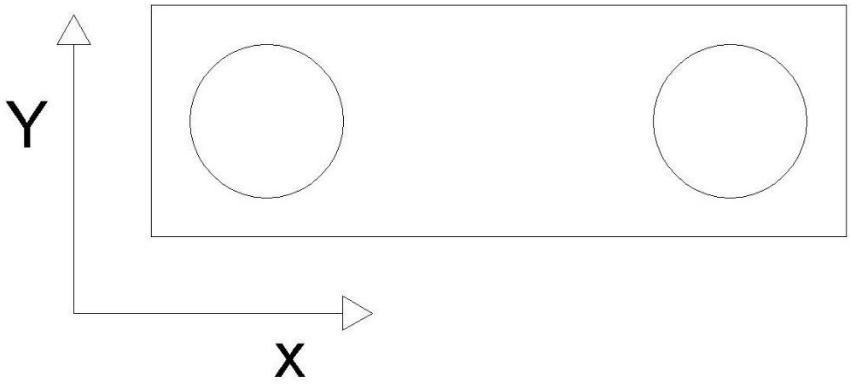

Figure 3.18 *Load directions of the 1x2 Pile-group*

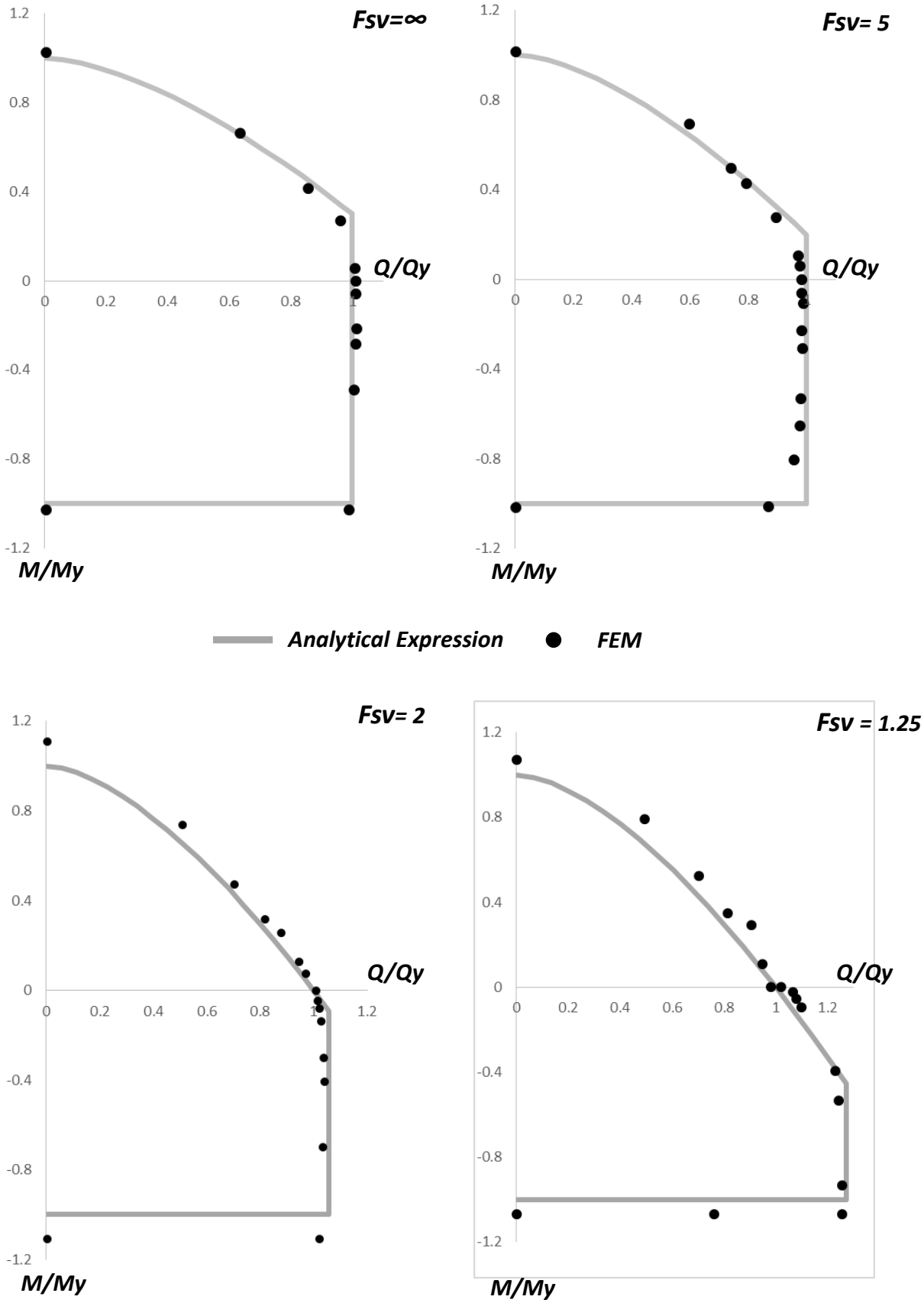

Figure 3.19(a) *Comparison between the data derived from the numerical experiments (points) and the analytical expression proposed for the yield surfaces of 1x2 Pile-group for 7 different factors, given in normalized values.*

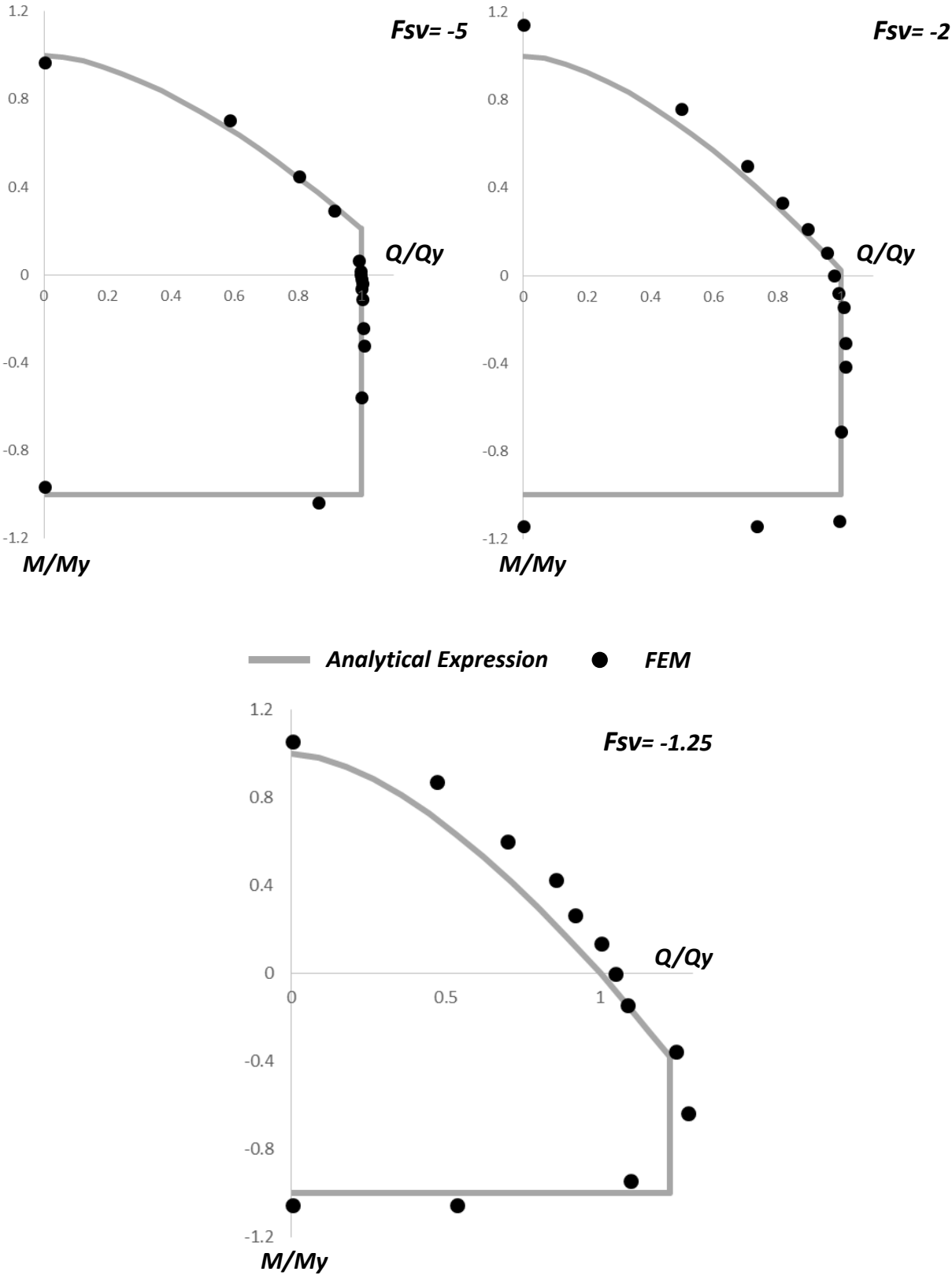

Figure 3.19(b) *Comparison between the data derived from the numerical experiments (points) and the analytical expression proposed for the yield surfaces of 1x2 Pile-group for 7 different factors, given in normalized values.*

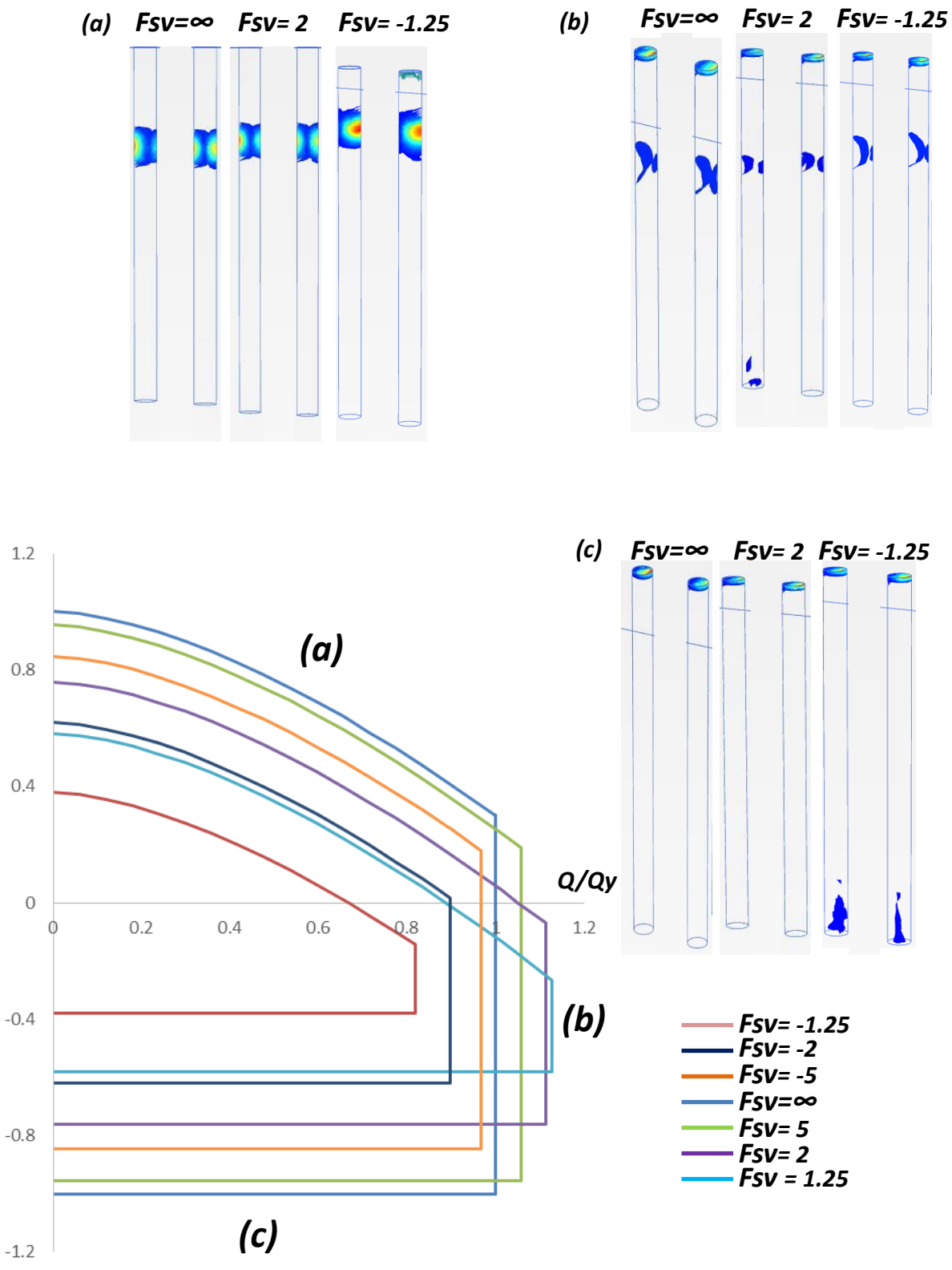

Figure 3.20 *Illustration of the plastic hinges through the plastic strain magnitude contours in the piles the for 3 distinct factors of safety against vertical loading for the three different failure mechanisms*

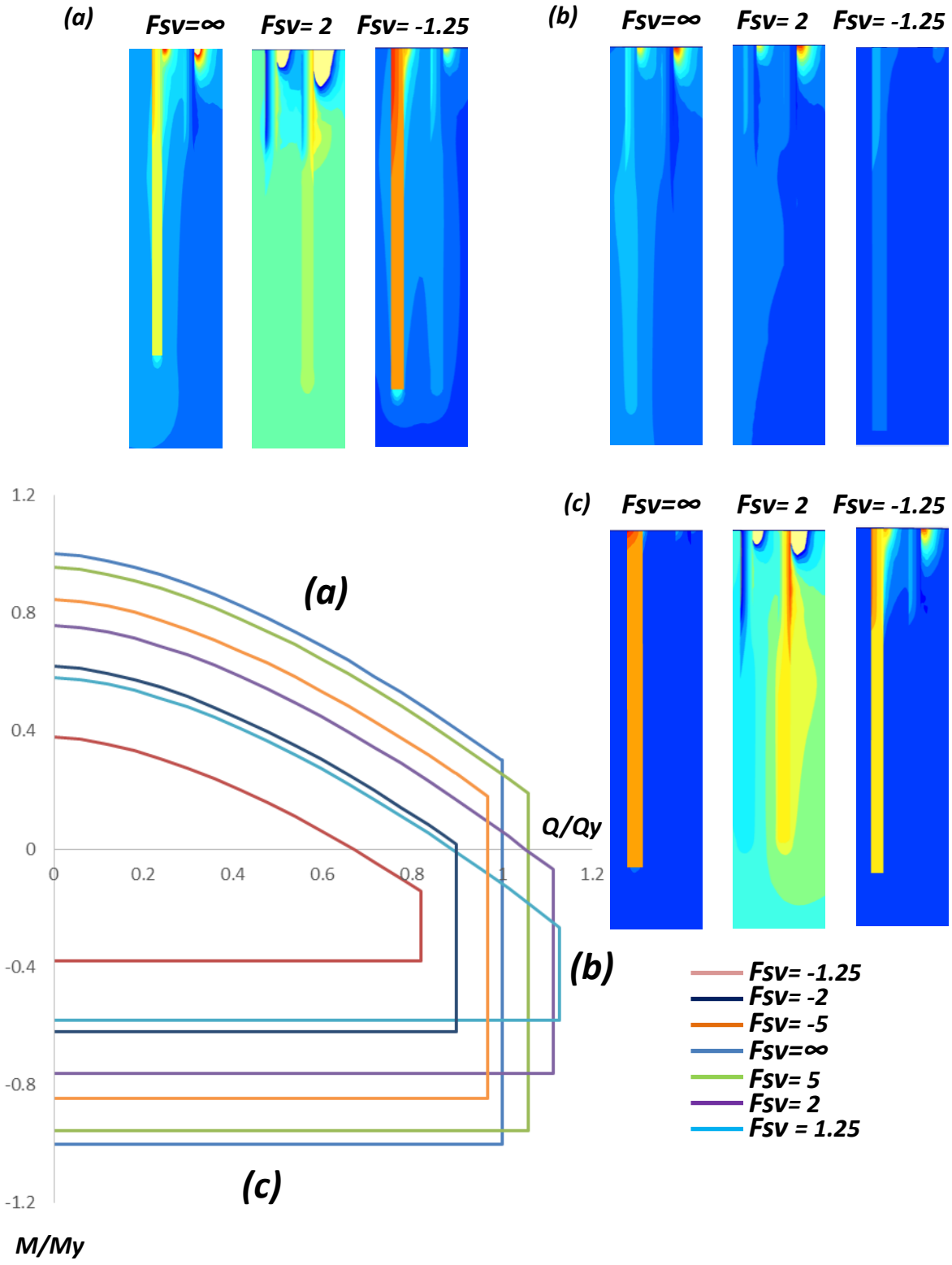

Figure 3.21 *Illustration of the vertical displacements magnitude of the piles for 3 distinct factors of safety against vertical loading for the three different failure mechanisms*

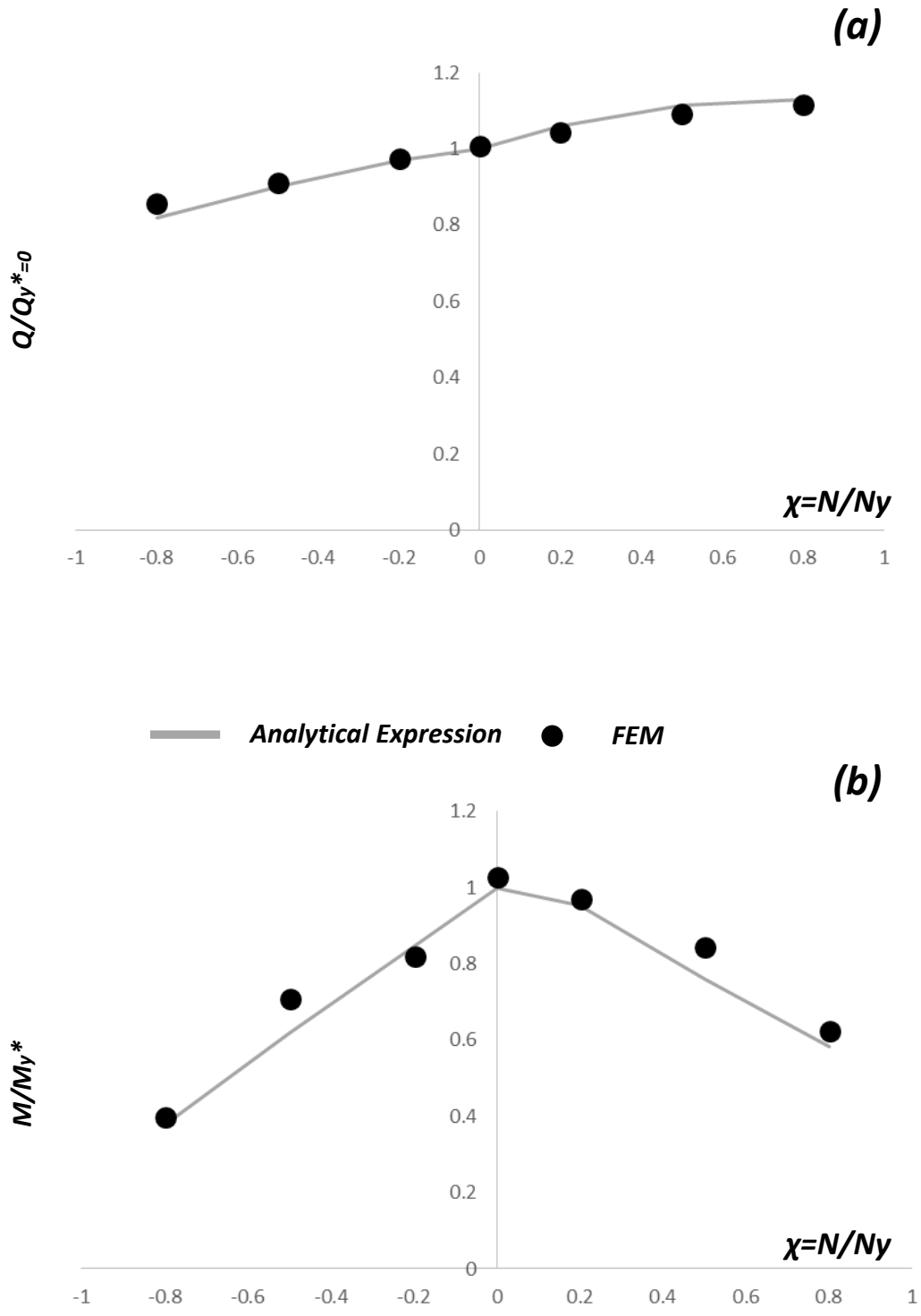

Figure 3.22 *The dimensionless* ***(α)*** *pure horizontal capacities* ***(b)*** *moment capacities of the 1x2 pile-group derived from the FE analyses (data points) are compared to the proposed analytical expression (lines).*

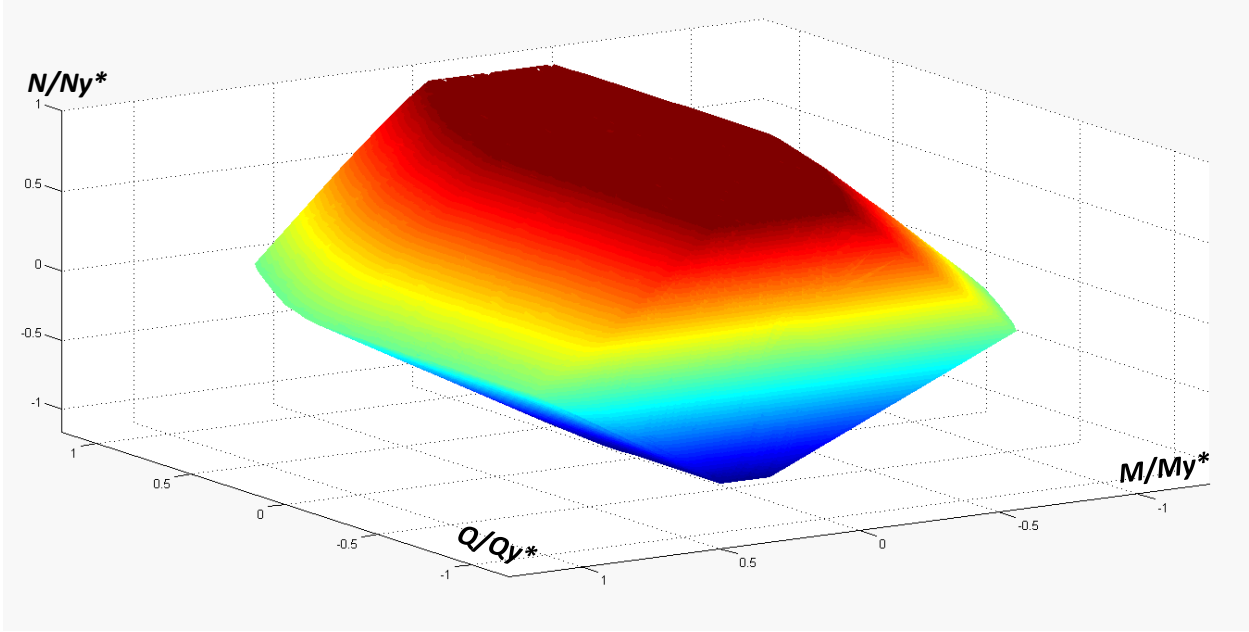

Figure 3.23 *Failure Surface (in 3-Dimensional M-Q-N space) of 1x2 Pile-group in cohesive soil*

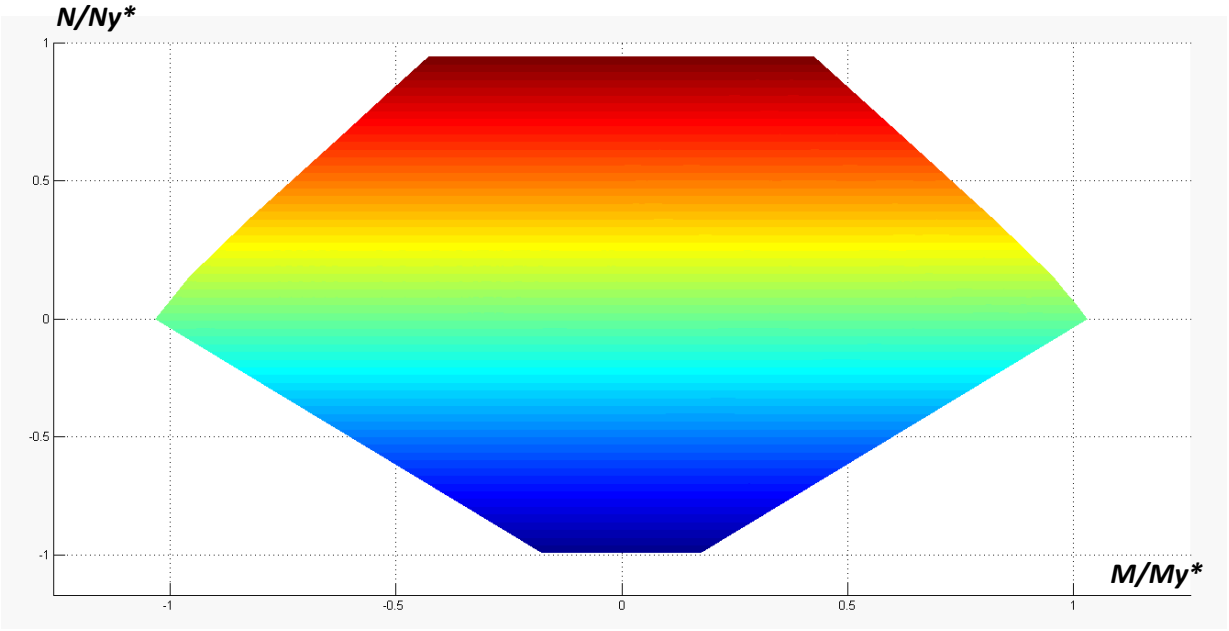

Figure 3.24 *Perspective of M-N Failure Surface (in 3-Dimensional M-Q-N space) of 1x2 Pile-group in cohesive soil*

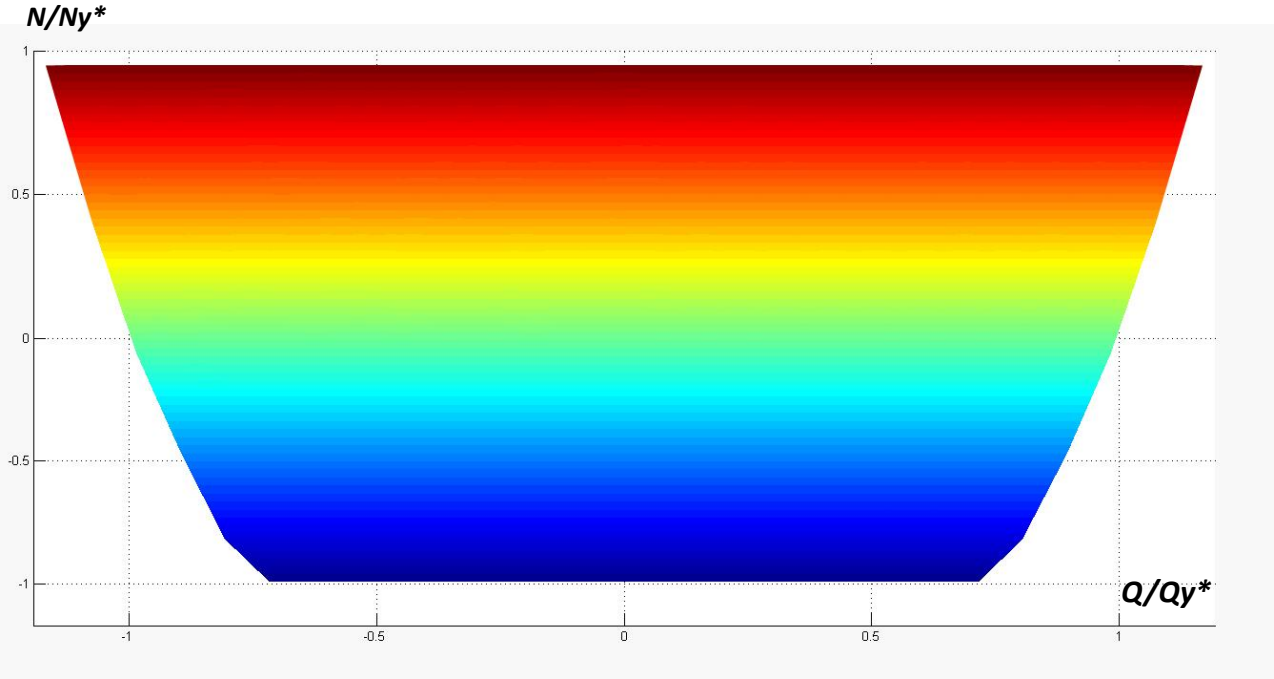

Figure 3.25 *Perspective of Q-N Failure Surface (in 3-Dimensional M-Q-N space) of 1x2 Pile-group in cohesive soil*

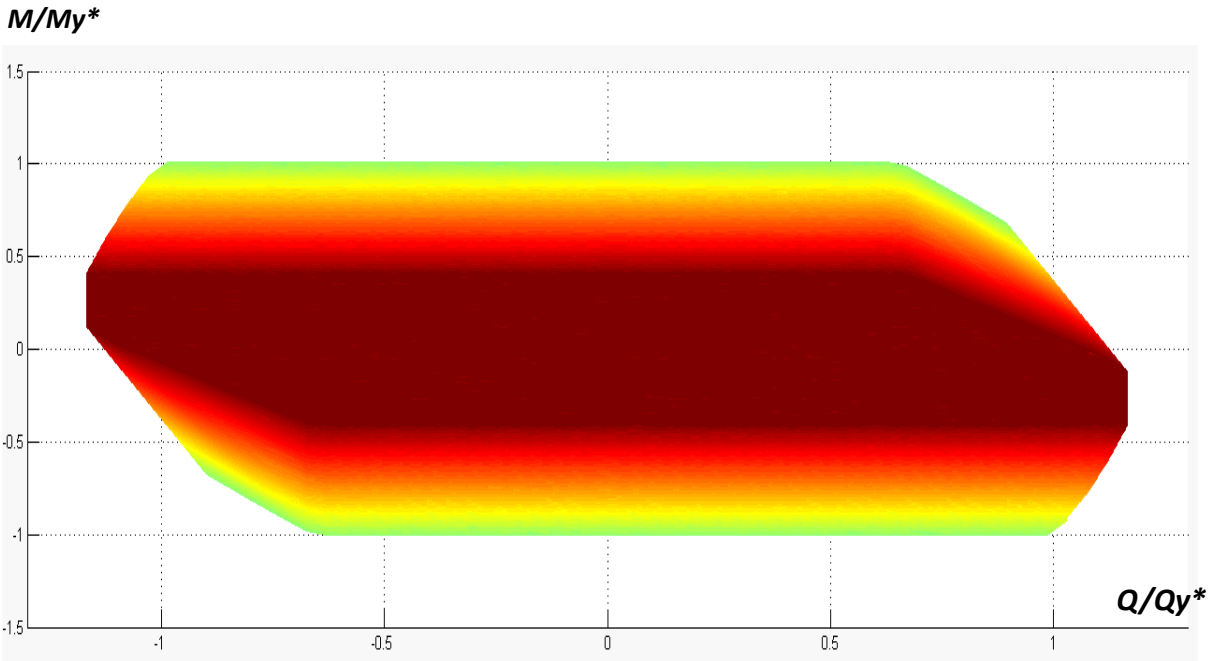

Figure 3.26 *Perspective of Q-M Failure Surface (in 3-Dimensional M-Q-N space) of 1x2 Pile-group in cohesive soil*

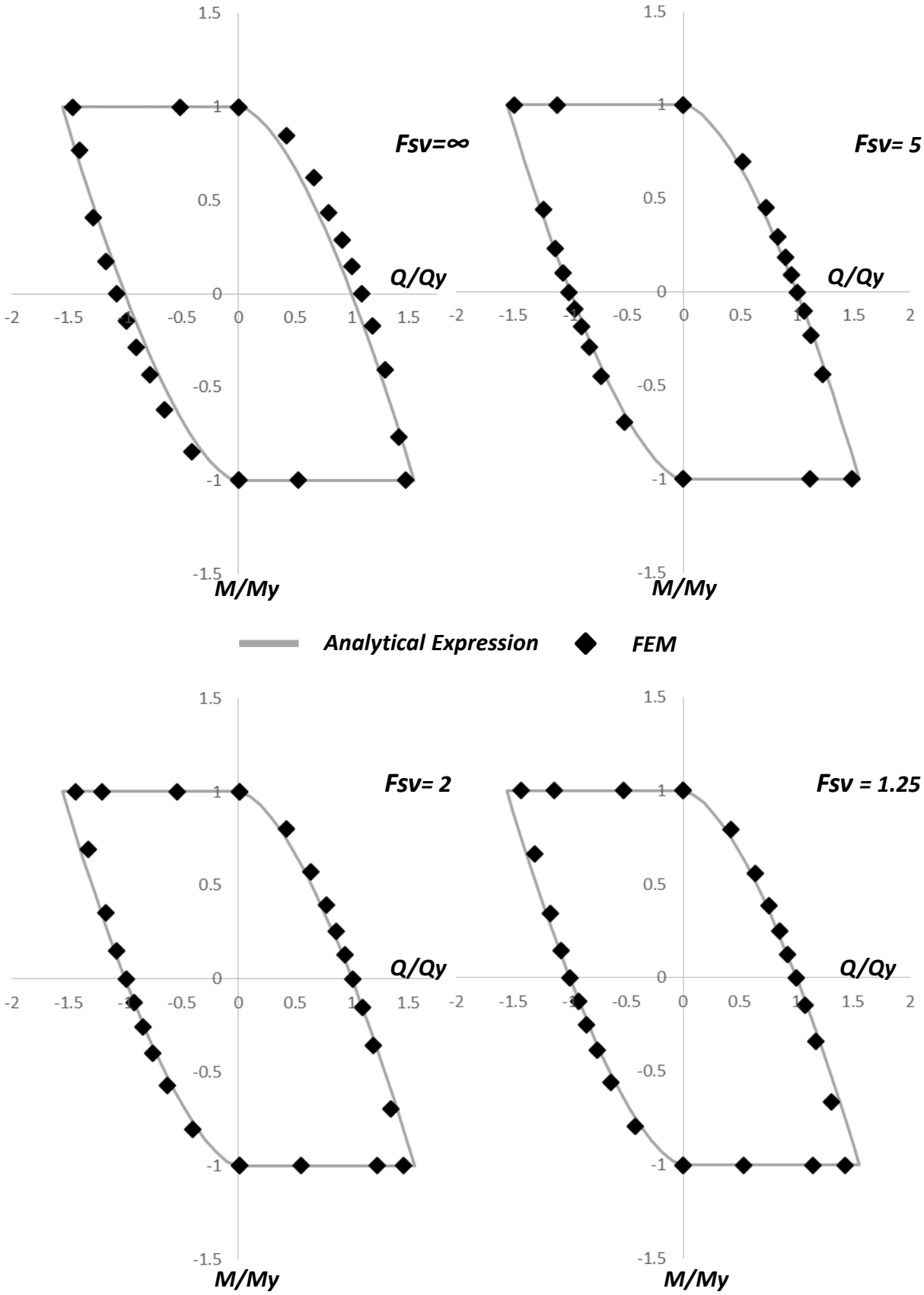

Figure 3.27 (a)*Comparison between the data derived from the numerical experiments (points) and the analytical expression proposed for the yield surfaces of 1x2 pile-group in Y direction for 7 different factors, given in normalized values.*

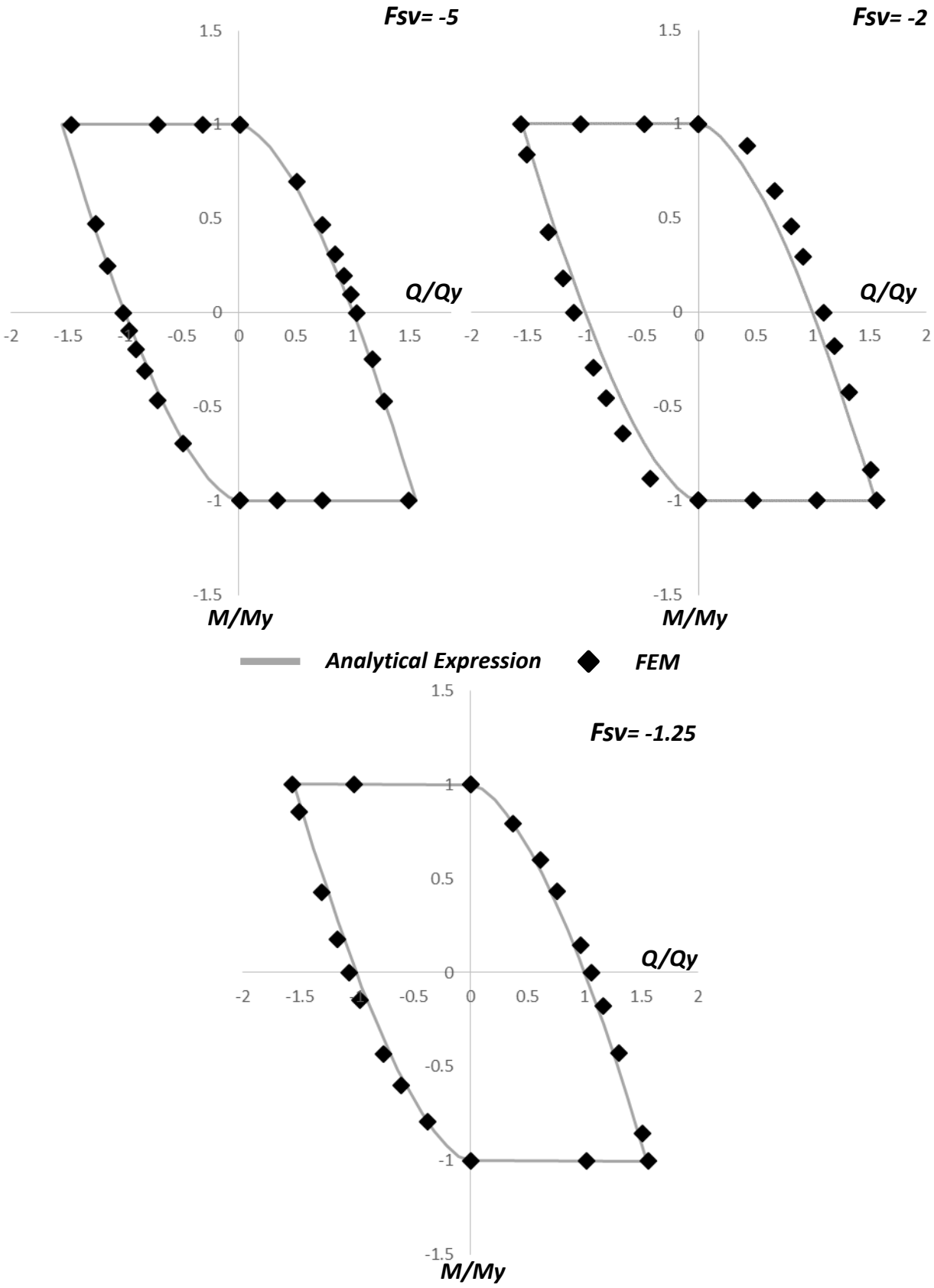

Figure 3.27 (b)*Comparison between the data derived from the numerical experiments (points) and the analytical expression proposed for the yield surfaces of 1x2 pile-group in Y direction for 7 different factors, given in normalized values.*

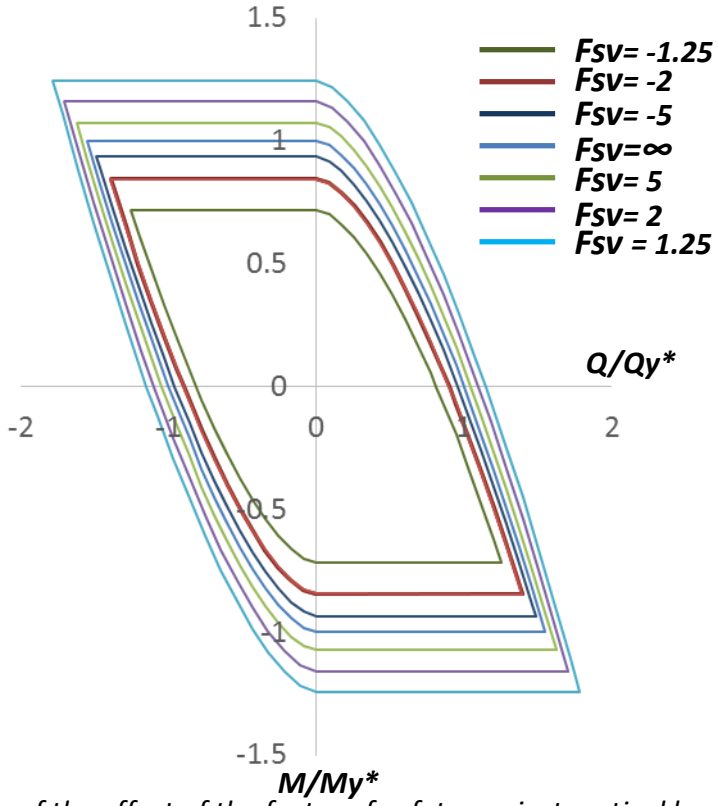

Figure 3.28 *Illustration of the effect of the factor of safety against vertical bearing capacity failure to the magnitude of the normalized interaction curves for 1x2 Pile-group under load in Y direction*

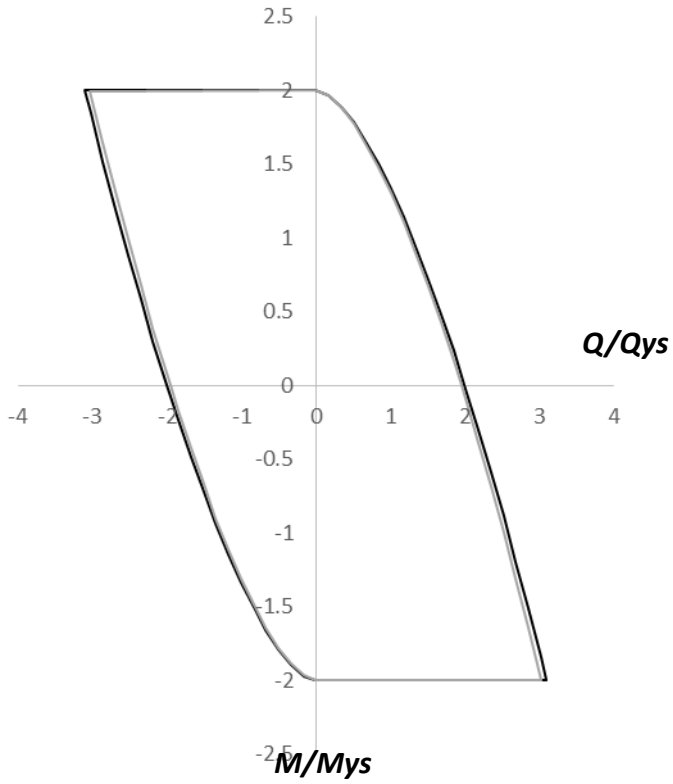

Figure 3.29 *Comparison of the 1x2 Pilegroup under load in Y direction with the response of the sum of two single flexible piles normalized to the capacity of the single flexible pile*

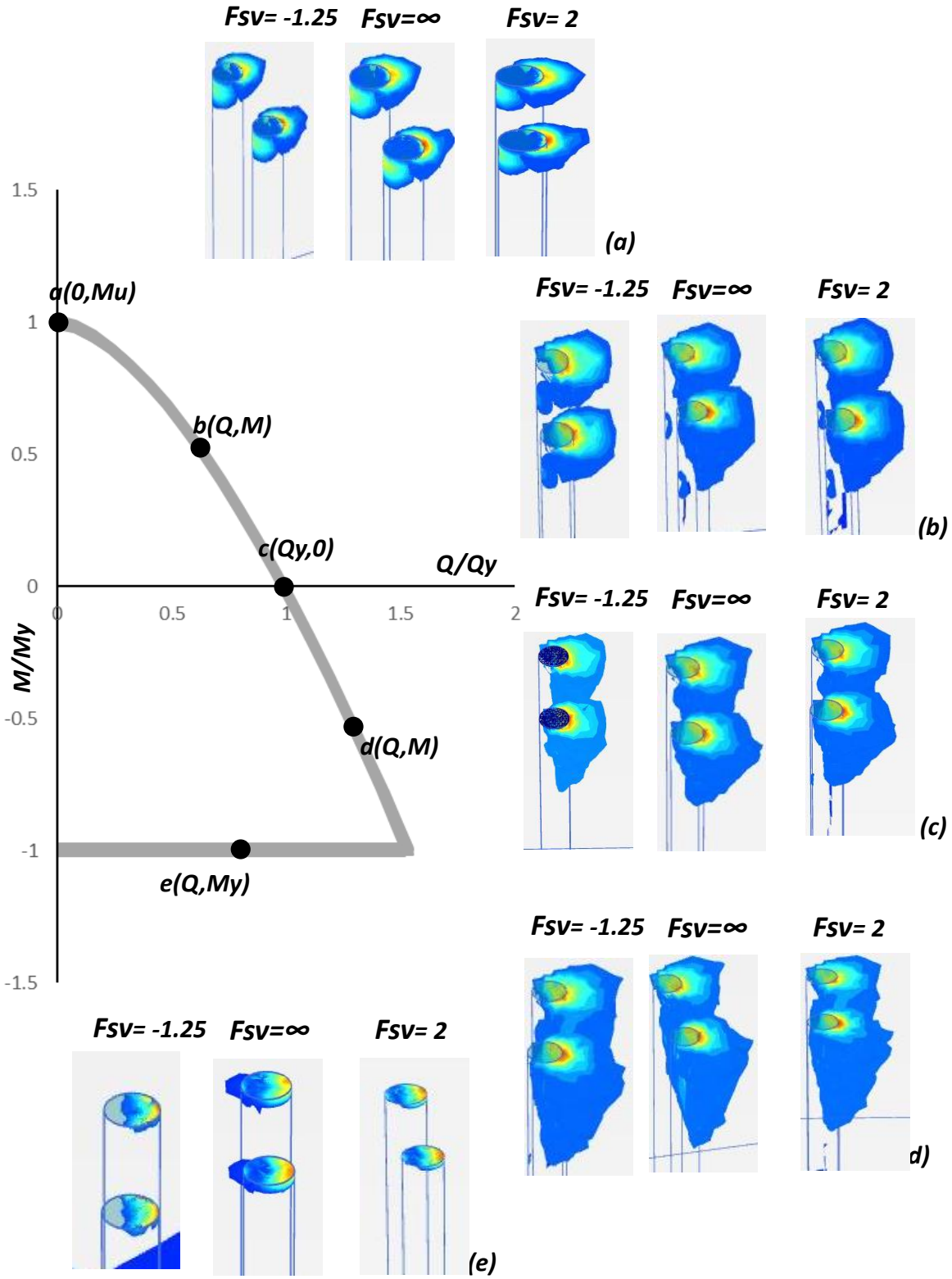

Figure 3.30 *Illustration of the plastic strain magnitude contours developed at characteristic points along the yield surface for 5 distinct factors of safety against vertical loading*

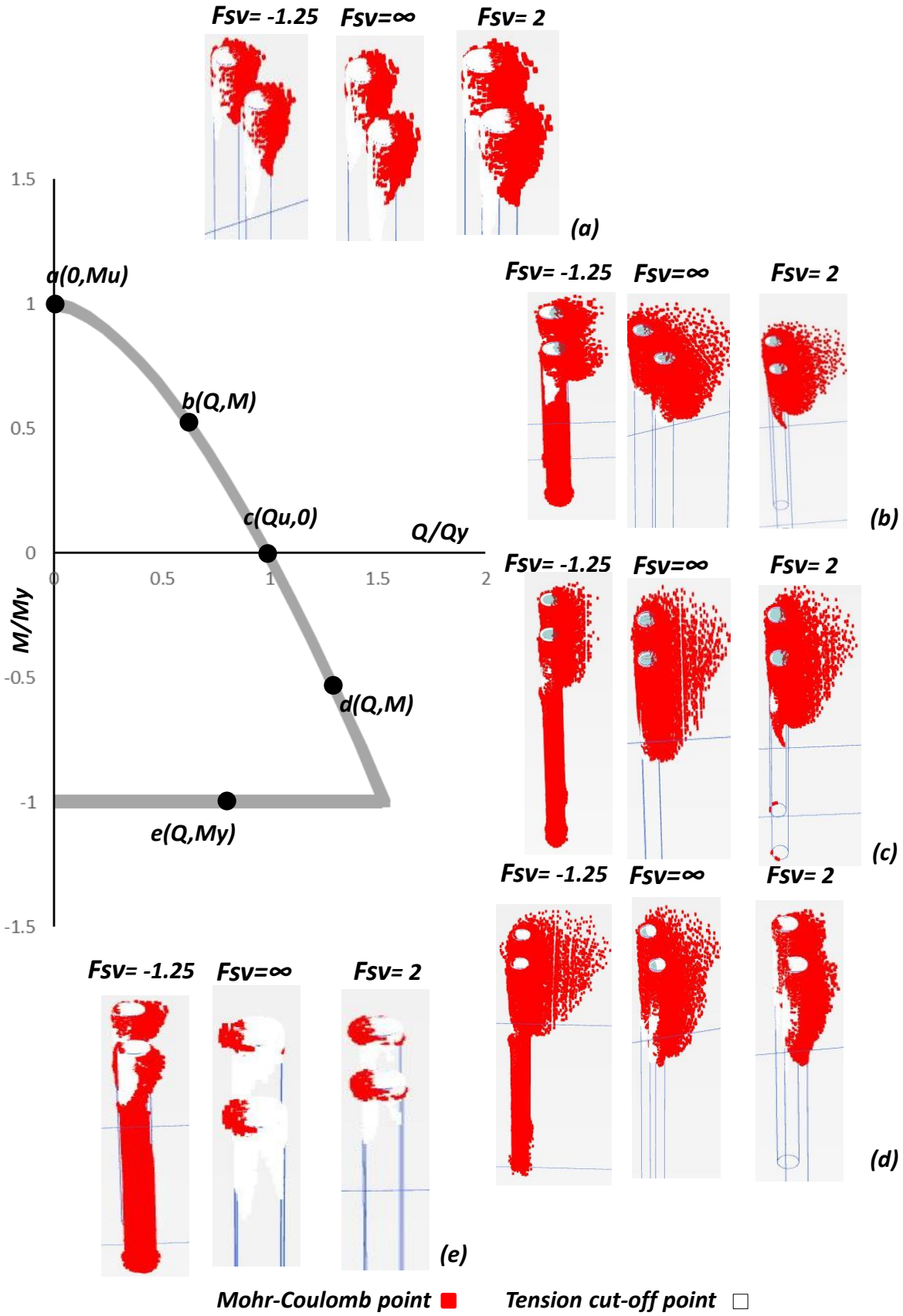

Figure 3.31 *Illustration of the Mohr-Coulomb and Tension cut-off points developed at characteristic points along the yield surface for 5 distinct factors of safety against vertical loading*

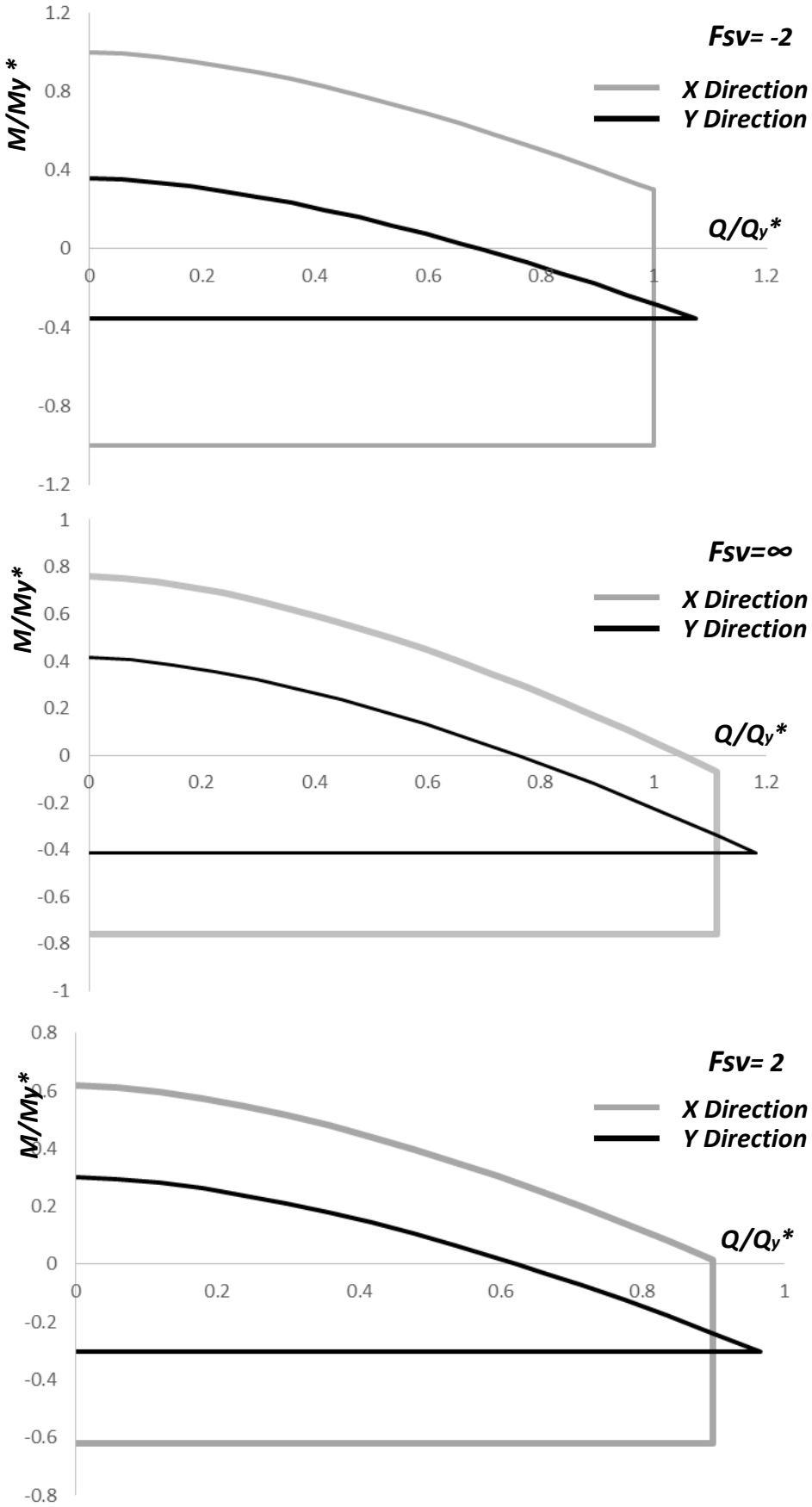

Figure 3.31 *Comparison of the behavior of the 1x2 Pile-Group under loading in X and Y direction for three different factors of safety*

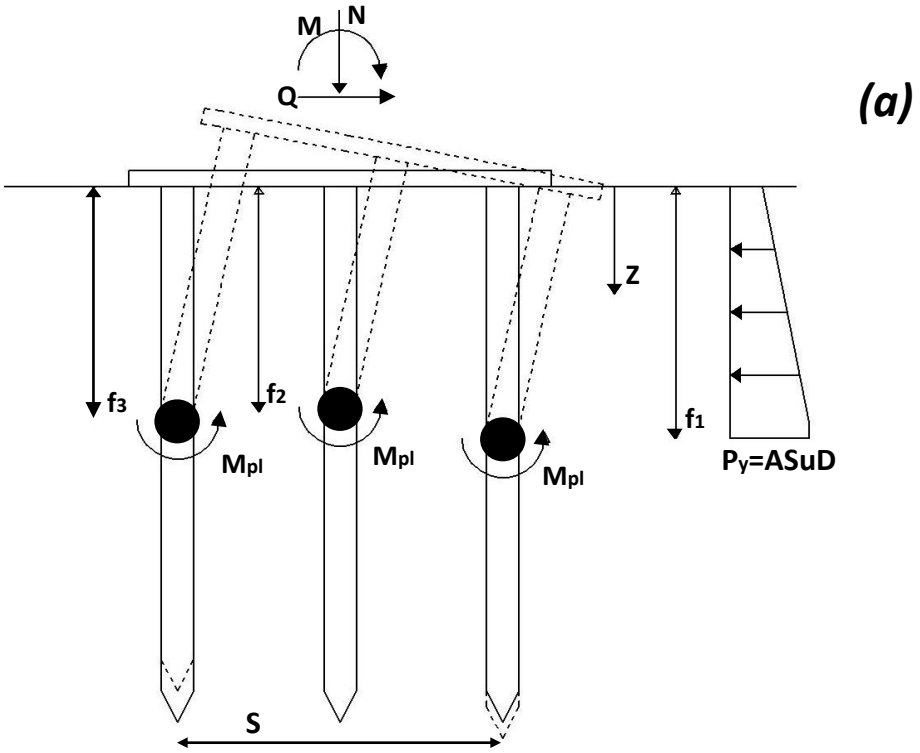

Figure 3.32(a) 2x2 *Pile-group embedded in cohesive soil with constant Su distribution with depth under diagonal combined loading:**(a)** failure type A*

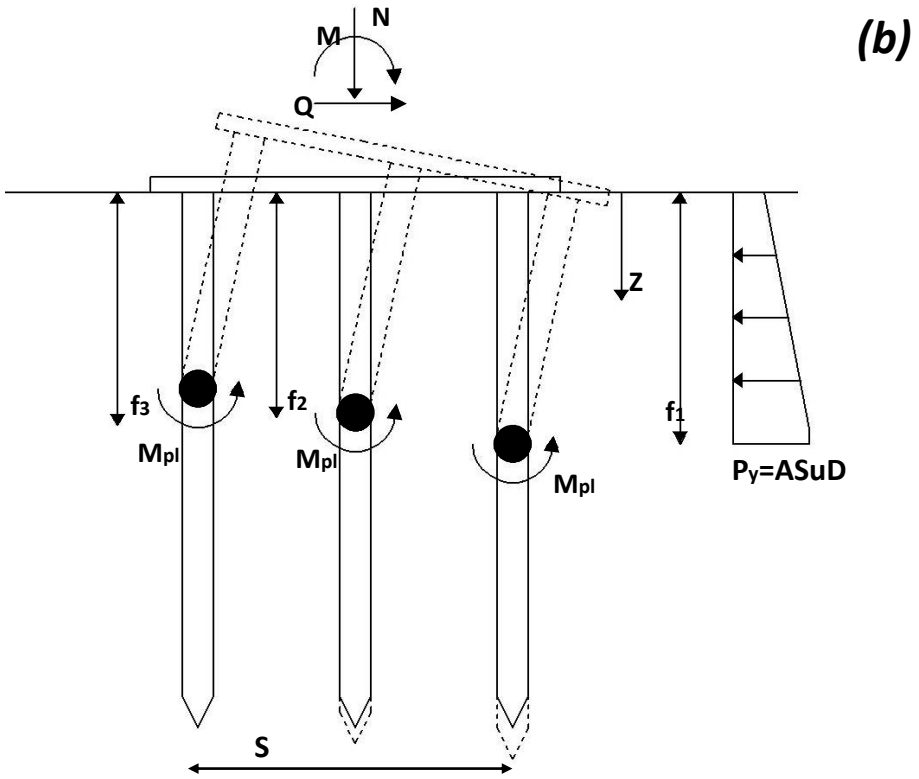

Figure 3.32(b) 2x2 *Pile-group embedded in cohesive soil with constant Su distribution with depth under diagonal combined loading:**(b)** failure Type B*

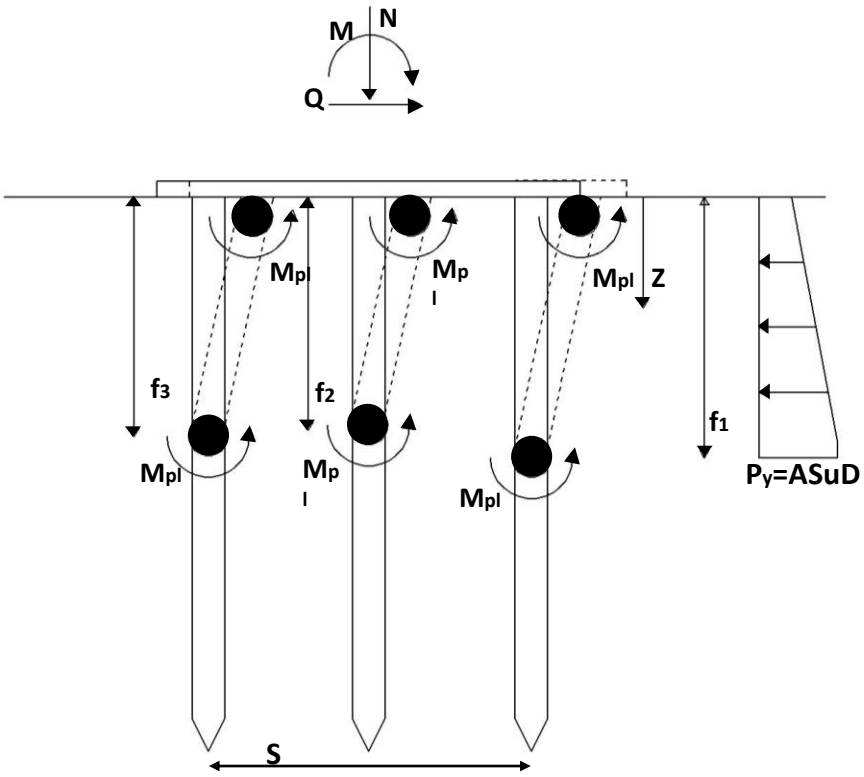

Figure 3.32(c) 2x2 *Pile-group embedded in cohesive soil with constant Su distribution with depth under diagonal combined loading:* ***(c)*** *failure Type C*

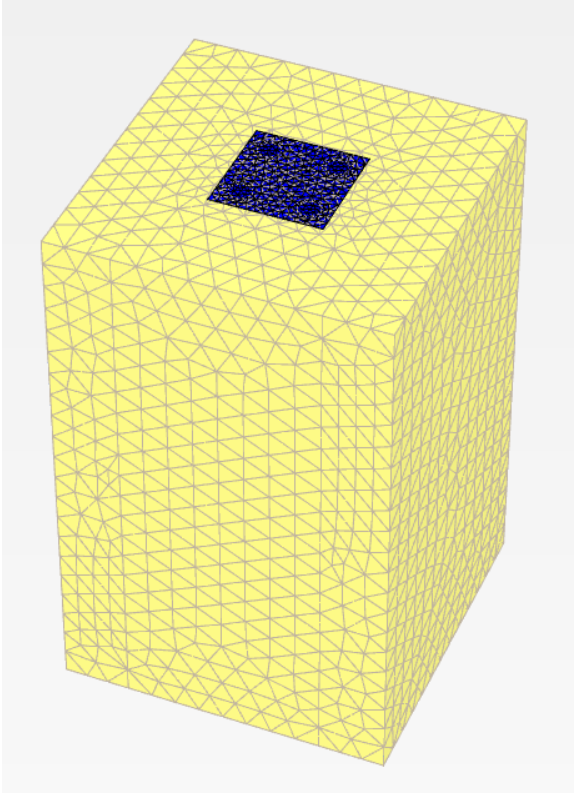

Figure 3.33 *Finite Element Model for 1x2 Pile-group in clay*

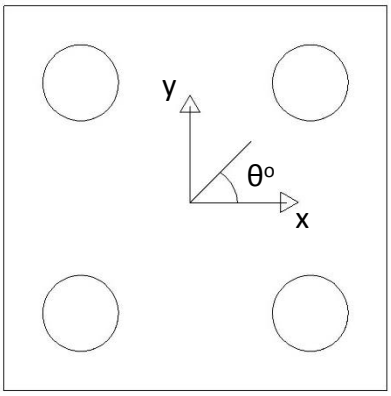

Figure 3.34 *Load directions of the 2x2 Pile-group:* ***(a)*** *in x direction* ***(b)*** *diagonal (ϑ=45o)*

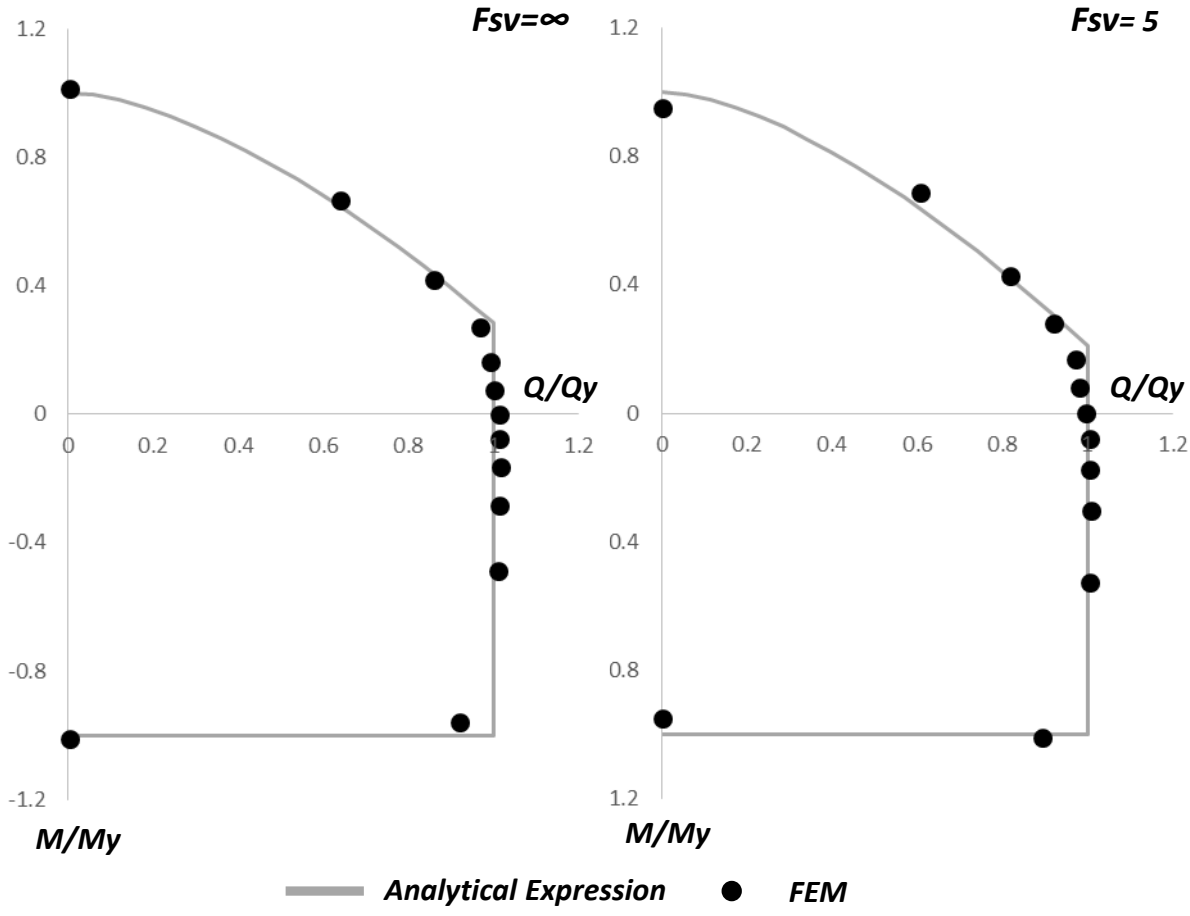

Figure 3.35(a) *Comparison between the data derived from the numerical experiments (points) and the analytical expression proposed for the yield surfaces of 2x2 pile-group in X direction for 7 different factors, given in normalized values.*

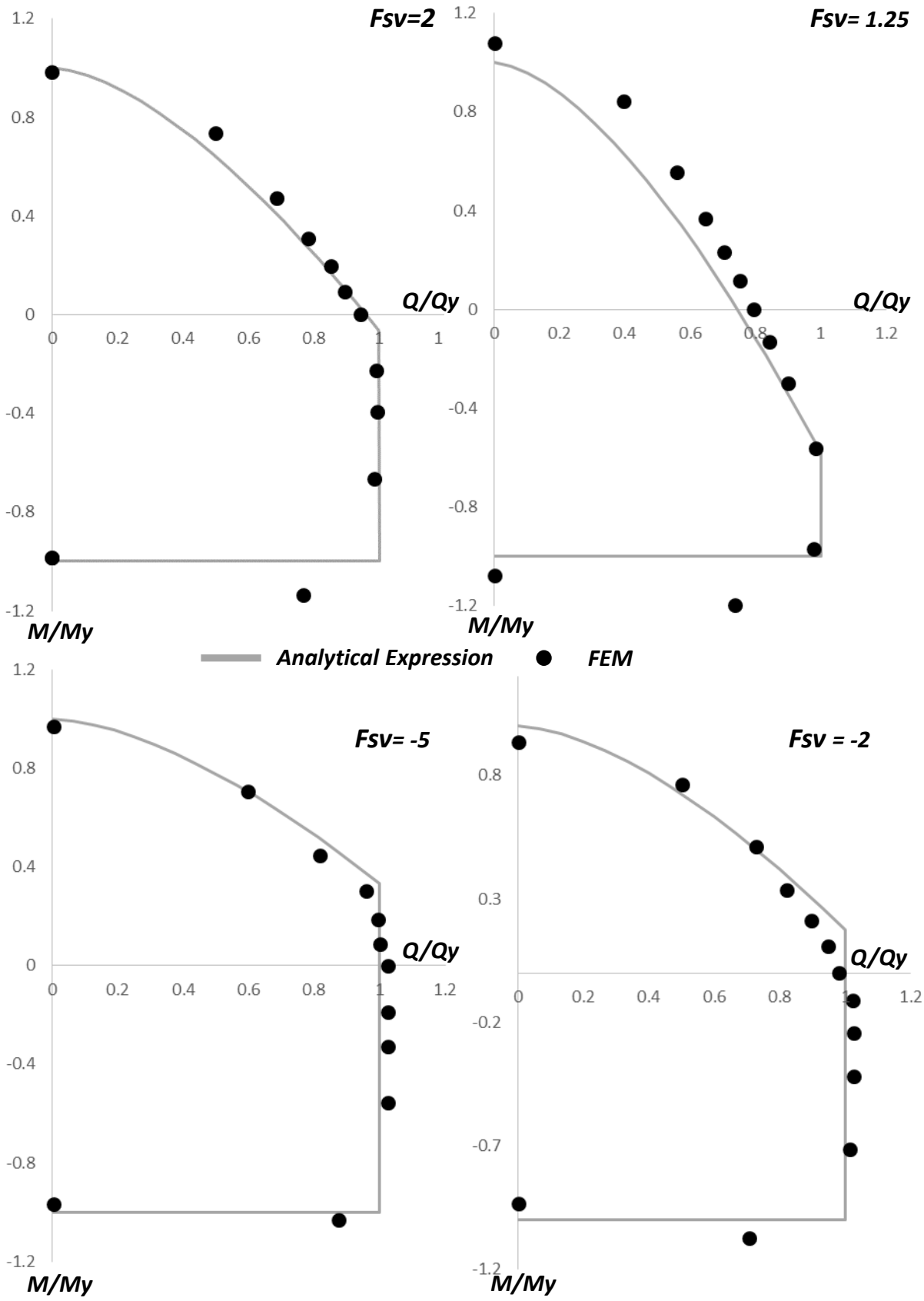

Figure 3.35(b) *Comparison between the data derived from the numerical experiments (points) and the analytical expression proposed for the yield surfaces of 2x2 pile-group in X direction for 7 different factors, given in normalized values.*

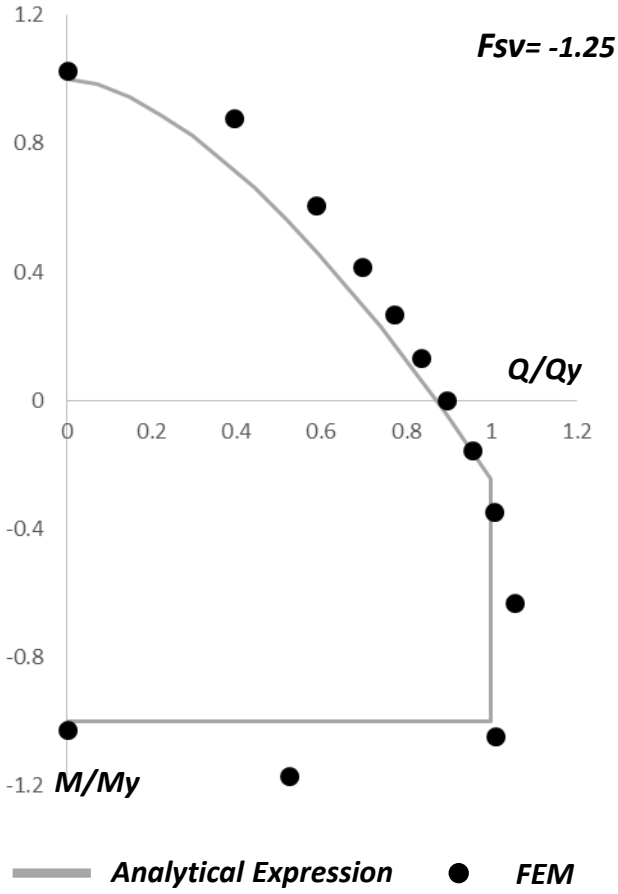

Figure 3.35(c) *Comparison between the data derived from the numerical experiments (points) and the analytical expression proposed for the yield surfaces of 2x2 pile-group in X direction for 7 different factors, given in normalized values.*

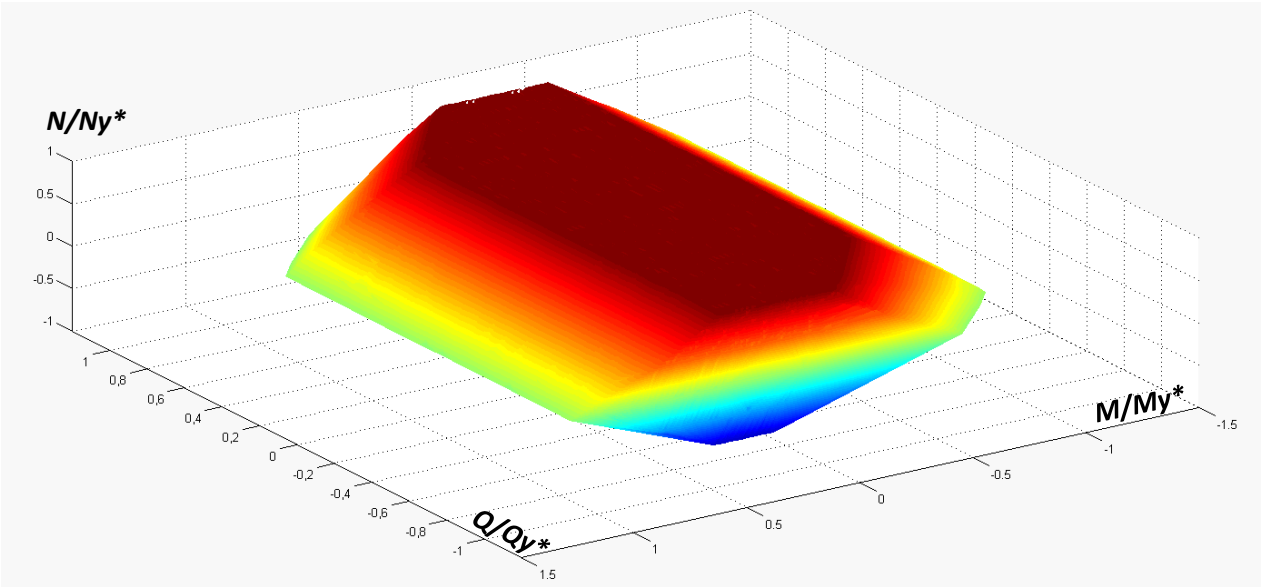

Figure 3.36 *Failure Surface (in 3-Dimensional M-Q-N space) of 2x2 Pile-group in cohesive soil*

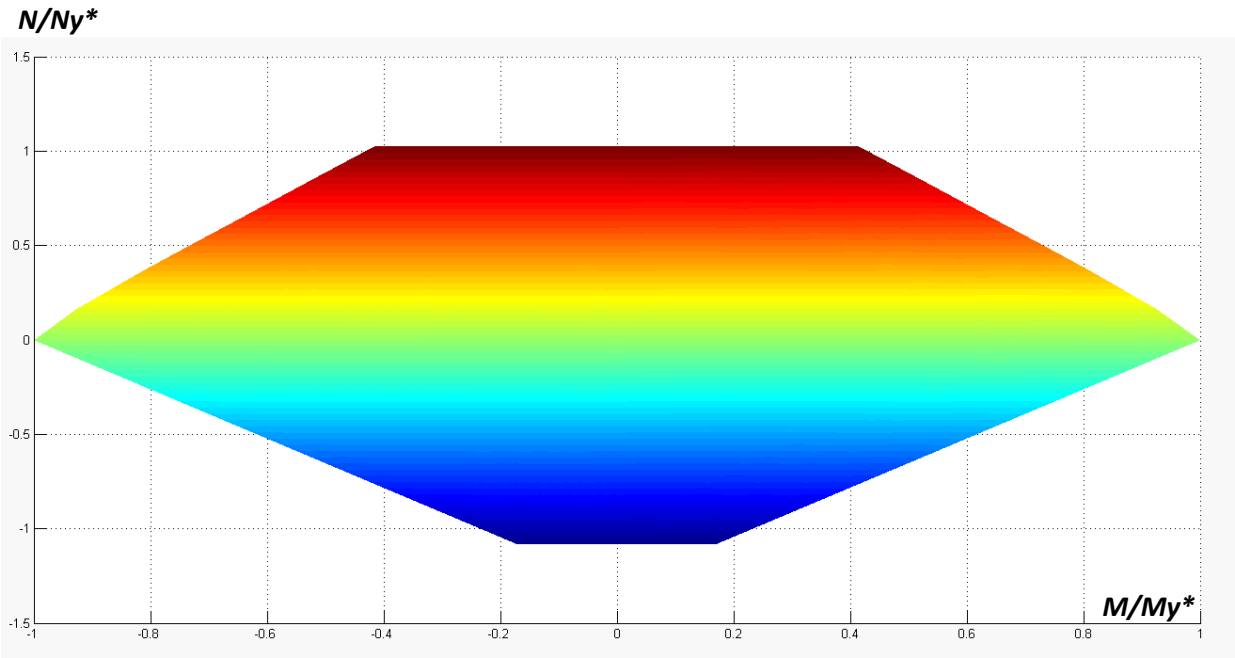

Figure 3.37 *Perspective of M-N Failure Surface (in 3-Dimensional M-Q-N space) of 2x2 Pile-group in cohesive soil*

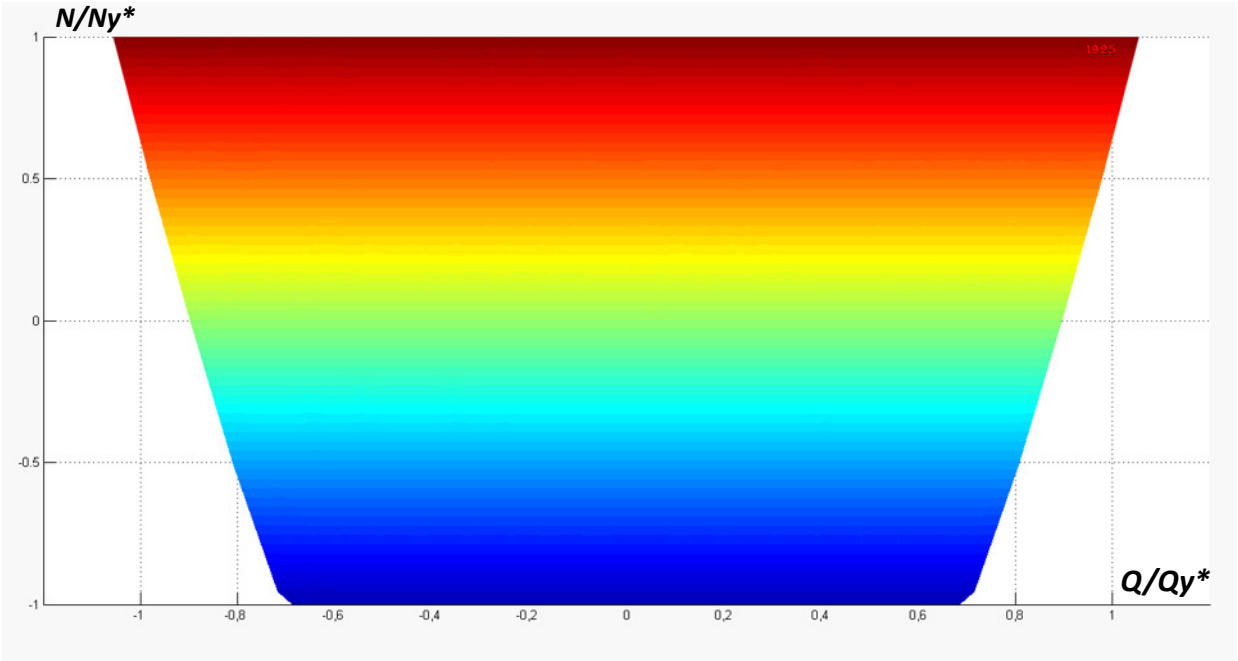

Figure 3.38 *Perspective of Q-N Failure Surface (in 3-Dimensional M-Q-N space) of 1x2 Pile-group in cohesive soil*

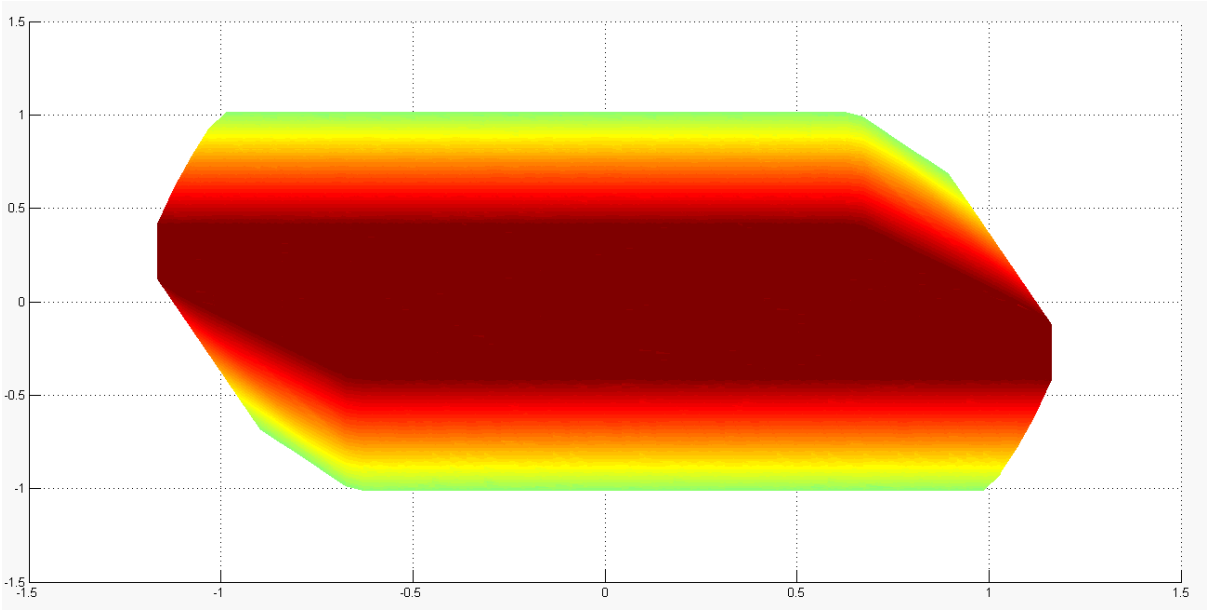

Figure 3.39 *Perspective of Q-M Failure Surface (in 3-Dimensional M-Q-N space) of 1x2 Pile-group in cohesive soil*

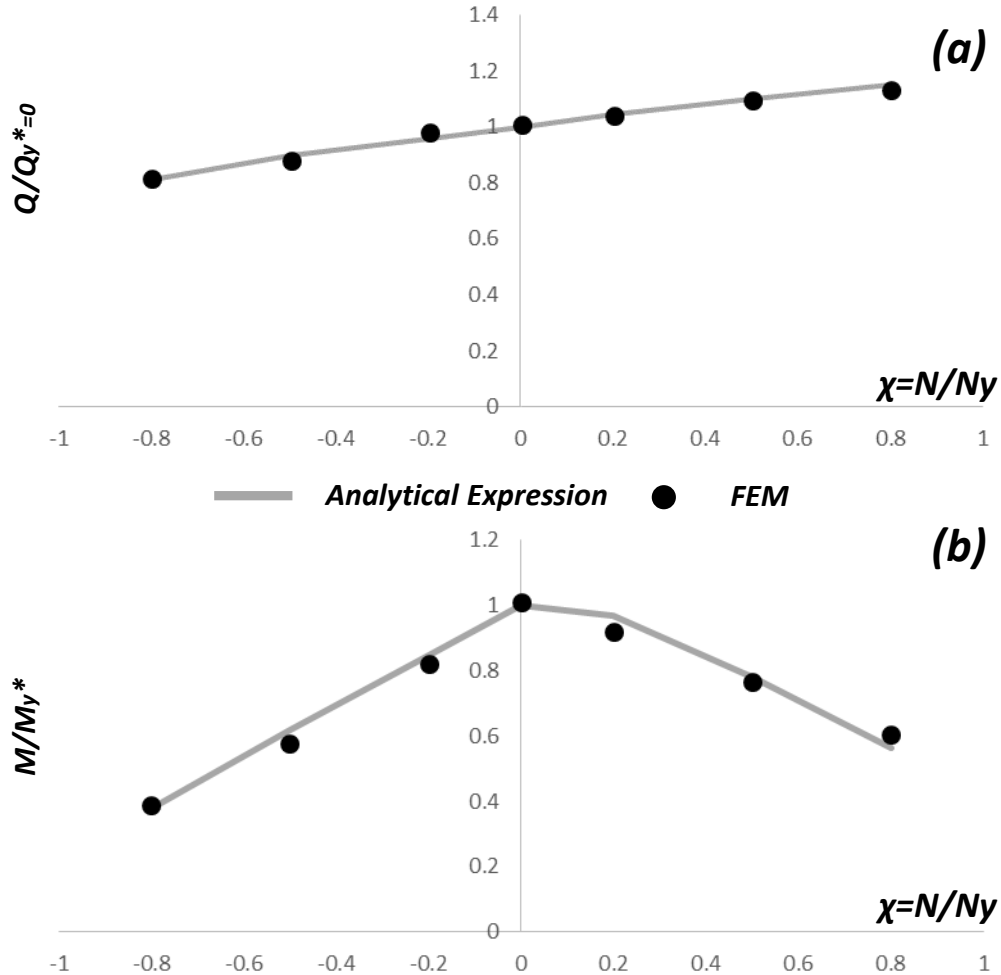

Figure 3.40 *The dimensionless* ***(α)*** *pure horizontal capacities* ***(b)*** *moment capacities of the 2x2 pile-group derived from the FE analyses (data points) are compared to the proposed analytical expression (lines).*

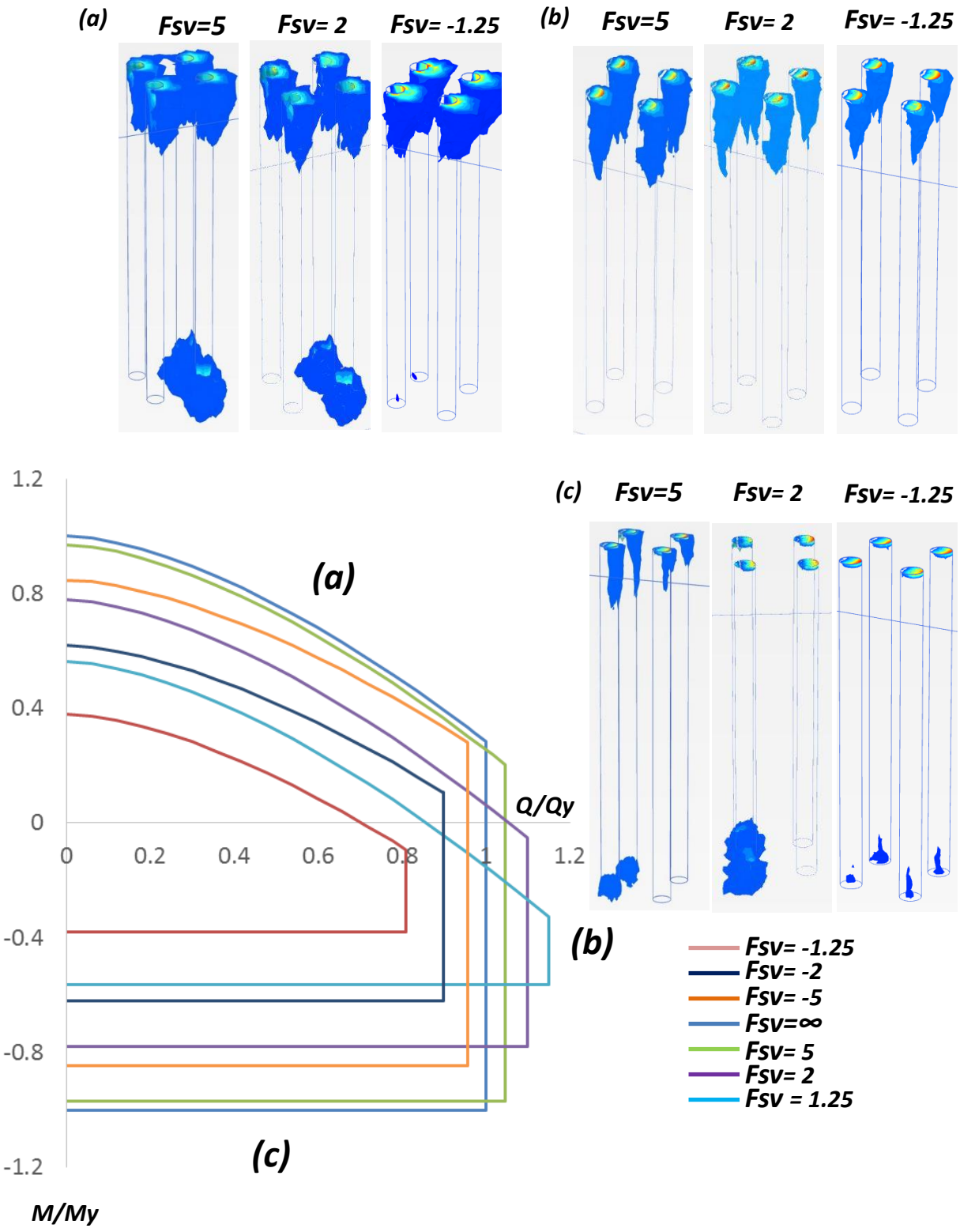

Figure 3.41 *Illustration of the plastic strain magnitude contours for 3 distinct factors of safety against vertical loading for the three different failure mechanisms*

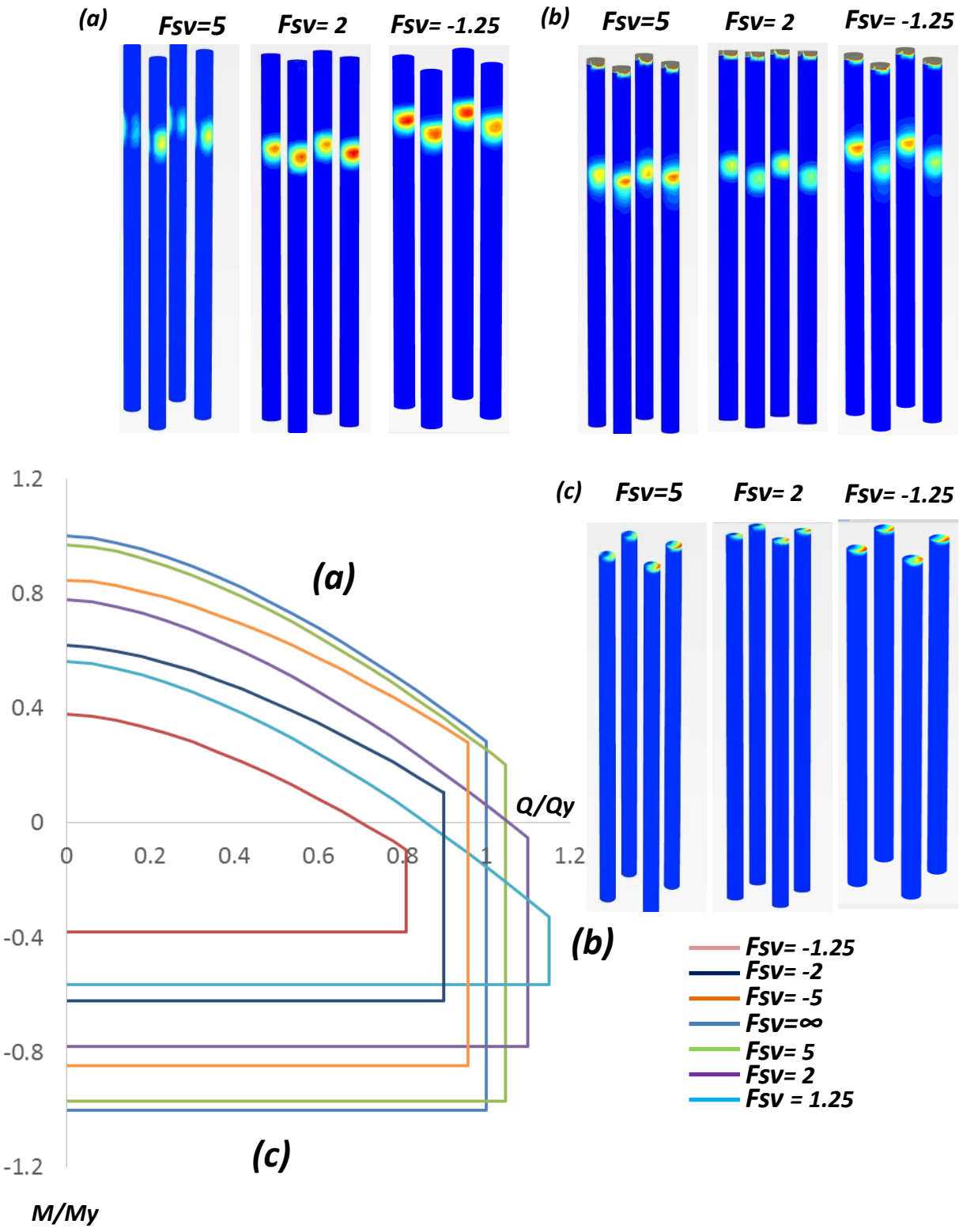

Figure 3.42 *Illustration of the plastic hinges of the piles for 3 distinct factors of safety against vertical loading for the three different failure mechanisms*

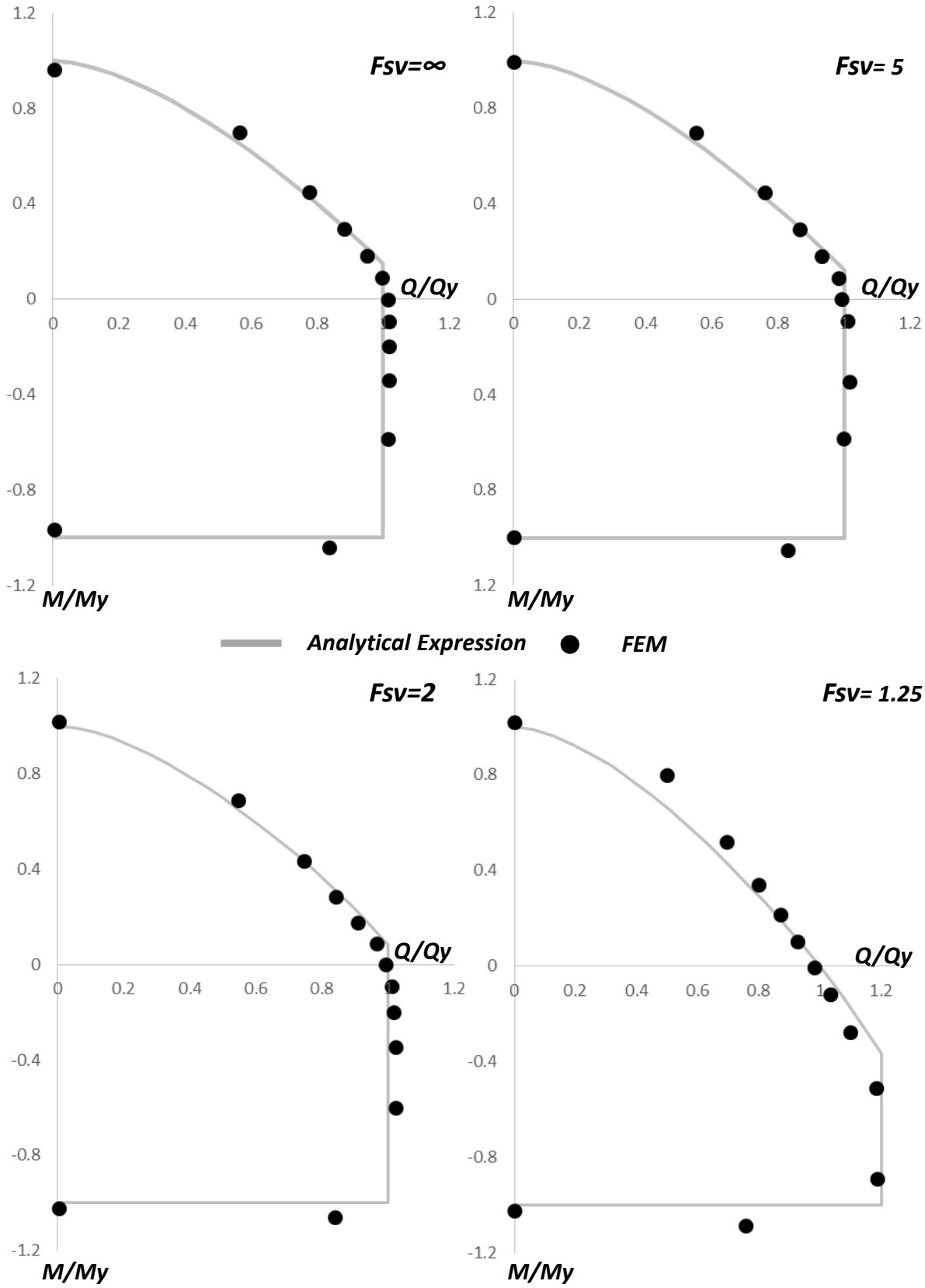

Figure 3.43(a) *Comparison between the data derived from the numerical experiments (points) and the analytical expression proposed for the yield surfaces of 2x2 pile-group in diagonal direction for 7 different factors, given in normalized values.*

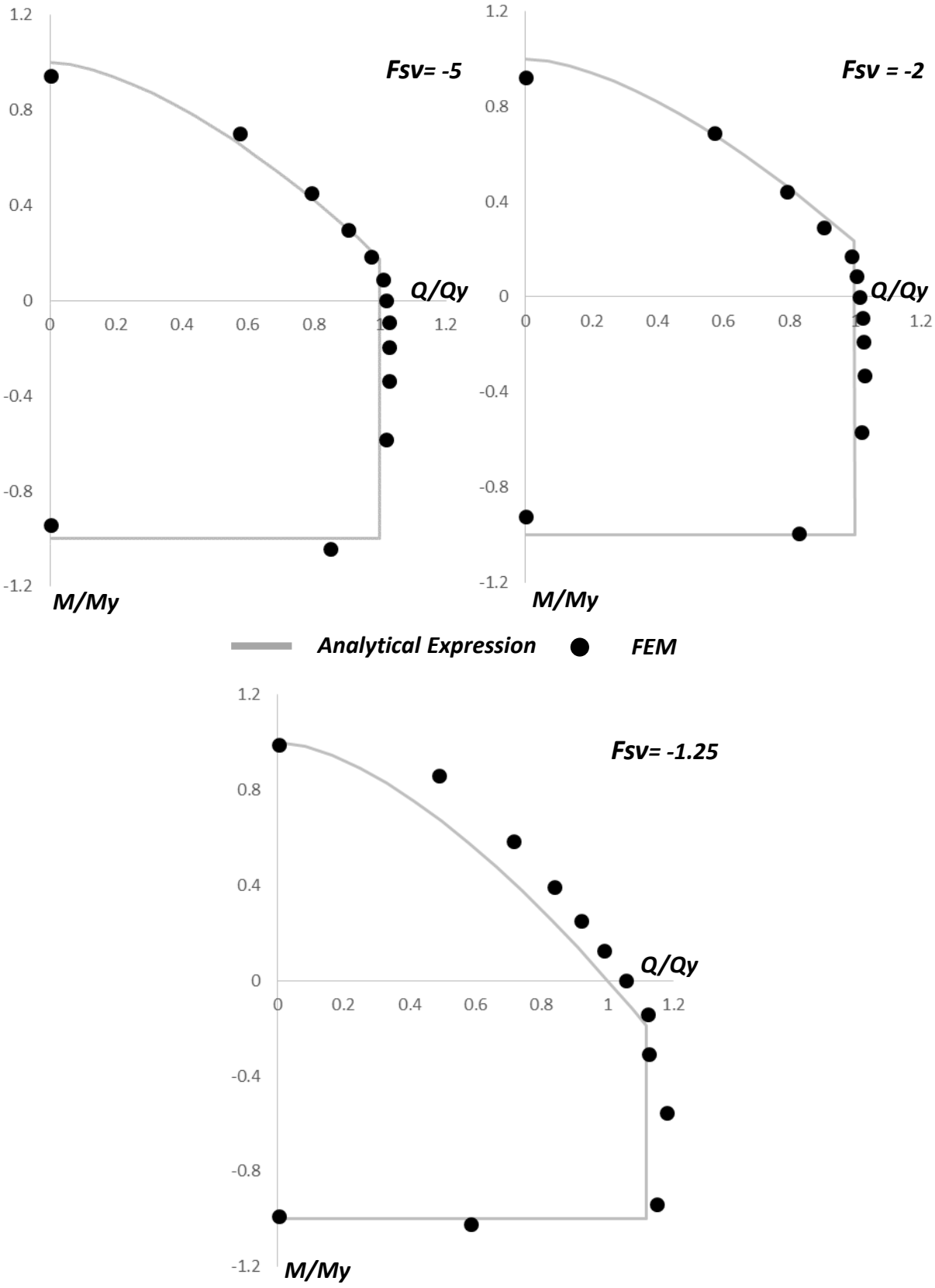

Figure 3.43(b) *Comparison between the data derived from the numerical experiments (points) and the analytical expression proposed for the yield surfaces of 2x2 pile-group in diagonal direction for 7 different factors, given in normalized values.*

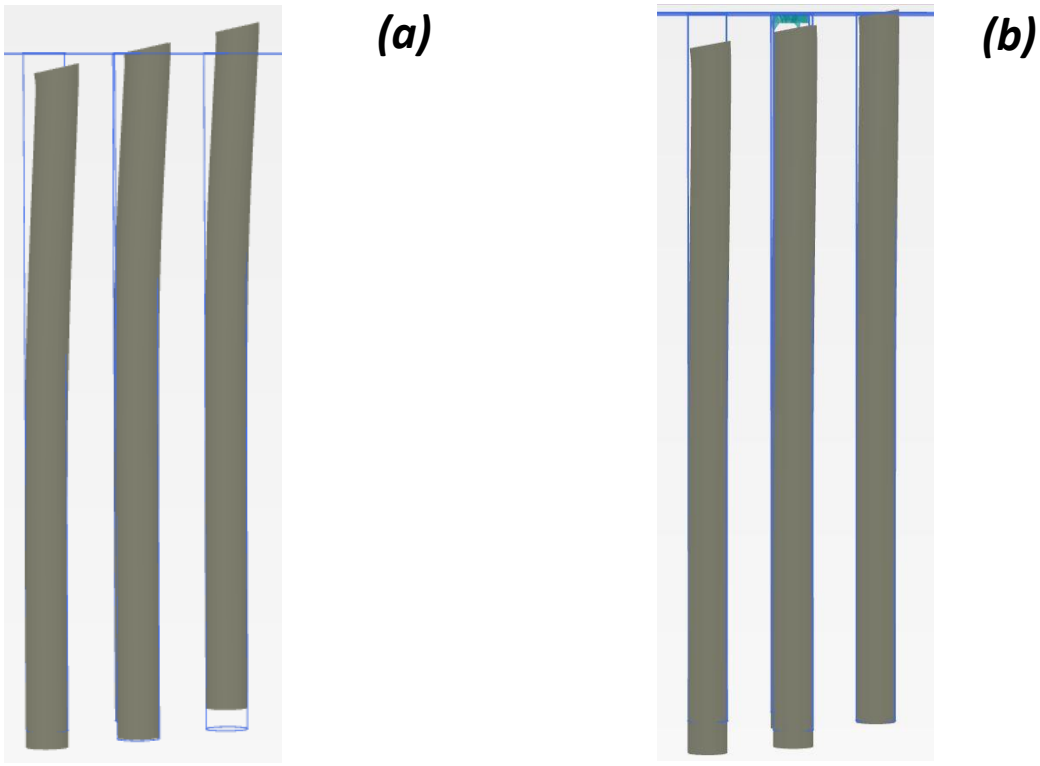

Figure 3.44 Illustration of the position of the pivot point at: ***(a)*** the head of the central piles for large factors of safety Fsv, ***(b)*** at the head of an outer pile for small factors of safety Fsv.

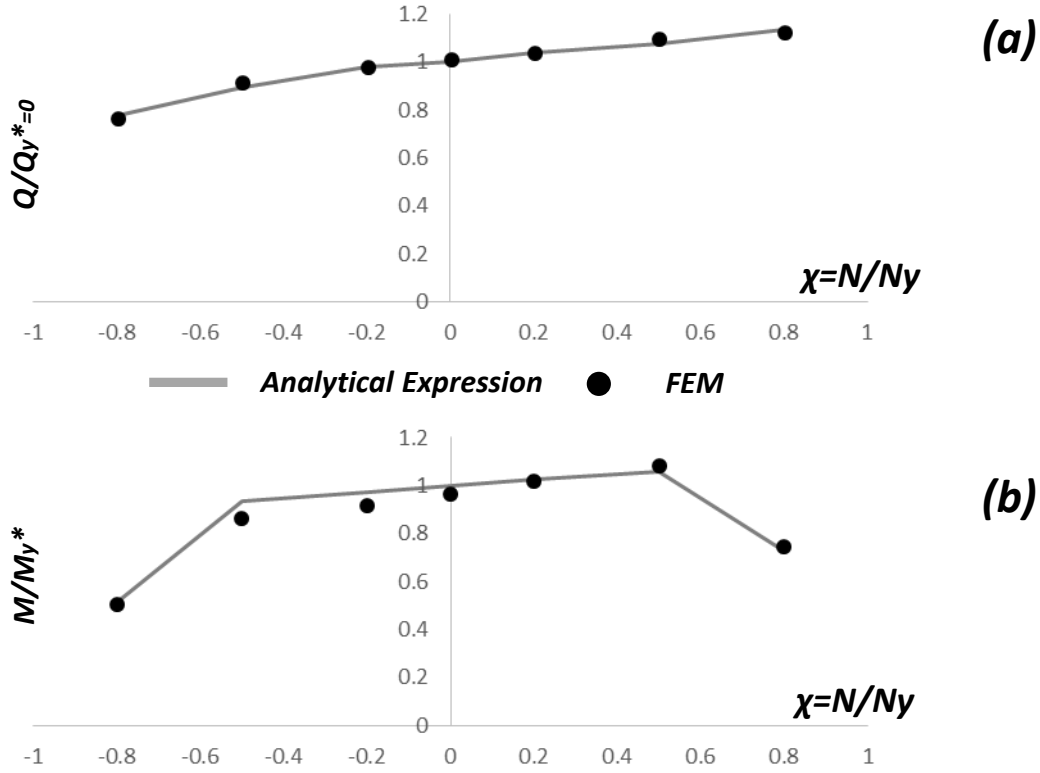

Figure 3.45 *The dimensionless* ***(α)*** *pure horizontal capacities* ***(b)*** *moment capacities of the 2x2 pile-group under combined loading in diagonal direction derived from the FE analyses (data points) are compared to the proposed analytical expression (lines).*

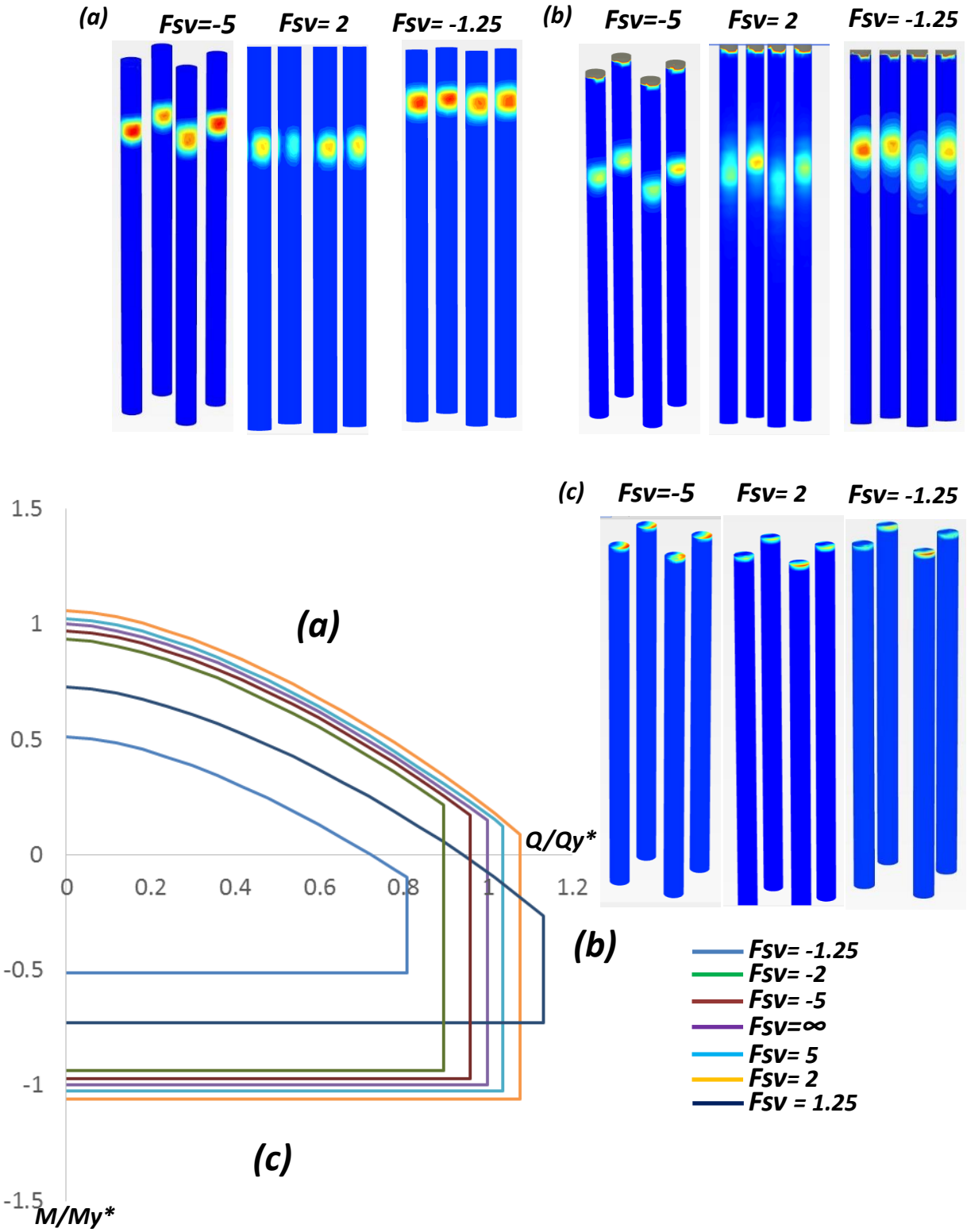

Figure 3.46 *Illustration of the plastic hinges of the piles for 3 distinct factors of safety against vertical loading for the three different failure mechanisms*

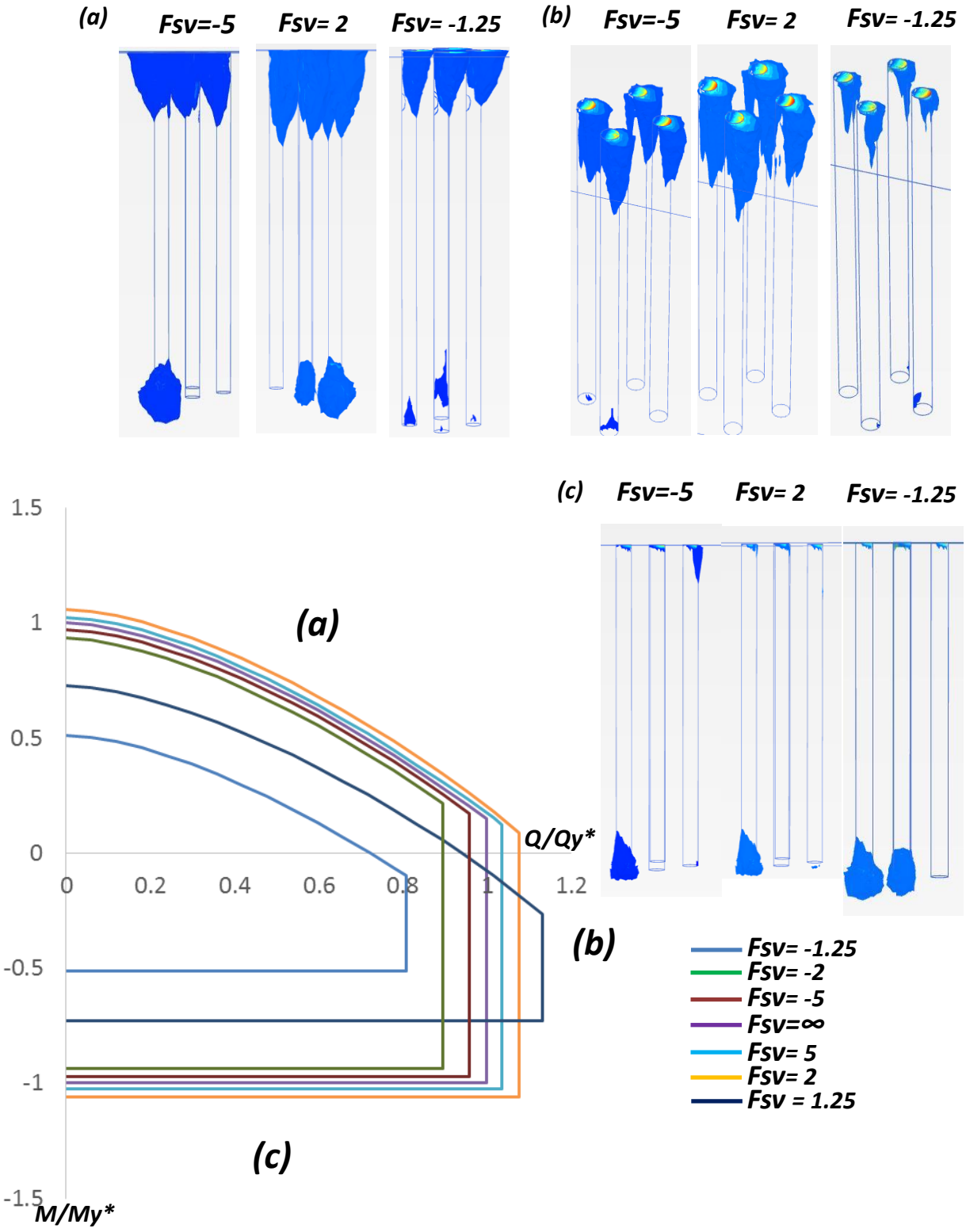

Figure 3.47 *Illustration of the the plastic strain magnitude contours for 3 distinct factors of safety against vertical loading for the three different failure mechanisms*

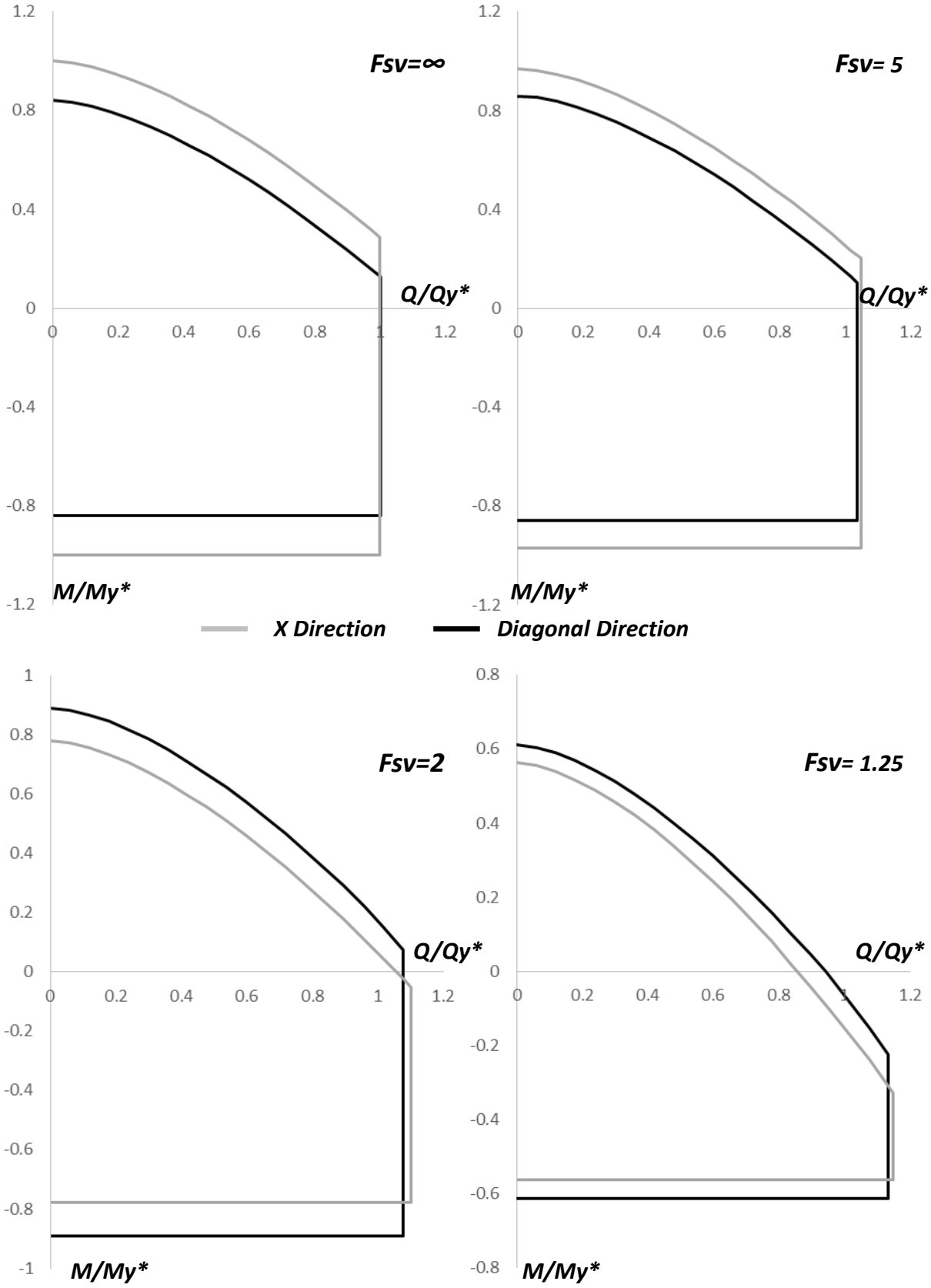

Figure 3.48(a) *Comparison between the 2x2 pile-group capacity under combined loading in x- and diagonal direction for the same factor of safety*

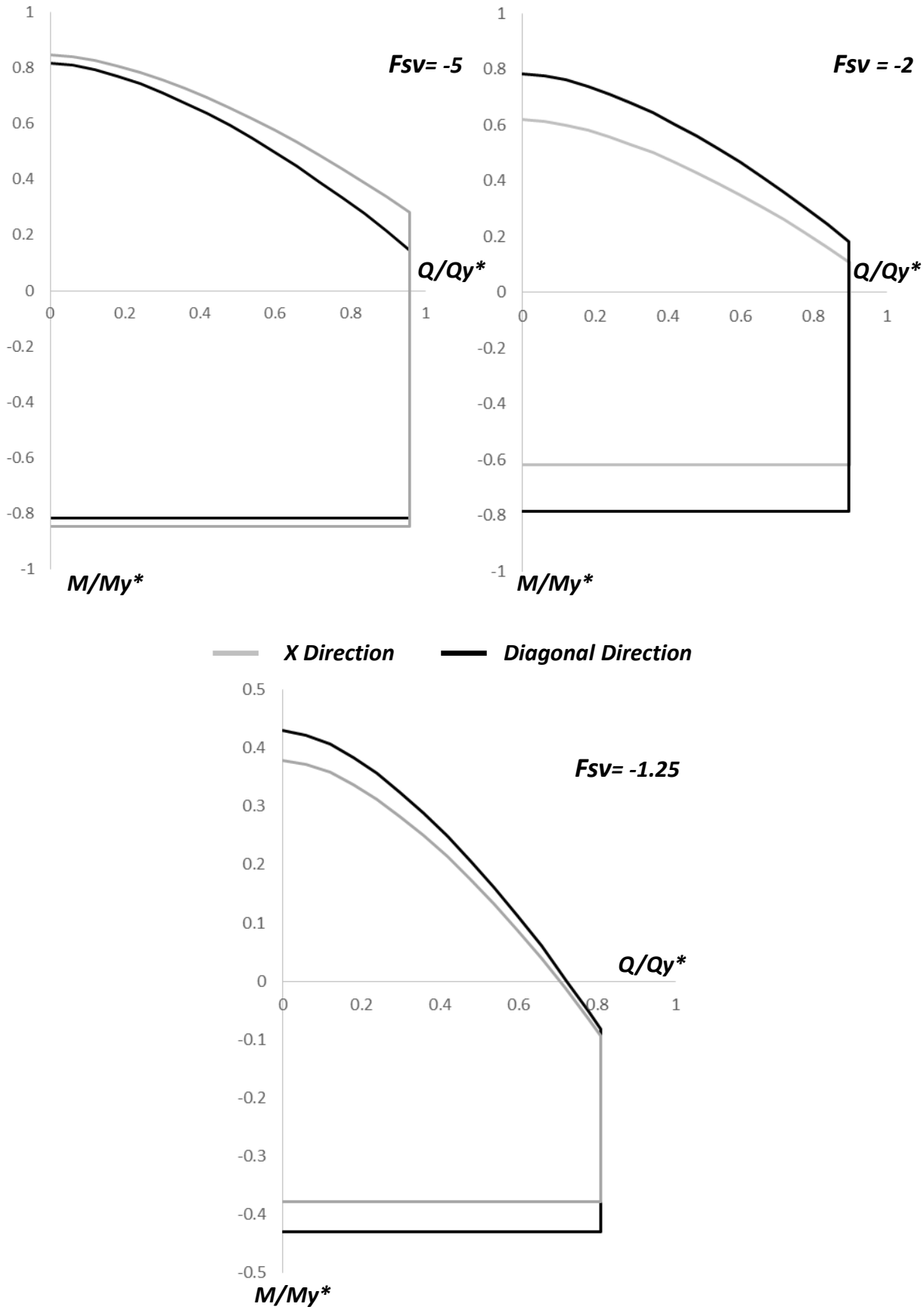

Figure 3.48(b) *Comparison between the 2x2 pile-group capacity under combined loading in x- and diagonal direction for the same factor of safety*

Chapter 4

Macroelement Modeling

4 Macroelement Modeling

4.1 Introduction

Many applications in civil engineering incorporate the uniform approach of the interaction effects observed in the structures, their foundations and the surrounding soil, which can display intense non-linear behavior, affecting the superstructure and its design. Due to the complicated, demanding, time consuming process for capturing the non- linear behavior of the soil and structure material and the geometrical non-linearities at the interface between the soil and the foundation (e.g. sliding, gapping, uplifting) geotechnical engineers have developed simplified mathematical models to encounter these kind of problems. These models can easily be installed in the software used by the structural engineers, in target of representing all these non-linearities at the level of the foundation, facilitating the precise dimensioning of the superstructure and the foundation. One basic category is the replacement of the surrounding soil with Winkler type springs **(*Fig.4.1*)**. In this method, the whole soil is substituted with uncoupled horizontal, vertical and rotational springs, which obey appropriate behavior rules (e.g. elastoplastic behavior). The assumption of the uncoupled springs has the advantage of the simple mathematical processing of the results, like the numerical integration of the local spring response with the aim of reproducing the general foundation behavior. The drawback of this model is the difficulty in the calibration of the spring parameters, which sometimes is insurmountable and at the same time this simplified assumption is unrealistic, as in all geotechnical problems the coupling of the various degrees of freedom is necessary. In the past, research has been conducted from various engineers for the representation of the foundation behavior in terms of Winkler modeling. *[Housner 1963; Chopra 1984; Chen and Lai 2003; Houlsby, Cassidy, Einav 2005; Einav, Cassidy 2005; Gerolymos and Gazetas 2006; Allotey, El Naggar 2007*].

A new category of mathematical modeling for the uniform reproduction of the soil-foundation interaction effects is developing the past years, which is based on the simulation of the total foundation system through macro-element modeling ***(Fig.4.2)***. In this case, the total soil-foundation system is replaced by a single element of 6 (3-D approach) or 3 (2-D approach) degrees of freedom, able to represent satisfactorily the systems behavior in terms of ''force-displacement'' in respect to a specific point of reference. [*Chatzigogos, Figini, Pecker and Salençon 2011*]. Extensive research has been performed in the specific model category for shallow foundations, which is related with the involvement of the plasticity theory. Roscoe και Schofield [*1956, 1957*] where the first who connected the study of foundations through a macro-element formulation with the plasticity theory. Nova και Montrasio [*1991*] through a series of experimental results managed to calibrate an elasto-plastic model of shallow foundation under the isotropic hardening law for the total soil-foundation system. This model was modified by Paolucci (1997) and extended by Pedretti (1997) for a more precise representation of the system behavior under cyclic loading. Crémer [*2001*] and Crémer et al. [*2001*] presented a more sophisticated macro-element model, by introducing two coupled response mechanisms:(a) the anelastic soil-foundation response and (b) the uplifting between the foundation and the soil under intense loading, providing the possibility of the independent activation of these two mechanisms depending the conditions of each examined problem.

In addition Le Pape and Sieffert [*2001*] used the model of Nova and Montrasio in scope of studying geotechnical earthquake engineering problems, basic their model to thermodynamic principals. Grange, Kotronis and Mazars [*2008*] developed an appropriate model for the representation of the circular shallow foundations behavior under 3 dimensional load. Finally Gerolymos and Souliotis [*2012*] have been one of the first macro-element approaches regarding caisson foundations.

It is clear that most research is focused on the shallow foundations, while almost none is done in the case for deeply embeeded and pile foundations. In this diploma thesis, one of the main goals is the compilation of an appropriate uniform mathematical tool through macro-element modeling, able to combine the mathematical expressions and the physical findings, in order to reproduce the

behavior of pile foundations without the need of new time-consuming 3-D finite element analysis. In the next sections the mathematical backround, the expressions and the laws combining all the tools for the macro-element model are presented, while its function is tested in comparison to the data derived from the numerical experiments.

4.2 Definition of the problem

The term Macro-element modeling originates from the scope of the macroscopic observation of the total foundation, providing the necessary information in terms of force-displacement and including all the mathematical and physical information in a single element. After determining all the theoretical aspects of the response of pile foundations, the quantification of the behavior through appropriate analytical expressions takes place, in target of incorporating them in the uniform mathematical tool presented in this chapter. Thus the connection between all those results and expressions through the correct laws and equations is performed and the examination of the validity of the model through the comparison with the results from the finite-element analysis.

Recent research has shown that the use of the laws and equations provided by the plasticity theory (work-hardening plasticity theory) can be immediate applicable in the elastoplastic foundation models for cohesive soils in undrained conditions [*Martin and Houlsby 2000*], while the soil-foundation system is replaced by a single element at under combined vertical, horizontal and moment load. It has been demonstrated that this approach provides better results in comparison to Winkler based model, as it is capable of representing fully realistically and easily the coupling between the various degrees of freedom, a point where the Winkler springs lack. Furthermore geotechnical engineers are already familiar with the physics that the work-hardening plasticity theory provides, because it has been utilized for the development of various constitutive soil material models (e.g. Cam-Clay constitutive model). It can macroscopically be claimed actually, that the application of the plasticity theory in the

pile foundation problems is the same with that used in the above mentioned constitutive laws, by simply replacing the appropriate parameters. The stresses and strains of the soil elements are substituted by the generalized loads (in 3-dimensional M-Q-N space) and the consequent displacements ((θ – u – v) respectively. Thus in the next sections the 4 main components [*Martin and Houlsby 2000*] of the process for developing the uniform mathematical tool are analyzed: (a) the definition of the elastic response of the foundation, through the appropriate elastic stiffness matrices for the active degrees of freedom, (b) the definition of the failure envelopes of the pile foundations (yield surfaces) in the generalized 3-dimensional M-Q-N space, which provide the limit between the elastic and the anelastic response of the system, (c) the definition of the appropriate plastic flow rule of the foundation's displacements, which provide the necessary information for the magnitude and the relation that have to each other the increments at the point of reference on the top of the foundation, at the time of the system's yielding, (d) the definition of the appropriate hardening law), which defines in which way and how much the plastic displacements influence the shape and the magnitude of the yield surfaces. During the development of the above mentioned components emphasis is given to the mathematical depiction of the process, while the physical perspective is already provided in the previous chapters of this thesis. In ***Fig.4.3*** a flowchart of the steps followed for the development of the macro-element formulation is provided, together with the influence of each of them to the response of the pile foundation in terms of 'force-displacement'.

In this thesis a macro-element model is developed able to simulate the behavior of a single flexible-pile foundation in cohesive soil and its expansion for a 1x2 pile-group.

4.3 Elastic Response

In order to capture the appropriate elastic response of pile foundations the suitable elastic stiffness matrices are formed. More specifically, for the representation of the foundation's behavior at small strains the correct stiffness expressions are selected from the bibliography for the horizontal and vertical degrees of freedom. These matrices associate the loads with the subsequent displacements and depend mainly

from the geometry of the foundation, its material properties and the elastic parameters of the soil.

In this thesis the monotonic load of the foundation under static condition is studied. Thus the elastic stiffness matrix at the top of the pile is formulated:

$$K_{el} = \begin{bmatrix} K_v & 0 & 0 \\ 0 & K_h & K_{hr} \\ 0 & K_{rh} & K_r \end{bmatrix} \quad \textbf{(4.1)}$$

where:

- K_v the elastic stiffness for the vertical direction
- K_h the elastic stiffness for the horizontal direction
- K_r the elastic stiffness against rotation
- $K_{hr}=K_{rh}$ the elastic interaction stiffness between the rotational and horizontal load

  The above mentioned parameters are according to Gazetas - Milonakis equal to:

$$K_v = E_p A_p \lambda \frac{\tanh(h\lambda) + \Lambda}{1 + \Lambda \tanh(h\lambda)} \quad \textbf{(4.2)}$$

$$K_h = 4E_p I_p g^3 \frac{\sin(2gh) + \sinh(2gh)}{-2 + \cos(2gh) + \cosh(2\,\mathrm{gh})} \quad \textbf{(4.3)}$$

$$K_r = 2E_p I_p g \frac{\sinh(2gh) - \sin(2\,\mathrm{gh})}{-2 + \cos(2gh) + \cosh h(2gh)} \quad \textbf{(4.4)}$$

$$K_{hr} = -2E_p I_p g^2 \frac{\cosh(2gh) - \cos(2gh)}{-2 + \cos(2gh) + \cosh(2gh)} \quad \textbf{(4.5)}$$

where:

$$\lambda = \sqrt{\frac{\delta G_s}{E_p A_p}}$$

$$\delta = \frac{2\pi}{\ln\left(\frac{5L(1-v)}{D}\right)}$$

$$\Lambda = \frac{Kb}{EpAp\lambda}$$

$$\mathrm{K}b = \frac{D \cdot Es}{1-v^2}$$

$$g = \left(\frac{kx}{4EpIp}\right)^{1/4}$$

$$kx = 1.2Es$$

Ep : Modulus of elasticity of the pile
Es : Modulus of elasticity of the soil
Ap : Area of the section of the pile
Ip : Moment of inertia of the pile
h : Depth of the tip of the pile
v : Soil's Poisson's ratio
D : Diameter of the pile
Gs : Soil's shear modulus of elasticity

The function of the above mentioned elastic stiffness matrix is displayed in ***Fig.4.4***, where only the head of the foundation is taken into account with the total properties of the soil-foundation system, while the rest of the pile and the surrounding soil are neglected.

4.4 Yield surfaces

The yield surfaces of pile foundations that are inserted in the model define the limit between the elastic and anelastic behavior of the soil-foundation system. Their shape and analytical expression are determined in a previous chapter of this thesis:

$$f = \left|\mathrm{sgn}(Q)\left(\frac{Q}{Qy}\right)^2 + \mathrm{sgn}(M)\left|\frac{M}{My}\right|\right| - 1 = 0 \qquad \text{for} \qquad \left|\frac{M}{My}\right| < 1 \qquad \textbf{(4.6)}$$

$$f = \left|\frac{M}{My}\right| - 1 = 0 \qquad \text{for} \qquad \left|\frac{M}{My}\right| = 1 \qquad \textbf{(4.7)}$$

$$f = \left|\frac{N}{Ny}\right| - 1 = 0 \qquad \textbf{(4.8)}$$

where:

$$Ny = Nt + (\frac{Nc}{2} - \frac{Nt}{2})(sign(N) + 1)$$

$$My = Mpl$$

$$Qy = \sqrt{2PyMpl}$$

Nc , Nt the ultimate compressive and tensile capacity respectively.

According to the above mentioned analytical expressions the estimation of the loading state of the pile foundation takes place. Knowing the geometry of the pile and the properties of the pile material and the soil (e.g. the undrained shear strength Su, the elasticity modulus) the total yield surfaces can be calculated and compared with the applied Load-Moment combination. Thus it is easily determined if the specific system behaves elastically or if the maximum capacity is reached.

Finally, after deriving the ultimate capacity of the foundation, the increments of the plastic displacements at the failure state are determined. In other words, the total representation of the post-elastic behavior of the pile is strived through the prediction of the developing plastic failure displacements through the adoption of an appropriate plastic flow rule.

4.5 Plastic flow rule

As it was previously proven by Gerolymos et al, and confirmed through the numerical experiments in this thesis, for the most accurate simulation of the pile foundation behavior in cohesive soil the election of an associated plastic flow rule with the connected consequence of the normality of the strains to the failure envelopes of the foundation is proposed. The use of the specific flow rule is convenient too, as

there is no need for the extraction of a new equation that would represent the plastic potential at the failure of the foundation, but the use of the same expressions is adequate. Thus the associate plastic flow rule is expressed in the following form:

$$\begin{Bmatrix} \partial w^{pl} \\ \partial u^{pl} \\ \partial \theta^{pl} \end{Bmatrix} = \begin{Bmatrix} \dot{w}_{pl} \\ \dot{u}_{pl} \\ \dot{\theta}_{pl} \end{Bmatrix} = \lambda \begin{Bmatrix} \dfrac{\partial f}{\partial N} \\ \dfrac{\partial f}{\partial Q} \\ \dfrac{\partial f}{\partial M} \end{Bmatrix} \qquad \textbf{(4.9)}$$

The above mentioned equations connect the alteration of the yield equation f in respect to the M, Q, N loads with the relative plastic displacements at the failure state. λ is a non-negative multiplication factor, which represents the magnitude of the plastic displacements at the failure, in respect to the M/Q/N ratio, under the basic presupposition that an elastoplastic load step remains on the yield surface [*Cassidy, Martin, Houlsby 2004*]. More specifically for the prediction of the development of plastic displacements the calculation of the partial derivatives of the yield function f is needed.

4.6 Hardening law

In a mathematical model, as the one developed in this thesis, that is based on the plasticity theory, the macroscopic foundation behavior in F-δ terms is determined exactly in the same way as in the soil material constitutive models, through a stress-strain relation: the load is applied increasingly and the mathematical model calculates numerically the up-to-date tangent stiffness matrices of the system at each step, producing the equivalent displacements. As in the classic plasticity theory, the change of a load vector of the foundation system in the yield surface leads to the development of elastic displacements exclusively. A load route that intersect the above mentioned yield surface (and remains on it) produces plastic displacements,

the incremental components of which are determined from the plastic flow rule that is adapted and the appropriate hardening law. E.g. Cassidy et al. [2004] developed a mathematical model based on plasticity theory for the study of the response of spudcan foundations used in offshore engineering. As displayed in ***Fig. 4.5.*** their project was based at the hardening law that depends exclusively at the vertical displacement of the soil-foundation system (singe- surface strain- hardening plasticity model), affecting the development of the yield surface in respect to the magnitude of the vertical load, as due to the special geometry of the specific foundation type, the embedment level depends principally to the vertical load applied and the consequent plastic vertical plunge. Thus the increase of the vertical load, magnifies the embedment extent, but also the system is closer to the maximum failure capacity in 3-dimensional M-Q-N space.

In the macro-element model developed here, a hardening law dependent to the produced work of the system is adopted (work-hardening plasticity theory). F is the vector of the load and δ the vector of the developed displacement. Thus the produced work W is equal:

$$W = F \cdot \delta , \qquad \textbf{(4.10)}$$

where:

$$F = \begin{Bmatrix} N \\ Q \\ M \end{Bmatrix} \text{ and } \delta = \begin{Bmatrix} w \\ u \\ \theta \end{Bmatrix}$$

As it is displayed in ***Fig.4.6.*** the pile foundation response is studied per ΔF steps, calculating the up to date tangent stiffness matrix of the system and by inverting it the increments of the displacement vectors are determined. Moreover three hardening parameters are inserted, able to describe every aspect of the studied foundation system: (a) parameter a, (b) parameter n and (c) parameter couple b and g.

Hardening parameters

(a) Monotonic load parameters.

The hardening parameter n controls the transition rate between the elastic part of the response to the yield state. A large value of the parameter n (e.g.10) depicts carefully a bilinear diagram ‘’force-displacement’’, while small values provide a smoother transition between the two areas, while plastic displacements occur even in low load levels. In ***Fig. 4.7*** the role of the n parameter is depicted according to Gerolymos and Gazetas (2006).

Moreover the parameter a defines the magnitude of the observed hardening and is equal with the ratio of the soil-foundation system after the yielding to the elastic one. In ***Fig 4.8*** the influence of parameter a in monotonic curves is presented. In the mathematical tool developed in this chapter, the most significant role has parameter n, while parameter a does not have a great effect on the results (a=1‰).

(b) load-reload parameters

The parameter couple b and g controls the shape of the load-reload curves (general shape of the loops under 6) cyclic loading). Gerolymos and Gazetas (2006) distinguish four basic shapes of loops depending on the b and g relation (***Fig.4.9***): i) when b-g=0.5,the stiffness at the opposite loading is equal with the stiffness of the principal loading, satisfying Masing criterion,(ii) when b=1 and g=0, where the loop degenerates into the monotonic curve(nonlinear elastic behavior, suitable for the representation of geometrical nonlinearities, but inappropriate for the elastic response of soil material), (iii) when b=0 and g=1 where the loop has a wider shape and the unload-reload stiffness much larger than the principal one and (iv) when b=0.9 and g=0.1, where the system response is similar to a nonlinear anelastic behavior. In this thesis b=g=0.5 is selected, due to the precision provided to the results.

4.7 Compilation of the uniform mathematical tool

Within the framework of deformation theory of classical elastoplasticity, the incremental total generalized displacement, *du* (displacements and rotations) is decomposed into the elastic and plastic components du^e and du^p by a simple superposition:

$$du = du^e + du^p \qquad \textbf{(4.11)}$$

The plastic strain increment is obtained from the flow rule:

$$du^p = \langle \lambda \rangle \frac{\partial g}{\partial F} \qquad \textbf{(4.12)}$$

In which *F* is the force vector in M-Q-N (moment, shear and axial forces) space.

Equation (2.2) implies normality to the plastic potential function g. *L* is a positive scalar of proportionality designated as the loading index. Substituting ***Eq. (4.12)*** into ***Eq. (4.11)*** and applying elasticity theory, the following generalized displacement generalized force relationship is obtained:

$$dF = K^e \left(du - \langle \lambda \rangle \frac{\partial g}{\partial F} \right) \qquad \textbf{(4.13)}$$

in which *Ke* is the elastic matrix. For a perfectly plastic material, the yield surface is fixed in stress space, and therefore plastic deformation occurs only when the stress path moves on the yield surface. Thus, the loading condition at failure is postulated by the following consistency equation:

$$df = 0 \Rightarrow \left(\frac{\partial f}{\partial F} \right)^T dF = 0 \qquad \textbf{(4.14)}$$

Combining ***Eqs (4.13)*** and ***(4.14)***, and after some algebra, the generalized displacement-generalized force relationship is reformulated into:

$$dF = K^{ep} du \qquad \textbf{(4.15)}$$

in which K^{ep} is the elasto-plastic matrix, given by:

$$K^{ep} = K^e \left[I - \Phi_g \left(\Phi_f{}^T K^e \Phi_g \right)^{-1} \Phi_f{}^T K^e \right]$$

(4.16)

in which *Φf* and *Φg* account for the failure surface and plastic flow rule, respectively:

$$\Phi_f = \frac{\partial f}{\partial F}, \Phi_g = \frac{\partial g}{\partial F} \qquad \textbf{(4.17)}$$

Due to the associated plastic flow rule:

$$\Phi_f = \Phi_g \qquad \textbf{(4.18)}$$

Hardening and hysteretic behavior is introduced by inserting the matrices *H1*, *H2* and hardening *parameter a* into ***Eq. (4.16)***:

$$K^{ep} = \begin{bmatrix} 1-a & 0 & 0 \\ 0 & 1-a & 0 \\ 0 & 0 & 1-a \end{bmatrix} K^e (I - BH_1H_2) + \begin{bmatrix} a & 0 & 0 \\ 0 & a & 0 \\ 0 & 0 & a \end{bmatrix} K^e \qquad \textbf{(4.19)}$$

where:

$$H_1 = \begin{bmatrix} (f(M,Q,N)-1)^n & 0 & 0 \\ 0 & (f(M,Q,N)-1)^n & 0 \\ 0 & 0 & (f(M,Q,N)-1)^n \end{bmatrix}$$

$$H2 = \begin{bmatrix} b + g \cdot sign(\Delta W) & 0 & 0 \\ 0 & b + g \cdot sign(\Delta W) & 0 \\ 0 & 0 & b + g \cdot sign(\Delta W) \end{bmatrix}$$

The terms in matrix *H1 and H2* are functions of the dimensionless hardening parameters *n, b, g* which are of the Bouc-Wen type (Gerolymos and Gazetas, 2005), Finally *B* is the abbreviation of the right-hand side term inside the parentheses of ***Eq. (4.16)***:

$$B = \Phi_g \left({\Phi_f}^T K^e \Phi_g \right)^{-1} {\Phi_f}^T K^e$$

For the expansion of the model in order to simulate a 1x2 pile-group the above mentioned matrices are extended to contain the properties of two piles and X is introduced to incorporate the interaction between the degrees of freedom of the piles and the transference of the loads and displacements to the pile-cap and vice versa.

$$X = \begin{bmatrix} 1 & 0 & x \\ 0 & 1 & 0 \\ 0 & 0 & 1 \end{bmatrix}, \qquad \textbf{(4.20)}$$

where x the distance of each pile from the center of the pile-cap.

4.8 Results

In ***Fig. 4.10*** to ***4.14*** the results of the developed model are presented, in scope of simulating the soil-pile and soil-pile-group system with one unique macro-element. More precisely the monotonic f-δ curves on the top of the foundation are displayed, as they were calculated through the mathematical tool and the derived data from the numerical experiments for various safety factors and load combinations.

In all cases, there is remarkable matching between the two methods in terms of horizontal load- horizontal displacement, vertical load-vertical displacement and moment-rotation. The precision of the mathematical tool appears not only in the

small strain region (elastic behavior), were the behavior of the system is ruled by the elastic stiffness matrix, but also in the failure area, where the response is governed by the associated plastic flow rule and the proportional yield surfaces of the foundation. In addition in the transition zone between the two above mentioned regions, where the system behavior is ruled by both the hardening law and the tangent stiffness matrices the fitting is more than satisfactory. This leads to the conclusion that every single component of the mathematical tool was carefully extracted, calibrated and designed in order to achieve the excellent capture of the foundation behavior. Thus the model is ready to be used through the appropriate changes in other types of soil too.

Another way to verify the correct simulation of the foundation and the usability of the method is by performing swipe tests, i.e. by introducing to the model instead of a combination of loads a combination of displacements until the systems failure. ***Fig.15-17*** show the excellent function of the model.

The model is extended by connecting two single piles by the appropriate kinematic constraints. Again, the matching between the prediction of the macroelement and the curves derived by the numerical experiments is more than satisfactory, as it is displayed in ***Fig. 4.18-20.*** The results are admirable, as the model is able to simulate the load distribution in the foundation system, i.e. the coupling between the moment and the axial force, the moment and the lateral force, the alteration of the plastic moment resistance of the pile material either by the axial load or the component of the moment that is distributed to the foundation as moment. In ***Fig.4.21*** and ***Fig.22*** the above mentioned mechanisms, verifying the appropriate function of the mathematical model, but also capturing the physical failure mechanism of the pile-group.

Figures

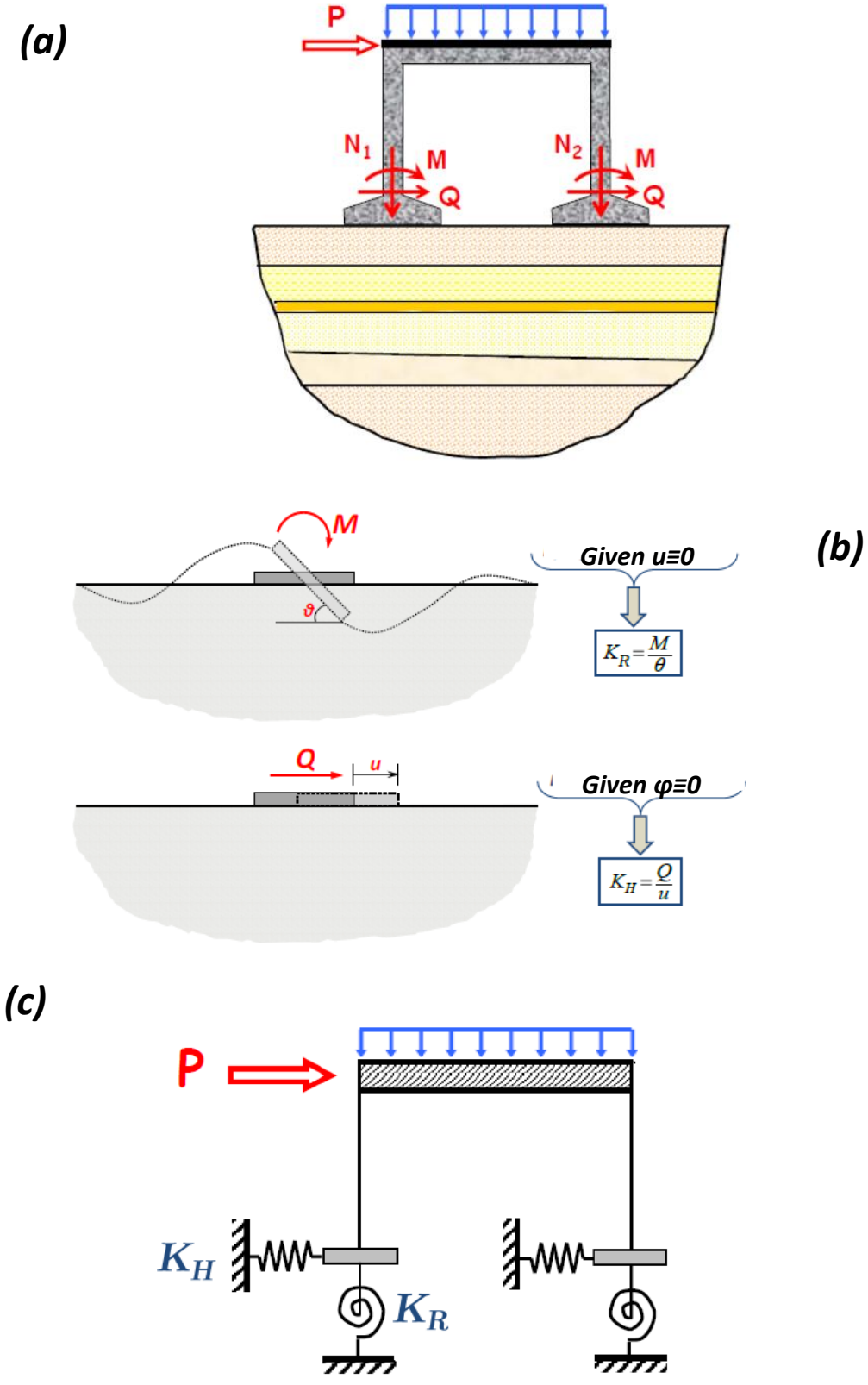

Figure 4.1 *The concept of using uncoupled Winkler springs:* ***(a)*** *structure grounded on a random layered soil,* ***(b)*** *uncoupled application of moment and horizontal force, determination of the stiffness coefficients and* ***(c)*** *substitution of the soil with the calculated springs*

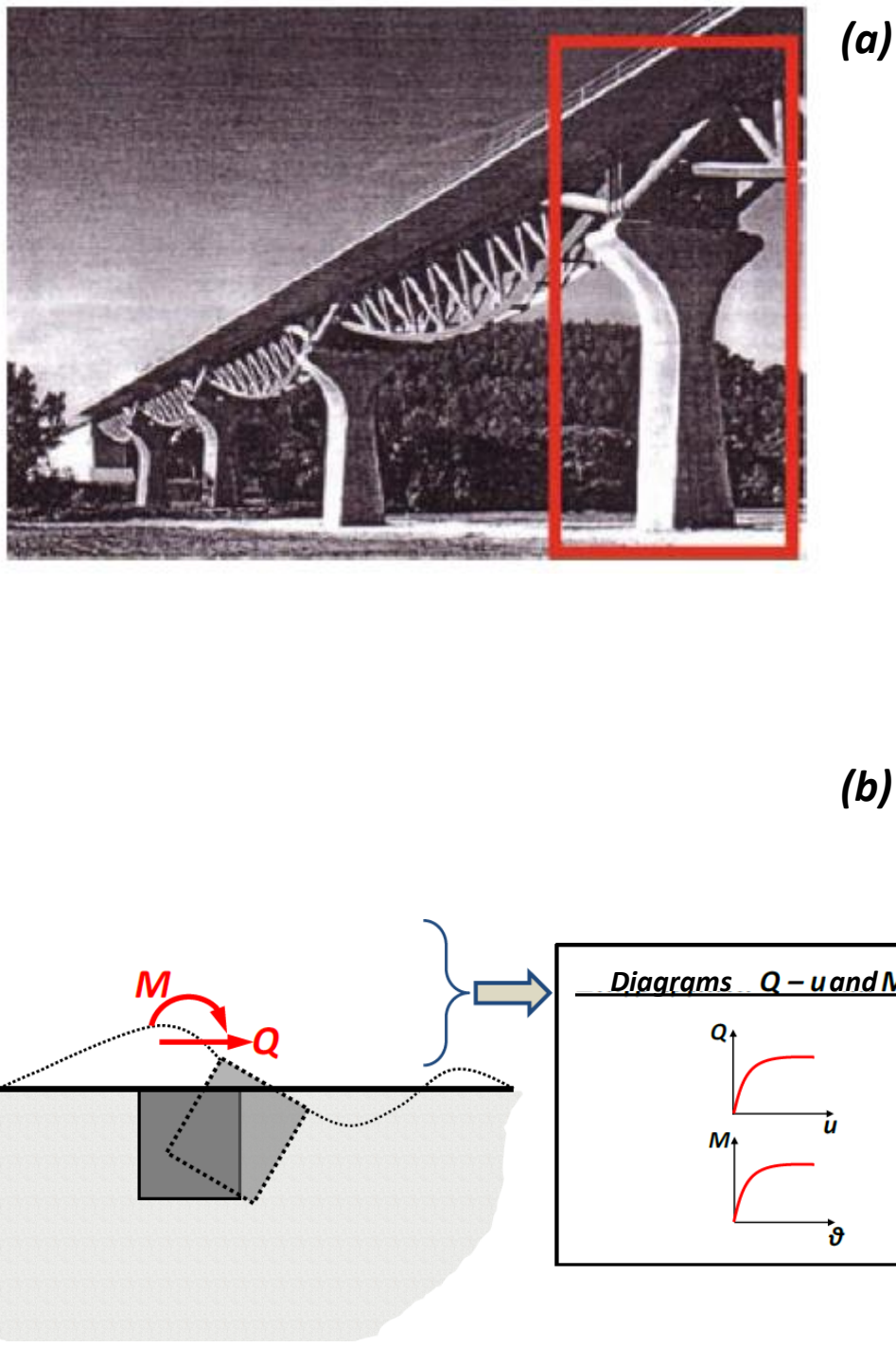

Figure 4.2 *The concept of simulating the foundation system with a macro-element: (a) conventional bridge pier grounded on a foundation (b) lateral loading of the foundation and extraction of the force displacement, moment-rotation curves (c) substitution of the soil and the foundation with a unique macro-element, able to reproduce the foundation system behavior, using as tools the above mentioned diagrams*

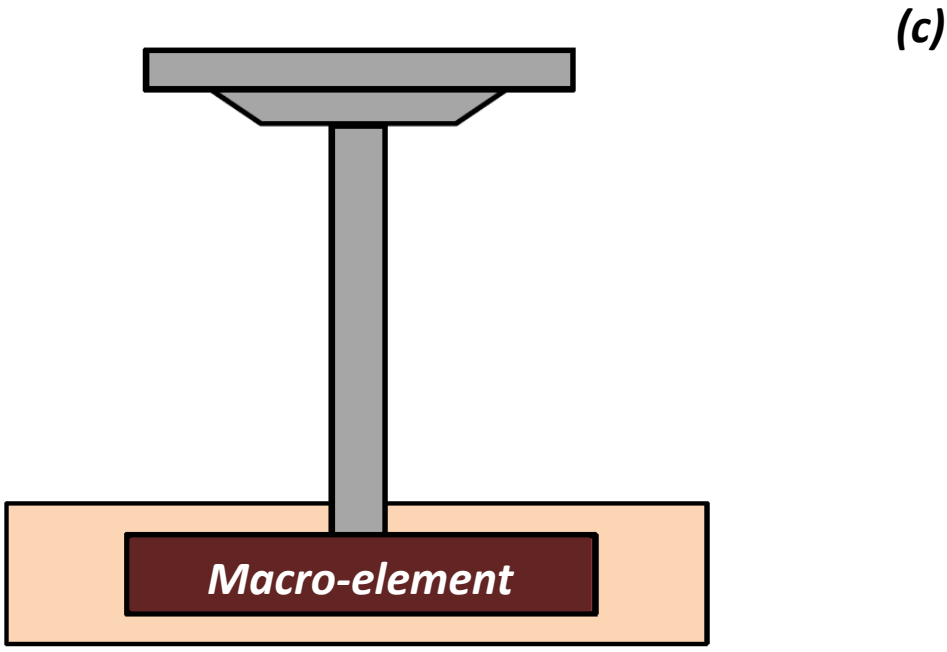

Figure 4.2 *The concept of simulating the foundation system with a macro-element: (a) conventional bridge pier grounded on a foundation (b) lateral loading of the foundation and extraction of the force displacement, moment-rotation curves (c) substitution of the soil and the foundation with a unique macro-element, able to reproduce the foundation system behavior, using as tools the above mentioned diagrams*

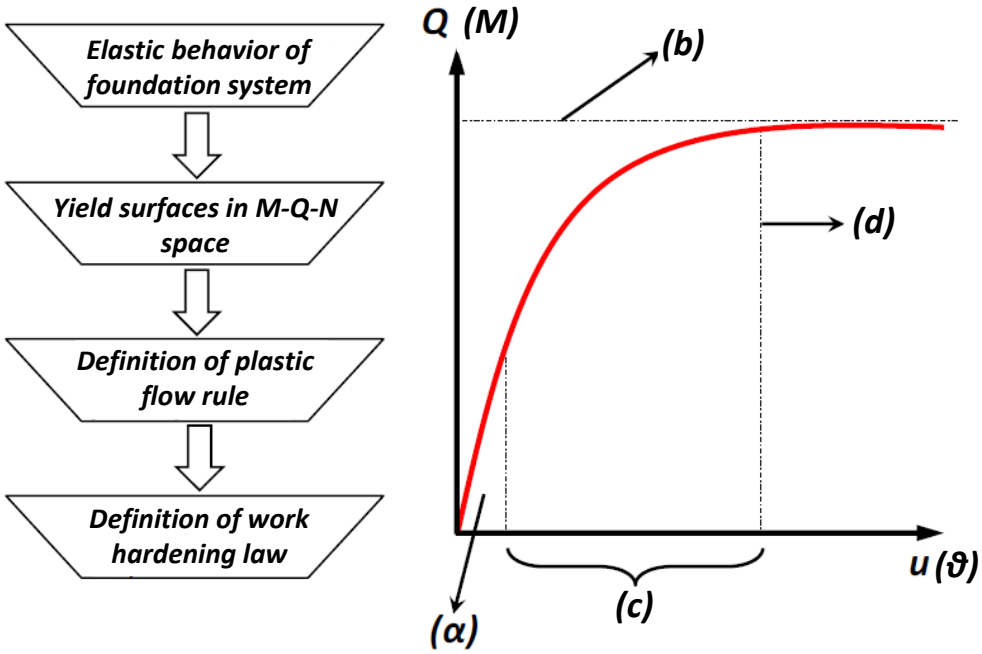

Figure 4.3 *The four components- steps for the development of a macro-element and their influence in the force-displacements diagrams.*

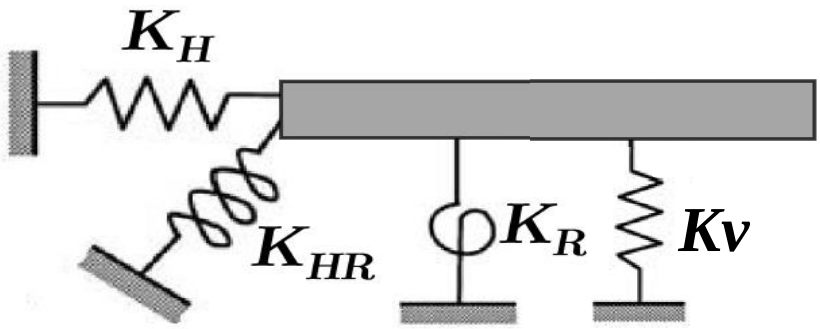

Figure 4.4 *Depiction of the elastic stiffness components on the head of the pile foundation, where the rest of the foundation and the surrounding soil are neglected (as far as the elastic part of the response is concerned).*

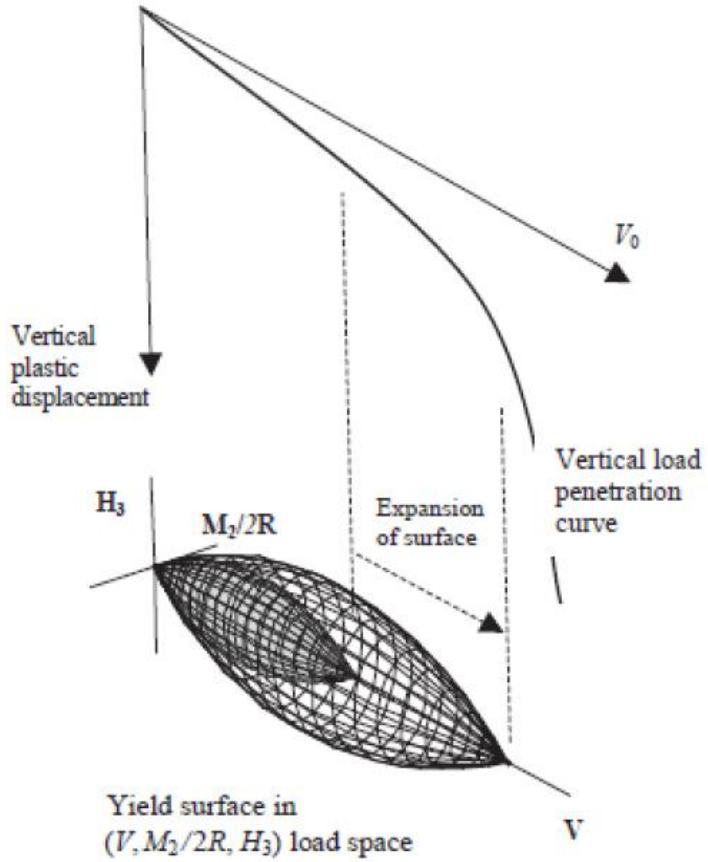

Figure 4.5 *Hardening law adapted by Cassidy et al. [2004] for the analytical expression of the response of spudcan foundations. The magnitude of the system's hardening depends on the level of the plastic vertical displacement. (strain- hardening plasticity model).*

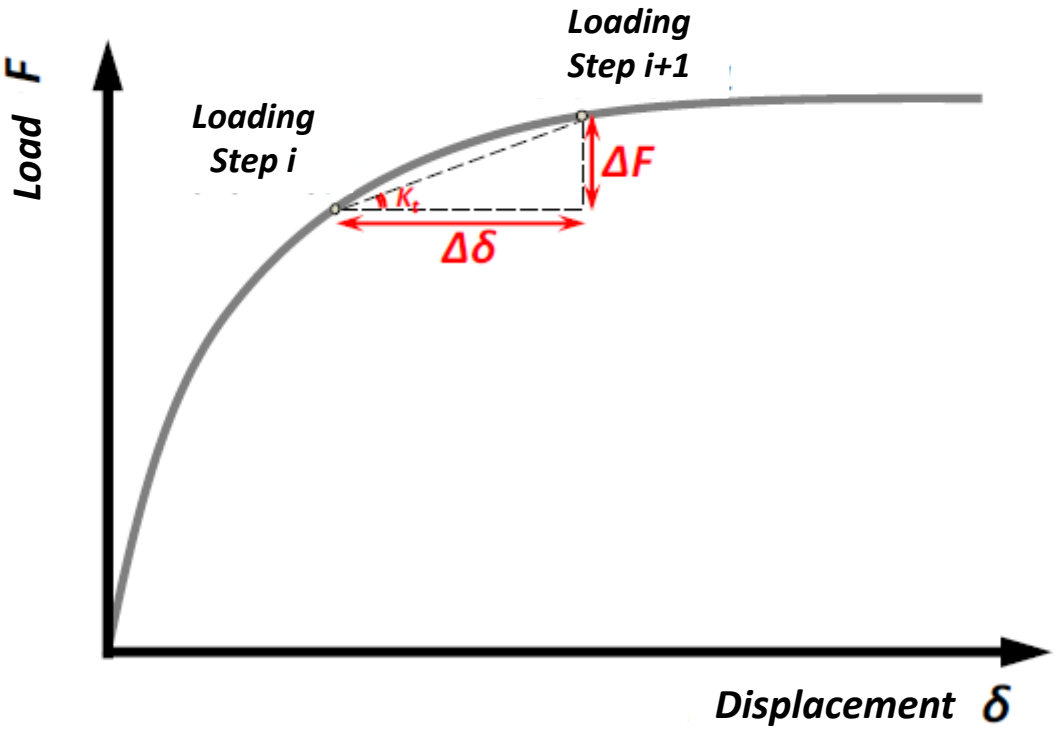

Figure 4.6 *The iterative development procedure of the mathematical tool: in step I the tangent stiffness matrix Kt is calculalted and the subsequent displacement Δδ is derived until the next loading step i+1. The shorter that is the step ΔF between two load steps, the preciser the procedure.*

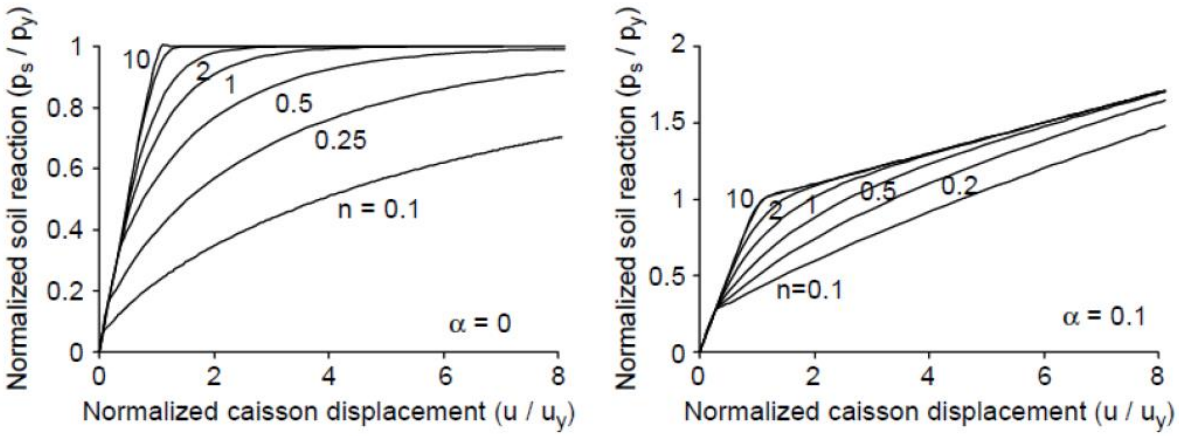

Figure 4.7 *Illustration of the influence of the hardening parameter n in the shape of the monotonic ''F-δ'' curves, for two values of the parameter a: (i) a = 0 and (ii) a = 0.1.*

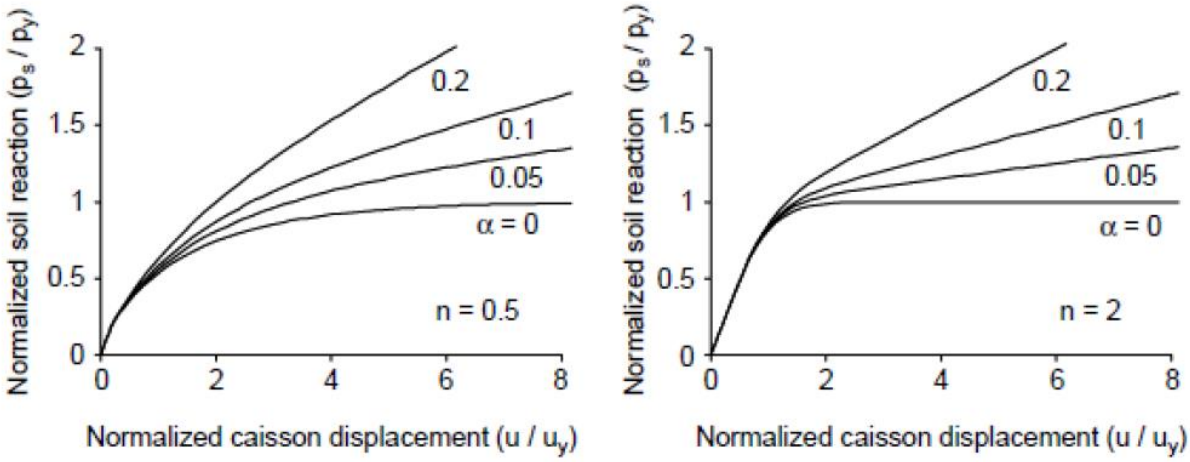

Figure 4.8 *Illustration of the influence of the hardening parameter a in the shape of the monotonic ''F-δ'' curves, for two values of the parameter n: (i) n = 0.5 and (ii) n = 2.*

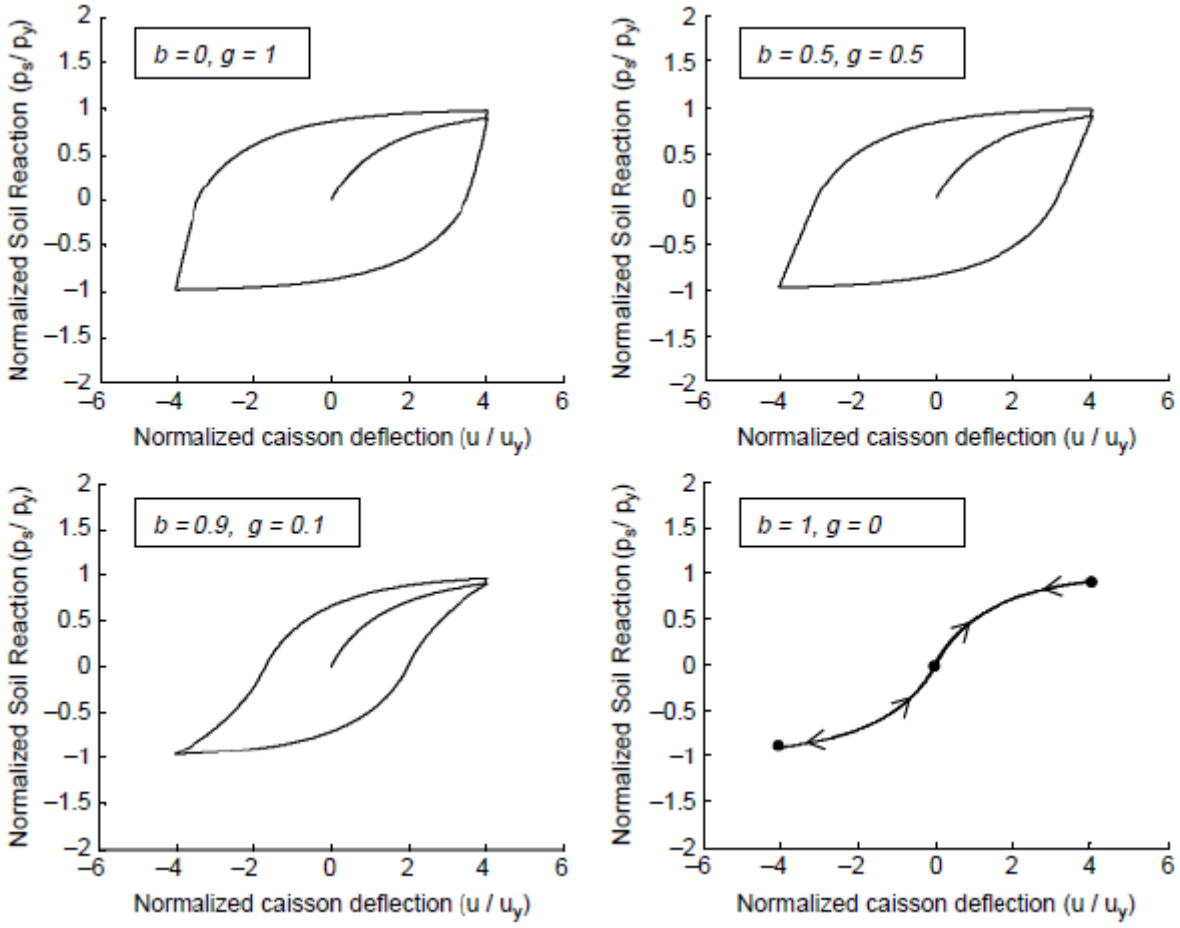

Figure 4.9 *Representation of the influence of the hardening parameters b and g, in the shape of the loops of embedded foundations (under cyclic loading). Four characteristic value couples can be identified [Gerolymos and Gazetas 2006]. In the present thesis, the values b = g = 0.5 are adopted, that satisfy the Masing criterion.*

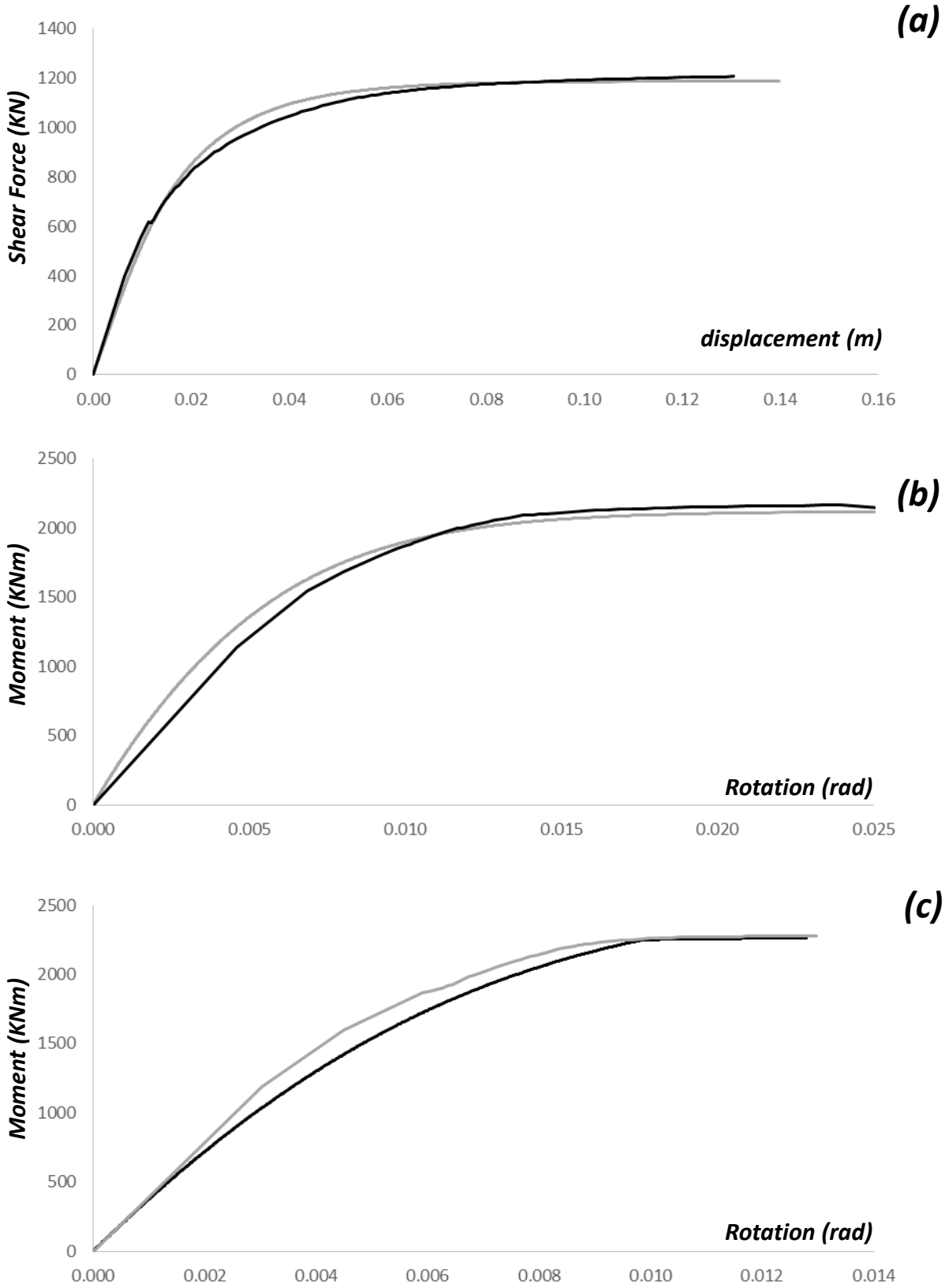

Figure 4.10 *Diagrams of (a) Force displacement for pure shear load for Fsv=∞, (b) Moment – rotation for pure moment for Fsv=∞, (c) Moment – rotation for pure moment for Fsv=5. With black lines are the curves extracted from the numerical experiments and with gray the prediction of the macro-element model*

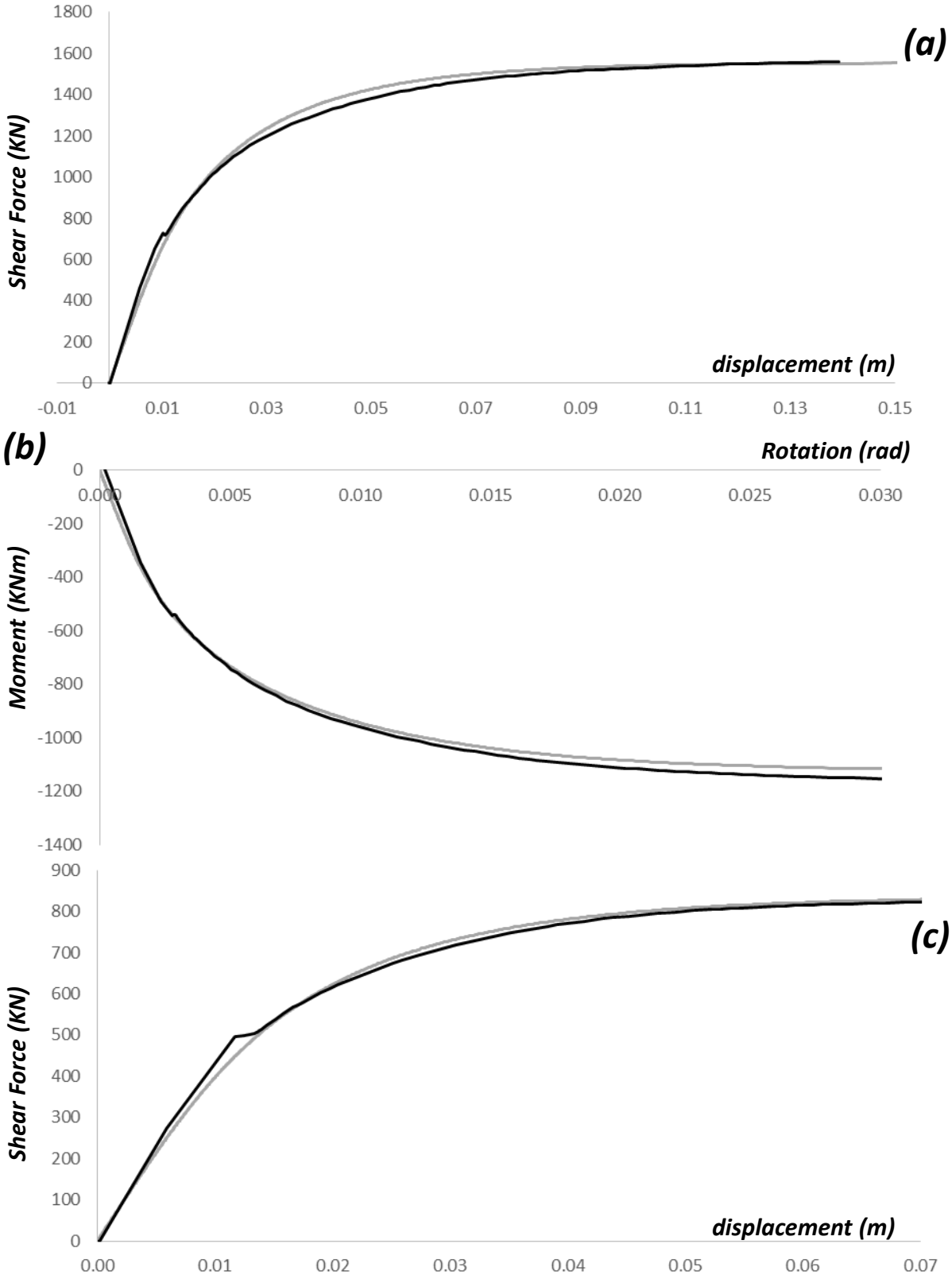

Figure 4.11 *Diagrams of (a) Force displacement for combined shear force – moment (ϑ=-36°) for Fsv=∞, (b) Moment – rotation for combined vertical force – moment (ϑ=-36°) for Fsv=∞, (c) Force displacement for combined shear force – moment (ϑ=52°) for Fsv=∞. With black lines are the curves extracted from the numerical experiments and with gray the prediction of the macro-element model*

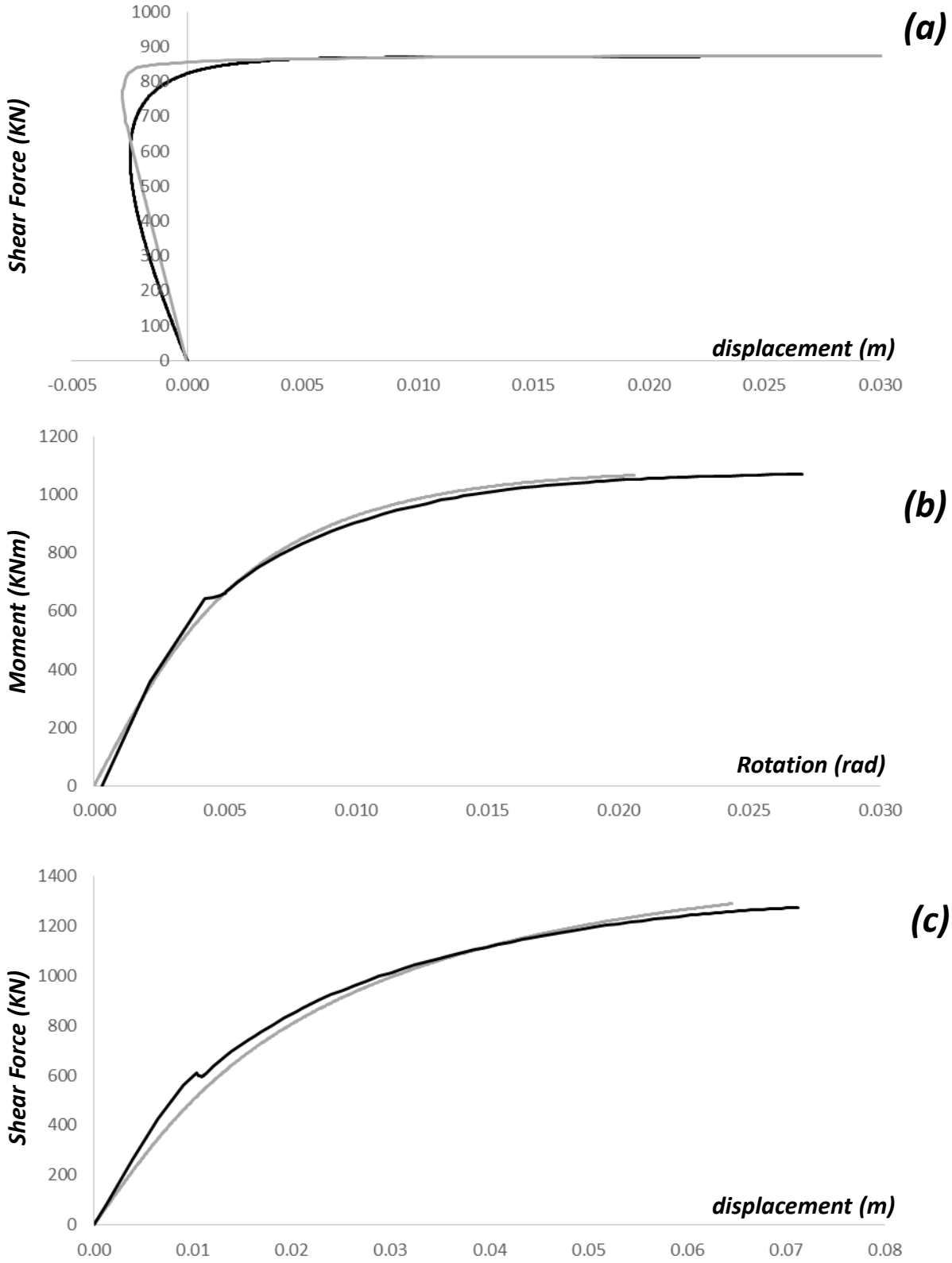

Figure 4.12 *Diagrams of (a) Force displacement for combined shear force – moment (ϑ=-70°) for Fsv=∞, (b) Moment – rotation for combined shear force – moment (ϑ=52°) for Fsv=∞, (c) Force pure vertical load for Fsv=2. With black lines are the curves extracted from the numerical experiments and with gray the prediction of the macro-element model*

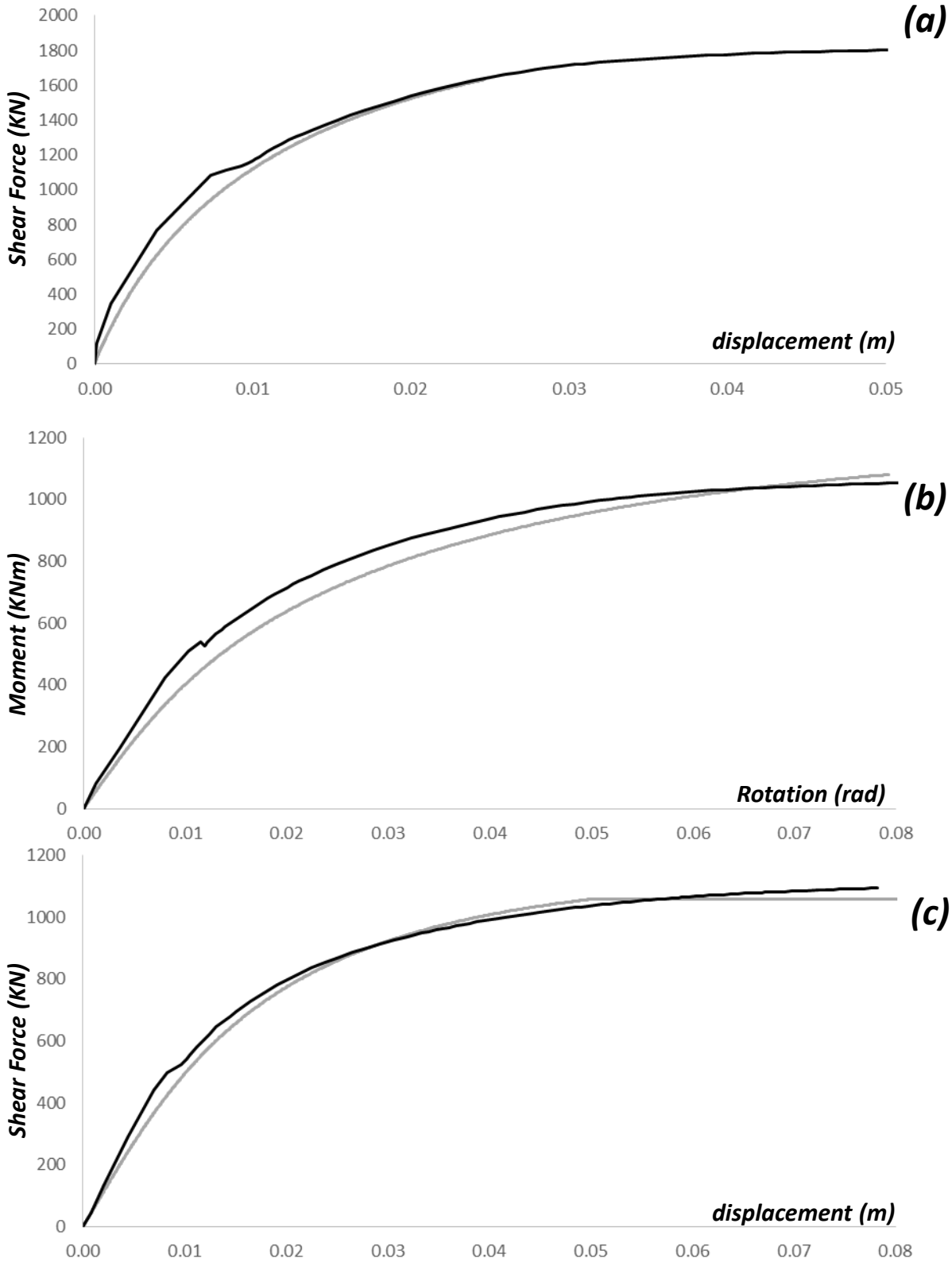

Figure 4.13 *Diagrams of (a) Force displacement for combined shear force – moment ($\vartheta=70^o$) for Fsv=2, (b) Moment – rotation for combined vertical force – moment ($\vartheta=36^o$) for Fsv=2, (c) Force pure vertical load for Fsv=-2. With black lines are the curves extracted from the numerical experiments and with gray the prediction of the macro-element model*

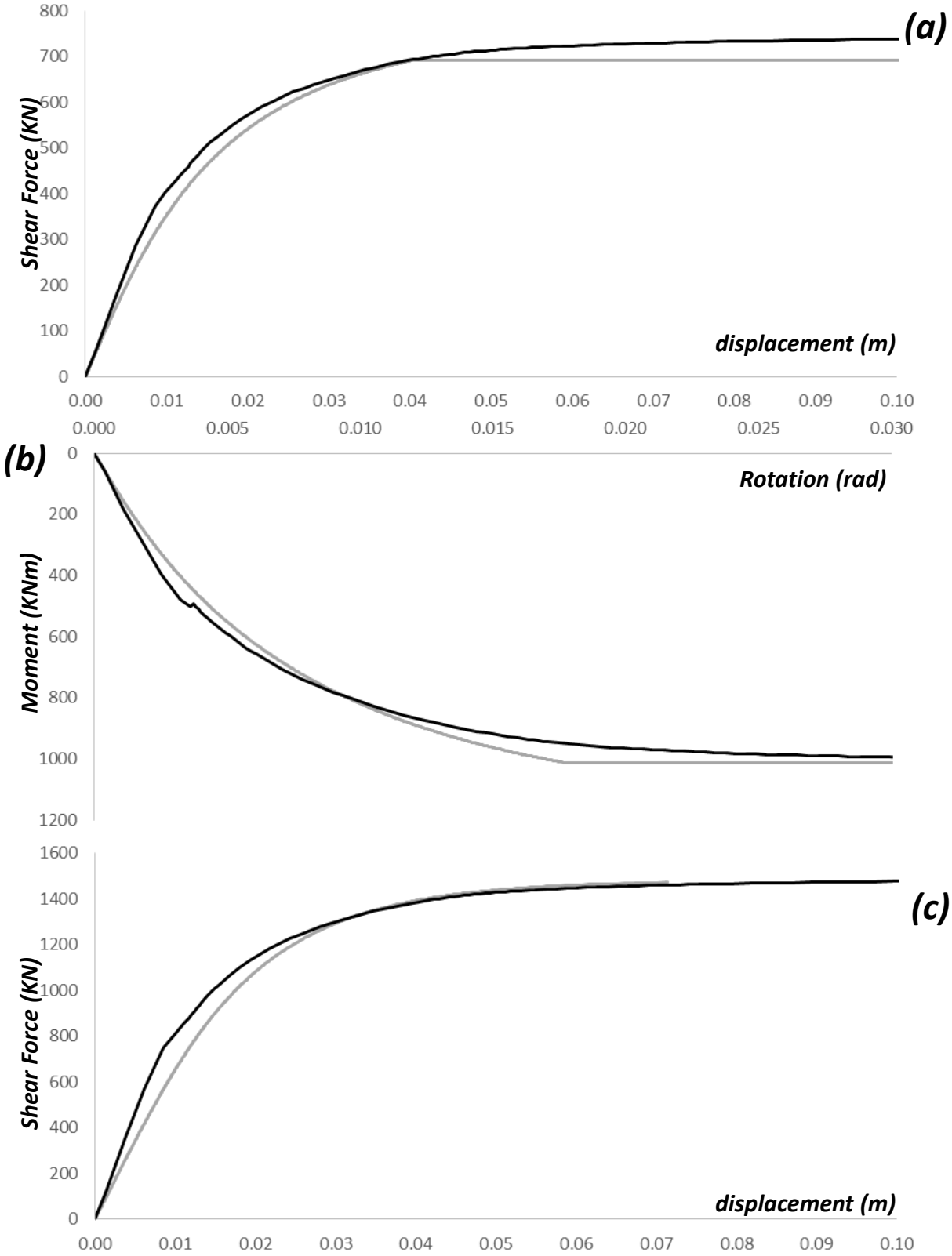

Figure 4.14 *Diagrams of (a) Force displacement for combined shear force – moment (ϑ=52°) for Fsv=-2, (b) Moment – rotation for combined shear force – moment (ϑ=-36°) for Fsv=-2, (c) Force displacement for combined vertical force – moment (ϑ=-36°) for Fsv=-2. With black lines are the curves extracted from the numerical experiments and with gray the prediction of the macro-element model*

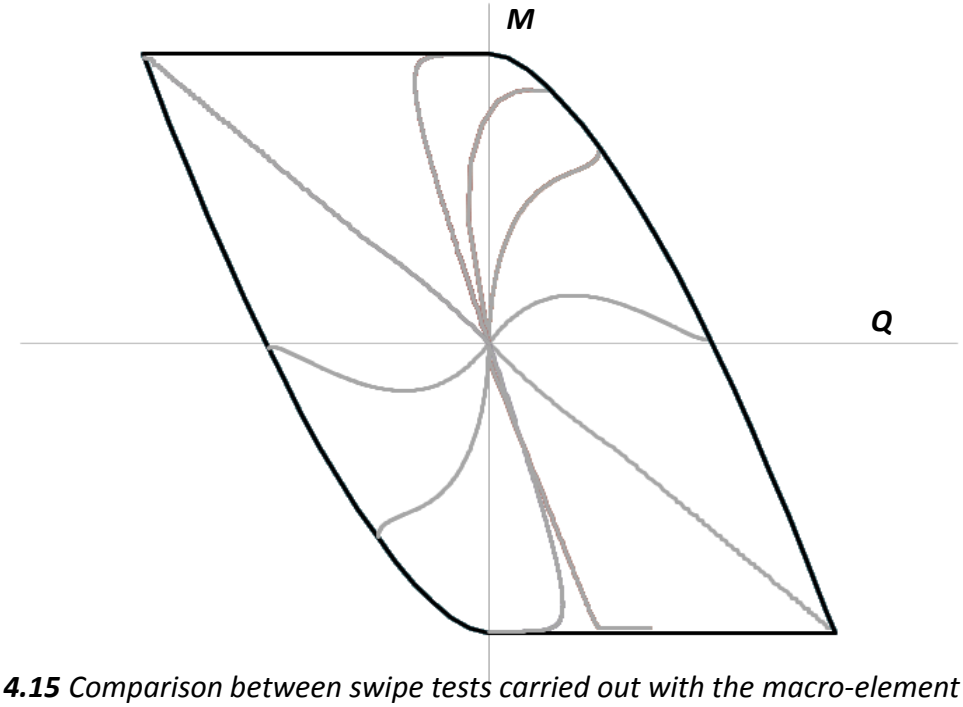

Figure 4.15 *Comparison between swipe tests carried out with the macro-element model and the interaction curves deduced from the analytical expressions for Fsv=∞*

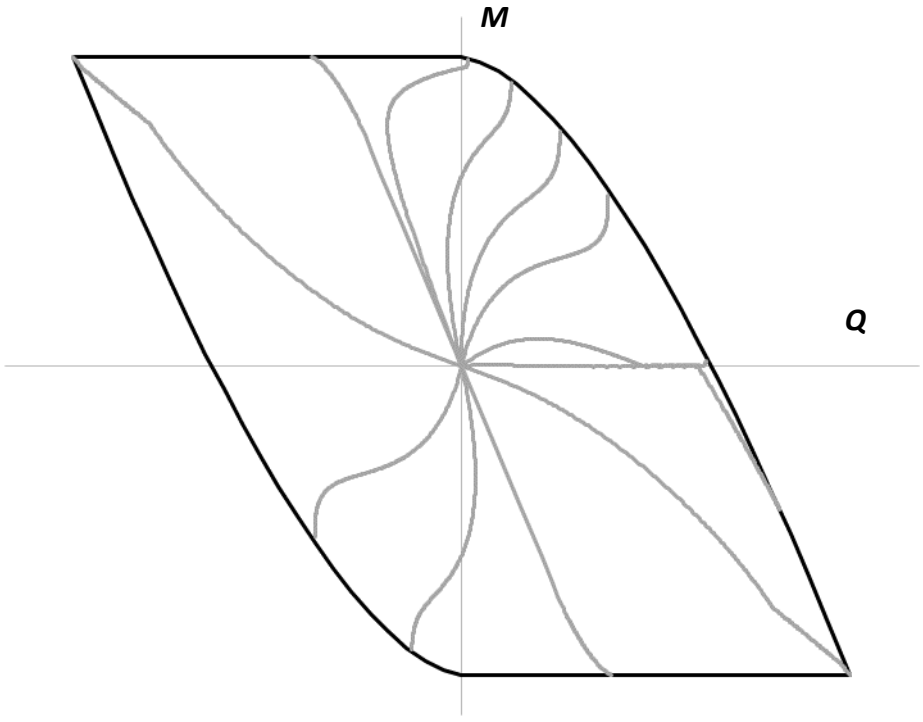

Figure 4.16 *Comparison between swipe tests carried out with the macro-element model and the interaction curves deduced from the analytical expressions for Fsv=1.25*

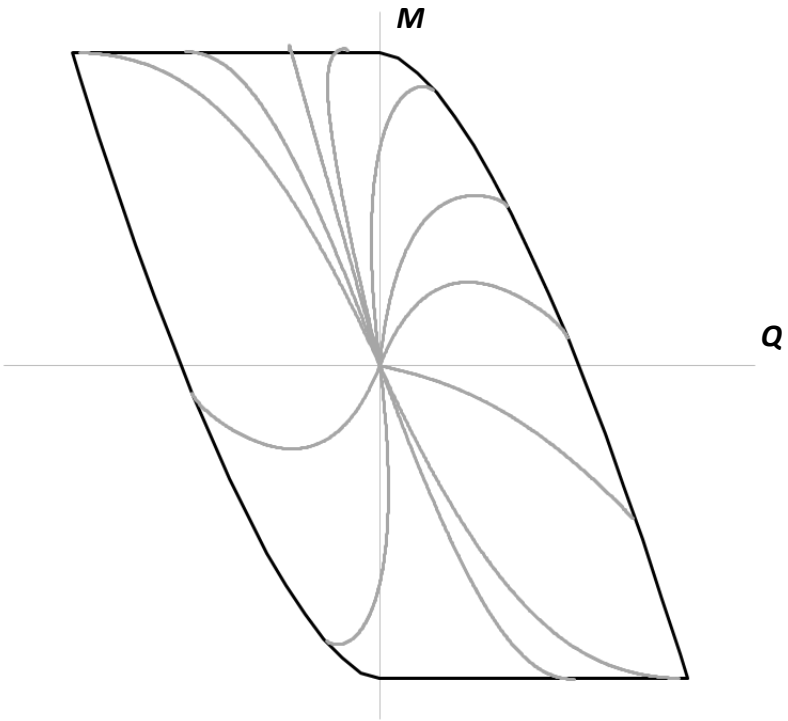

Figure 4.17 *Comparison between swipe tests carried out with the macro-element model and the interaction curves deduced from the analytical expressions for Fsv=-2*

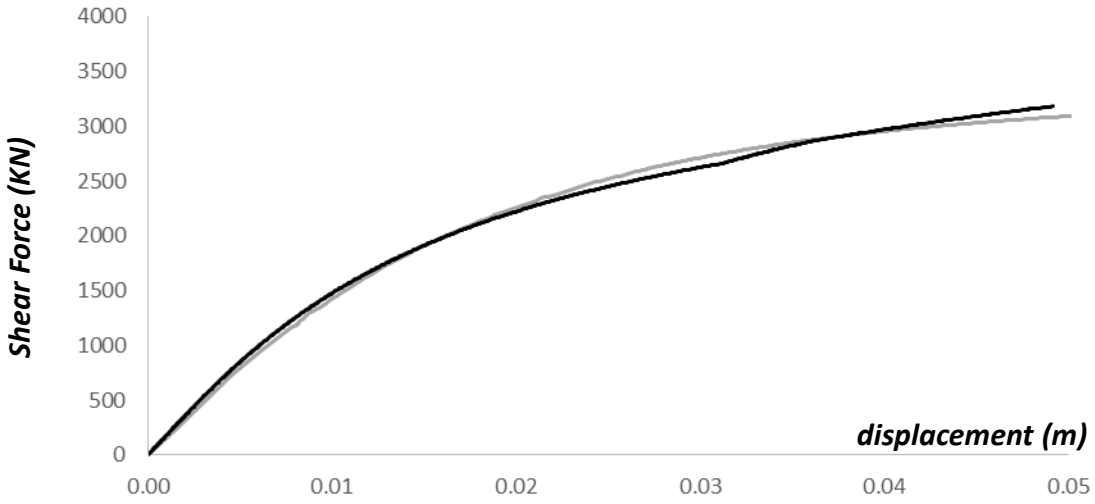

Figure 4.18 *Diagram of force displacement for pure shear load for Fsv=∞, . With black line is the curve extracted from the numerical experiments and with gray the prediction of the macro-element model*

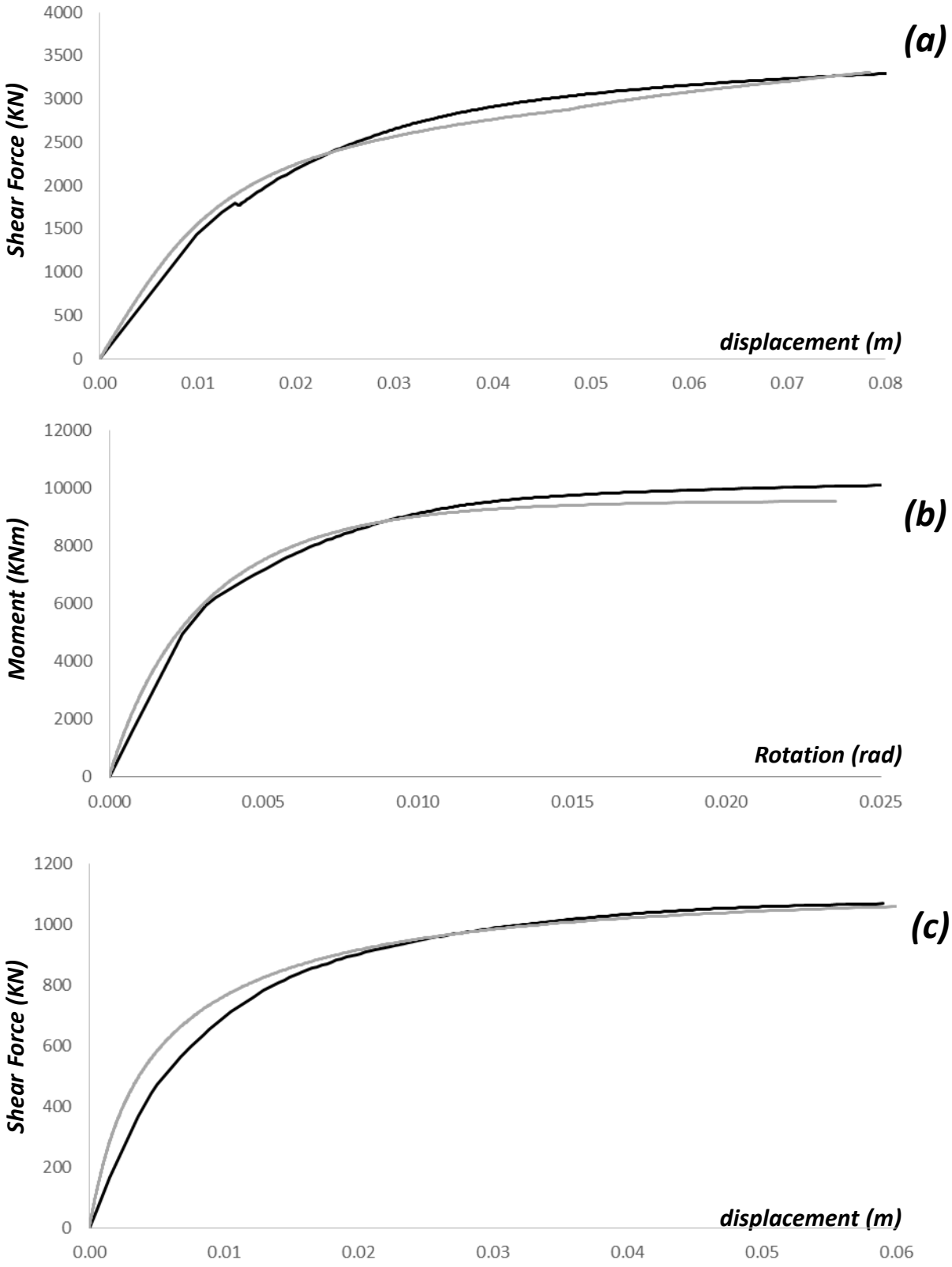

Figure 4.19 *Diagrams of (a) Force displacement for combined shear force – moment ($\vartheta=30^o$) for Fsv=∞, (b) Moment – rotation for pure moment for Fsv=-5, (c) Force displacement for combined shear force – moment ($\vartheta=75^o$) for Fsv=-1.25. With black lines are the curves extracted from the numerical experiments and with gray the prediction of the macro-element model*

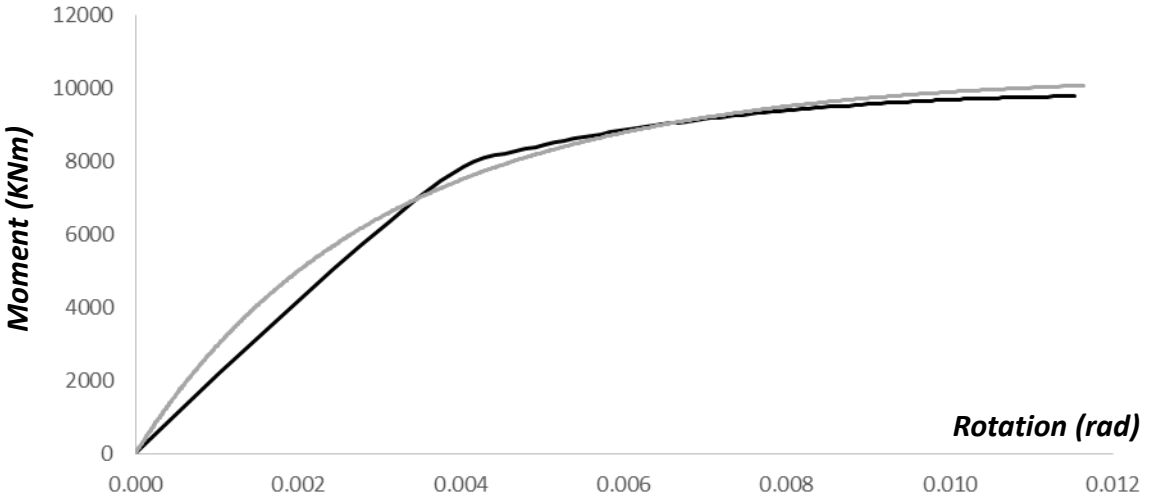

Figure 4.20 *Diagram of force displacement for pure moment for Fsv=2, . With black line is the curve extracted from the numerical experiments and with gray the prediction of the macro-element model*

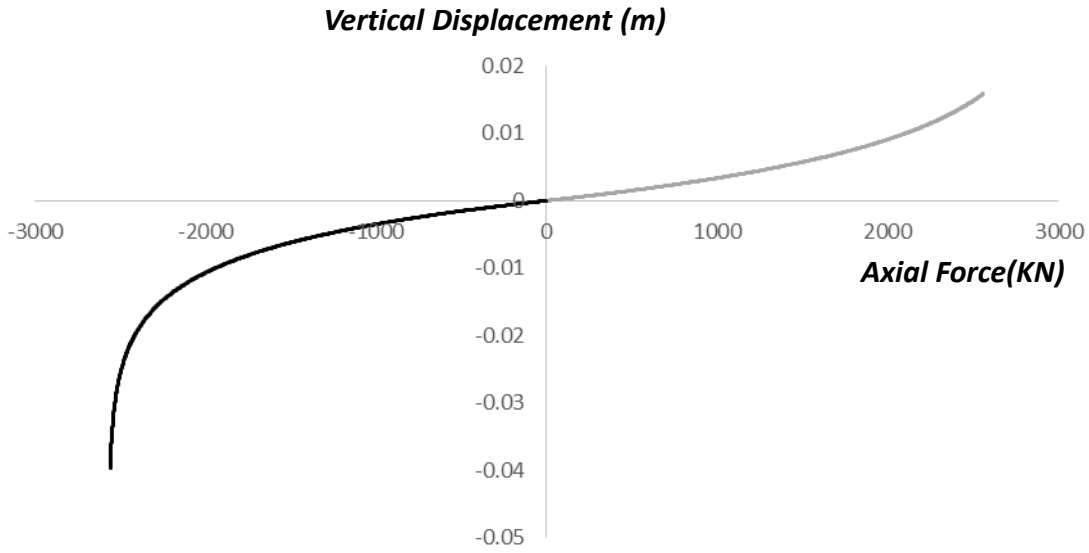

Figure 4.21 *Diagram of axial force – vertical displacement for pure moment for Fsv=∞. The stress is caused by the axial component of the moment. The black line represents the axial failure of the pile under tension, while the gray line displays the axial force applied to the compressed pile.*

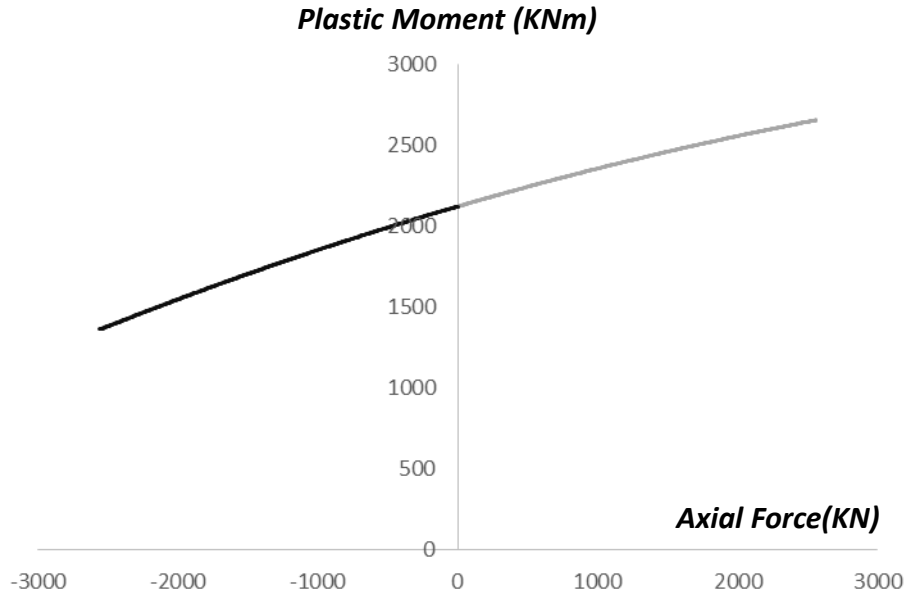

Figure 4.22 *Diagram of the alteration of the plastc moment resistance of the pile material due to the axial component of thepure moment for Fsv=∞. With black and gray line is presented the moment resistance of the pile under tension and compression respectively.*

Chapter 5

Conclusions and recommendations

5 Conclusions and recommendations

5.1 Conclusions

This thesis dealt with the response of pile foundations resting on an undrained clay profile with an increasing undrained shear strength with the depth subjected to combined axial and lateral static monotonic loading.

Our first aim was to develop a new approach able to simulate in finite element modeling the pile behavior accurately. Taking into consideration the drawbacks and weaknesses of the existing methods a new tool is designed capable of capturing the pile material properties and response in elasticity, in plasticity and incorporating the effects of random loading.

Our second aim was to provide insight to the failure envelopes of a single flexible pile and a 1x2 and 2x2 pile-group under combined M-Q-N loading, including the effects of soil-pile nonlinearities. Following the work of Gerolymos et al in the case of single pile, we determine analytical expressions that represent these failure envelopes, able to experience both sliding and gapping.

Our third aim was to develop a uniform mathematical tool, known as macroelement modeling capable of representing the total behavior of a pile from elasticity to total plasticity, extending to simulate a 1x2 pile-group response too.

The important conclusions that were drawn from this thesis are presented below:

- A new macroscopic approach was developed under the Mohr-Coulomb i.e. Tresca failure criterion for simulating circular piles behavior. Its verification was focused in various concrete pile diameters (0.8m, 1m, 1.5m) with different reinforcements (1%, 1.5%, 2%), analytically and in finite element modelling. The results where more than satisfactory, as the approach is able to simulate the pile behavior in elastoplasticity, in terms of moment-curvature and to include the interaction between the external loads and the

pile material properties, as well as the soil-pile interaction. The calibration of the approach can be easily be conducted through the following steps:

1. Extraction of the failure envelope of the studied circular pile.
2. Using the derived mathematical expressions and an optimization tool the calibration of the parameters of the model can be performed.
3. The variables are inserted in the finite element model in the appropriate soil model together with the other elastic pile parameters
4. Verification of the approach can be done by extracting the failure envelopes in the finite element program and comparing the moment-curvature diagrams.

- The failure envelopes of a single flexible pile in cohesive soil are derived. The pile is modeled by the previously derived approach. Various moment- lateral load combinations are applied under different safety factors against axial failure and the interaction diagrams are created. The total 3- dimensional in M-Q-N space yield surface of the pile is designed. It is being confirmed that the shape of the envelopes is constant regardless the axial load, while the e equations proposed by Gerolimos et al are extended by introducing the alteration of the pile plastic moment due to the change of the axial load. Finally the normality of the plastic displacements increment is ascertained, confirming the associated plastic flow rule.

- The interaction diagrams in both directions of a 1x2 pile group in cohesive soil are derived. In the direction where the full pile-group function is activated shape of the curves is not constant, but varies in respect to the axial load. Analytical expressions are proposed able to describe the pile-group behavior, while the failure mechanisms are examined and classified in two basic categories: the system's ultimate capacity is reached by the development of one plastic hinge at each pile and the axial failure of one of the two or by the development of two plastic hinges at each pile. The first mechanism concerns the failure under combined axial, moment and lateral load where the

moment has major contribution, with the pivot point located at the head of the compressive pile, while the second is activated when the system reaches its ultimate lateral capacity, while the pile-group is practically not rotated. In the vertical direction the pile-group functions as the sum of two single piles influenced by the interaction of the piles due to their distance. The shape of the failure envelopes remains constant as in the case of the flexible pile and the failure mechanisms are equal, while the normality of the plastic displacements increment is also analytically verified. Finally the moment – lateral load capacities for the same safety factors in the two direction are compared, displaying the overstrength provided when the full pile-group function is activated.

- The behavior of a 2x2 pile group in normal and diagonal direction was investigated. In the normal direction the pile-group behaves as the 1x2, having the same failure mechanisms and similar failure envelopes. These results were expected due to the geometrical resemblance of the two pile-groups. Moreover the relevant analytical expressions where derived. Interesting is the fact that the failure envelopes under diagonal combined loading have similar shape with the ones derived for the 1x2 and 2x2 pile–group, in spite of the alteration of the failure mechanisms. A conclusion very contributive in the research of capturing a generalized relation for the extraction of the failure envelopes of random pile-groups. For big safety factors where the moment has major contribution, the pile-group rotates in respect to the two central piles and the system reaches its ultimate capacity by the development of one plastic hinge at each piles and the axial failure of one outer pile. In contrary close to axial failure the pivot point is located at the outer compressed pile and the group resistance is depleted by one plastic hinge development at each pile and the axial failure of two. In both cases when the system reaches its ultimate lateral capacity two plastic hinges develop at each pile. The capacities for the same safety factor for the two different loading directions are compared. In both cases the lateral resistance

is practically the same. It is notable that for big safety factors the pile-group in x direction provides larger moment resistance, while as the axial load increases the pile-group under diagonal loading shows more strength.

- A macro-element model was developed able to simulate the soil-pile foundation behavior from elasticity to full plasticity. This model incorporates 4 components: a) elasticity, b) failure envelopes, c) associative plastic flow rule and d) hardening law. The elastic stiffness matrices were formed using the existing bibliography, while the previously extracted failure envelopes were inserted in the mathematical tool. An associative plastic flow rule was chosen, as its validity is analytically confirmed, while a hardening law provides the system the non-linear behavior. The results were compared with those from the numerical experiments both by applying a combination of loads until the systems failure or by introducing prescribed displacements on the top of the pile (swipe tests) until the system reaches its maximum capacity. The matching verified the correct and accurate development of the modp el, as it has the ability to capture the pile – soil foundation in elasticity, plasticity and in the transition zone between the two. Furthermore this model was extended by incorporating two flexible piles with the appropriate kinematic constraints and simulating the behavior of a 1x2 pile-group comparing it with the failure envelopes derived previously. The mathematical model can simulate it satisfactorily.

5.2 Recommendations for future research

In this last section, some suggestions for future work on the extensive subject of macro-element modeling of pile foundations is provided:

- The development of the macroscopic circular pile approach for different pile material (e.g. steel). Moreover the incorporation of the approach in other constitutive models, extending its use to a wider range of problems.

- The examining of pile-groups with different number of piles and geometry, in order to capture a generalized behavior of this type of foundations. Furthermore the influence of the interface nonlinearities can be investigating in the response and failure state of the system.

- In addition, this work should be extended to the study of dynamic problems and especially seismic excitations, justifying the initial adoption of an undrained shear strength profile. Thus numerical experiments regarding the dynamic response of pile foundations can be held, incorporating the results in the extracted macroelement model and extending its function to the capture of the total foundation behavior.

- Finally a different soil profile can be utilized (e.g. sand), investigating the behavior of the pile macroscopic approach, the pile foundation response and modifying the developed macroelement model in order to simulate the different conditions.

`

Chapter 6

References

6 References

American Petroleum Institute (API), 2000, Recommended practice for planning, designing and constructing fixed offshore platforms-working stress design, *API Recommended Practice 2A-WSD (RP 2A-WSD)*, 21st edn.

Bransby M.F., Randolph M.F., 1998, "Combined loading of skirted foundations", *Geotechnique*, 48(5), pp 637-655

Broms B.B.., 1964a, "Lateral resistance of piles in cohesive soils", *Journal of Soil Mechanics and Foundation Division*, ASCE 90(SM2), pp 27-63.

Broms B.B.., 1965, "Design of laterally loaded piles", *Journal of Soil Mechanics and Foundation Division*, ASCE 91(SM3), pp 77-99.

Cassidy MJ, Martin CM, Houlsby GT. Development and application of force resultant models describing jack-up foundation behaviour. Marine Structures 2004; 17:165–193.

Chatzigogos, C. T., Figini, R., Pecker, A. and Salençon, J. (2011). A macroelement formulation for shallow foundations on cohesive and frictional soils. Int. J. Numer. Anal. Meth. Geomech. 2011; 35:902–931

Cho Y., Bang S., 2002, "Inclined Loading Capacity of Suction Piles", *Proceedings of the 12th International Offshore and Polar Engineering Conference*, Kitakyushu, Japan May 26-31, pp 827-832.cohesive soil", *Geotechnique*, Vol 34 (4), pp 613-623.

Comodromos EM and Bareka SV (2009) "Response evaluation of axially loaded fixed-head pile groups in clayey soils", International Journal for Numerical and Analytical Methods in Geomechanics, Vol. 33, No. 17, pp. 1839-1865

Comodromos EM and Papadopoulou MC (2012) "Response evaluation of horizontally loaded pile groups in clayey soils", Geotechnique, Vol. 62, No. 4, pp 329-39.

Correia AA (2011) A pile-head macro-element approach to seismic design of monoshaft-supported bridges, PhD Thesis, ROSE School, IUSS Pavia, Italy

Correia AA, Pecker A, Kramer SL, Pinho R (2012) A pile-head macro-element approach to seismic design of extended pile-shaft-supported bridges. In: Proceedings of the 2nd international conference on performance-based design in earthquake geotechnical engineering. Taormina, Italy, Paper No. 7.03, May 28–30

Crémer C, Pecker A, Davenne L. Cyclic macro-element for soil-structure interaction: material and geometrical non linearities. International Journal for Numerical and Analytical Methods in Geomechanics 2001; 25: 1257 – 1284.

Crémer C. Modélisation du comportement non linéaire des fondations superficielles sous séisme. PhD thesis, Laboratoire de Mécanique et de Technologie, ENS – Cachan, France, 2001. Das, B., 1995. Fundamentals of soil dynamics. *Elsevier.*

Davidson, H., 1982. *Laterally loaded drilled pier research,* Pensylvania: Gai Consultans, Inc.: Electric Power Research Institute.

Gerolymos N, Gazetas G (2006) Development of Winkler model for static and dynamic response of caisson foundations with soil and interface nonlinearities. Soil Dynamics and Earthquake Engineering 26 (2006), pp 363–376

Gerolymos N., (2012), "A macro-element model for nonlinear static and dynamic response of piles", research program final report, PEVE 2008

Gerolymos N., Gazetas G., (2005). "Phenomenological Model Applied to Inelastic Response of SoilPile Interaction Systems", *Soils & Foundations*, Japanese Geotechnical Society, Vol. 45(4), p.p. 119-132

Gerolymos N., Zafeirakos A. , Souliotis Ch. (2012). "Insight to failure mechanisms of caisson foundations under combined loading : a macro-element", Proceedings of the First Bulletin of the Second International Conference on Performance–Based Design in Earthquake Geotechnical Engineering, 28-30 May, Taormina (Italy).

Gerolymos, N. & Gazetas, G., 2006. Winkler model for lateral response of rigid caisson foundations in linear soil. *Soil Dynamics and Earthquake Engineering,* Volume 26, pp. 347-361.

Gerolymos, N., Drosos, V., Gazetas, G. (2009). Seismic response of single-column bent on pile: evidence of beneficial role of pile and soil inelasticity. Bull Earthq Eng 7(2): 547–573 Special Issue:Earthquake Protection of Bridges.

Gourvenec, S. (2007). Failure envelopes for offshore shallow foundation under general loading, Geotechnique, 57(9): 715~728.

Grange S., Kotronis P. and Mazars J. (2008). A macro-element for a circular foundation to simulate 3D soil–structure interaction. Int. J. Numer. Anal. Meth. Geomech. 2008; 32:1205–1227

Houlsby, T., Kelly, R. B., Huxtable, J. & Byrne, B. W., 2005. Field trials of suction caissons in clay for offshore wind turbine foundations. *Geotechnique,* Volume 5, pp. 287-296.

J.H. Atkinson (2007): “The Mechanics of Soils And Foundations”

Le Pape Y, Sieffert JG. Application of thermodynamics to the global modelling of shallow foundations on frictional material. International Journal for Numerical and Analytical Methods in Geomechanics 2001; 25:1377–1408.

Matlock, H. (1970): Correlations for design of laterally loaded piles in soft clay, Paper No. OTC 1204, Proc. 2nd Annual Offshore Technology Conference, Houston, Texas, 1,577-594

Meyerhof G., 1995, “Behaviour of pile foundations under special loading conditions: 1994 R.M. Hardy keynote address”, *Canadian Geotechnical Journal*, Vol 32 (2), pp 204-222.

Montrasio, L., and Nova, R. 1988. Assestamenti di una fondazione modello sotto carico inclinato: risultati sperimentali e modellazione matematica. Rivista Italiana di Geotecnica, 22(1): 35 – 49.

Mylonakis G. PhD (1995) “Contributions to static and seismic analysis of piles and pile-supported bridge piers’’, State University of New York at Buffalo

Nova, R. & Montrasio, L. (1991). Settlements of shallow foundations on sand. Geotechnique 41, No. 2, 243–256.

PLAXIS3D, 2012. *Material Models.* Delft, The Netherlands: Plaxis b.v..

PLAXIS3D, 2012. *Scientific Manual.* Delft, The Netherlands: Plaxis b.v..

Poulos H.G., Davis E.H., 1980, *Pile Foundation Analysis and Design*

Prager, W. (1959). An introduction to plasticity. Reading, MA: Addison-Wesley.

Randolph, M. F. (1981): The response of flexible piles to lateral loading, Geotechnique, 31(2), 247-259

Reese L.C., Van Impe W.F., 2001, *Single Piles and Pile Groups under Lateral Loading*, A.A.Balkema. Rotterdam

Reese, L. C., Cox, W. R. and Koop, F. D. (1975): Filed testing and analysis of laterally loaded piles in stiff clay, Paper No. OTC 2312, Proc. &th Offshore Technology Conference, Houston, Texas, II, 672-690

Ricceri, G., and Simonini, P. 1989. Interaction diagrams for shallow footings on sand. In Proceedings of the 12th International Conference on Soil Mechanics and Foundation Engineering, Rio de Janeiro, 13 – 18 August 1989. A.A. Balkema, Rotterdam, Netherlands. pp. 89 – 95.

Tomilson M. J, Woodward J. (2007): “Pile Design and Construction Practice”
Varun, 2006. *A simplified model for lateral response of caisson foundations,* s.l.: s.n.